On Automation in Anesthesia

Soltesz, Kristian

2013

Document Version:
Publisher's PDF, also known as Version of record

On Automation in Anesthesia

Kristian Soltész

LUND
UNIVERSITY

Department of Automatic Control

Department of Automatic Control
Lund University
PO Box 118
SE-221 00 Lund
Sweden

PhD Thesis
ISRN LUTFD2/TFRT--1096--SE
ISSN 0280–5316
ISBN 978-91-7473-484-3

Printed in Sweden by Media-Tryck.
Lund 2013

Szeretett Nagytatámnak

Abstract

The thesis discusses closed-loop control of the hypnotic and the analgesic components of anesthesia. The objective of the work has been to develop a system which independently controls the intravenous infusion rates of the hypnotic drug propofol and analgesic drug remifentanil. The system is designed to track a reference hypnotic depth level, while maintaining adequate analgesia. This is complicated by inter-patient variability in drug sensitivity, disturbances caused foremost by surgical stimulation, and measurement noise. A commercially available monitor is used to measure the hypnotic depth of the patient, while a simple soft sensor estimates the analgesic depth. Both induction and maintenance of anesthesia are closed-loop controlled, using a PID controller for propofol and a P controller for remifentanil. In order to tune the controllers, patient models have been identified from clinical data, with body mass as only biometric parameter. Care has been taken to characterize identifiability and produce models which are safe for the intended application. A scheme for individualizing the controller tuning upon completion of the induction phase of anesthesia is proposed. Practical aspects such as integrator anti-windup and loss of the measurement signal are explicitly addressed. The validity of the performance measures, most commonly reported in closed-loop anesthesia studies, is debated and a new set of measures is proposed. It is shown, both in simulation and clinically, that PID control provides a viable approach. Both results from simulations and clinical trials are presented. These results suggest that closed-loop controlled anesthesia can be provided in a safe and efficient manner, relieving the regulatory and server controller role of the anesthesiologist. However, outlier patient dynamics, unmeasurable disturbances and scenarios which are not considered in the controller synthesis, urge the presence of an anesthesiologist. Closed-loop controlled anesthesia should therefore not be viewed as a replacement of human expertise, but rather as a tool, similar to the cruise controller of a car.

Acknowledgments

It is with the direct or indirect help from several persons that I have come to write this thesis. With the reservation of forgetting anyone of you, I would explicitly like to acknowledge the following persons.

My supervisor professor Tore Hägglund has been ever supporting in my work. Your engagement and mentoring has meant a lot to me. You have always encouraged me and contributed to an atmosphere in which it has been truly enjoyable to work. You have also served as a role model, in a much broader context than that of automatic control.

Professor Karl Johan Åström has been a great source of inspiration and has been the source of several key ideas around which I have worked.

The administrative staff at the department, being Britt-Marie Mårtensson, Ingrid Nilsson, Eva Schildt, Agneta Tuszynski, Eva Westin, Monika Rasmusson and Lizette Borgeram have all been very kind, knowledgeable and helpful.

At the University of British Columbia I would like to acknowledge professor Guy Dumont and post doctoral fellows Jin-Oh Hahn and Klaske van Heusden for introducing me to an interesting research topic. I would also like to thank Dr. Mark Ansermino and the staff at the anesthesia department of the British Columbia Children's Hospital in Vancouver.

I would like to thank all fellow PhD students at the department for interesting discussions. In particular my former office mate Magnus Linderoth has provided material for discussions of almost everything, including relevant topics.

Research engineers Rolf Braun, Pontus Andersson, Anders Blomdell, Leif Andersson and Anders Nilsson have taught me many interesting things related to computers, lab processes and workshop machines which I am sure will come to use regularly.

Finally I would like to thank my wife Ingrid, my family and my friends in Lund and Vancouver.

Financial Support

The Swedish Research Council through the LCCC Linnaeus Center is gratefully acknowledged for financial support.

Contents

Preface

Motivation

Closed-loop control has found its successful application in a wide range of fields, stretching from indoor temperature control, to robotics or tracking in DVD players. However, it has had a comparably limited impact in the field of medicine.

The suggestion of controlling drug delivery for maintaining an adequate anesthetic state during surgery is an exception and was proposed and demonstrated already in the 1950s [Soltero et al., 1951]. There has since emerged numerous studies on the topic, utilizing a wide range of control strategies. However, little has changed in clinical practice. One contributing reason to this is the justified concern regarding patient safety. This is foremost manifested through the regulatory challenges facing any candidate system, particularly in North America [Manberg et al., 2008]. In order to achieve a broad clinical acceptance, it must therefore be demonstrated that a candidate system is safe and that it provides a benefit over manual drug dosing.

The potentials of closed-loop controlled anesthesia is that it is expected to decrease drug dosage and facilitate post-operative recovery while increasing patient safety and decreasing the workload of the anesthesiologist [Hemmerling et al., 2010], [Liu et al., 2006], [Struys et al., 2001]. It might also reduce the variability in drug dosing between anesthesiologists [Mackey, 2012]. This has been confirmed by several studies, as mentioned in Section 1.2 of the thesis. It is therefore rather questions concerning patient safety, which are currently inhibiting a wider clinical acceptance. In fact, several clinical studies, including [Absalom and Kenny, 2003] and [Haddad et al., 2011], report poor robustness, manifested as oscillatory response of the control system for some cases.

It is unlikely that one control system (of practical complexity) will be able to account for all patients in all anesthesia situations. In fact, this is not needed in the presence of an anesthesiologist, who can intervene during cases when the system does not perform satisfactory. This could pose a con-

cern when it comes to system performance, but an acute threat to patient safety can be avoided by introducing hard low-level bounds on e.g. drug infusion rates, which confine the closed-loop system to an operational envelope from within which poor performance can easily be recovered by switching to manual mode.

With what has been mentioned in mind, the main motivation behind the work resulting in the thesis has been to demonstrate the safety and potential of a closed-loop anesthesia system, both in simulation and clinically. This includes showing that simple low-order models and controllers are adequate for the task and that analgesia can be successfully controlled, in the absence of a reliable dedicated clinical monitor, by using a simple soft sensor approach. In order to show this, an appropriate set of performance measures is required. However, the measures most frequently used in closed-loop controlled anesthesia were adopted from another context, for which they were tailored. Another motivator has therefore been to establish a set of performance measures which more closely reflects the clinical outcome.

A more detailed motivation of the work behind the thesis relies on technical and medical aspects. Consequently, it is not given here, but rather integrated into the remainder of the text.

Contributions

Papers

Parts of the work underlying the thesis have been previously published or accepted for publication. References to the corresponding papers are chronologically listed below, together with a brief description of their contribution to the thesis. The role of the author in the work behind each paper is explicitly stated.

Paper I Soltész, K., J.-O. Hahn, G. A. Dumont, and J. M. Ansermino (2011). "Individualized PID control of depth of anesthesia based on patient model identification during the induction phase of anesthesia". In: *Proc. IEEE Conference on Decision and Control and European Control Conference*. Orlando, USA.

The two customary approaches to controlling the hypnotic depth component of anesthesia is to use either robust or adaptive techniques. The shortcoming of the robust techniques is that they need to be very conservative, due to large inter-patient variability in drug sensitivity. Meanwhile, continuously adaptive techniques are challenged by the presence of unmeasurable disturbances, mainly resulting from surgical stimulation, as well as measurement noise. The paper presents an alternative where a robust controller is used during the initial induction phase of anesthesia, during which there is

no surgical stimulation. The response of the patient to the hypnotic drug is subsequently used to re-tune the controller and the re-tuned controller is employed throughout the remainder of the procedure. Consequently, individualized control is achieved, while avoiding the issues related to continuous adaptation. The proposed scheme is evaluated in simulation on a set of previously published patient models, identified from clinical data.

K. Soltész wrote the simulation software, proposed the controller tuning and was the main author of the manuscript.

Paper II Soltész, K., K. van Heusden, G. A. Dumont, T. Hägglund, C. L. Petersen, N. West, and J. M. Ansermino (2012b). "Closed-loop anesthesia in children using a PID controller: a pilot study". In: *Proc. IFAC Conference on Advances in PID Control*. Brescia, Italy.

The first study with a PID controller-based automatic drug delivery system for propofol anesthesia in children is presented. It is shown that a robustly tuned PID controller is capable of delivering safe and adequate anesthesia. The design process of the control system is reviewed. Results are discussed and compared to those of two previous studies in adults.

K. Soltész designed the controller in the underlying study, based on patient models identified by K. van Heusden. He also wrote the simulation software used prior to clinical evaluation. The manuscript was assembled by K. Soltész, with useful input from the co-authors.

Paper III Soltész, K., G. A. Dumont, K. van Heusden, and J. M. Ansermino (2012a). "Simulated mid-ranging control of propofol and remifentanil using EEG-measured hypnotic depth of anesthesia". In: *51st IEEE Conference on Decision and Control*. Maui, USA.

The paper suggests an extension of an existing, clinically evaluated, closed-loop drug delivery system for hypnotic depth control using propofol. The extension introduces closed-loop administration of the analgesic drug remifentanil, thus forming a multiple-input single-output (MISO) control system. Remifentanil acts in, and is metabolized at, a significantly faster time scale than propofol. Direct control of analgesia is hindered by the current absence of a reliable real-time nociception monitor. However, several hypnotic depth monitors respond to nociception. Sudden changes in the measured hypnotic depth are frequently caused by changes in noxious stimulation. The novelty of this work lies in increasing the disturbance rejection bandwidth of the control system for hypnotic depth by directing the high frequency content of its control error to a remifentanil controller. A control system based on this simple soft sensor approach was implemented and tuned using the same patient models as in Paper II. The performance of the system was demonstrated in a realistic simulation scenario.

K. Soltész proposed the structure and tuning of the additional control loop, with technical input from K. van Heusden, G. A. Dumont and T. Häg-

glund. J. M. Ansermino provided clinical information necessary for tuning the controller and devising realistic simulations.

Paper IV van Heusden, K., G. A. Dumont, K. Soltész, C. L. Petersen, A. Umedaly, N. West, and J. M. Ansermino (2013a). "Clinical evaluation of robust PID control of propofol anesthesia in children". *IEEE Transactions on Control System Technology*. In press.

This paper is based on the same study as Paper II, but presents the entire study involving 102 closed-loop controlled anesthesia cases. The initial controller was deliberately tuned conservatively, as described in Paper II. A slightly more aggressive controller tuning was supported by the extended set of patient models available after the first 23 clinical cases using the initial controller.

The paper was written foremost by K. van Heusden. K. Soltész was involved in the data analysis and controller tuning prior to, and during, the clinical study and assisted in assembling the manuscript.

Paper V Soltész, K., J.-O. Hahn, T. Hägglund, G. A. Dumont, and J. M. Ansermino (2013b). "Individualized closed-loop control of propofol anesthesia: a preliminary study". *Biomedical Signal Processing and Control* **8** (6), pp. 500–508.

This paper is an extended journal version of Paper I, giving a more in-depth analysis of what one could expect to achieve from an individualized hypnotic depth control scheme.

K. Soltész wrote the simulation software, proposed the controller tunings and was the main author of the manuscript.

Paper VI West, N., G. A. Dumont, K van Heusden, C. L. Petersen, S. Khosravi, K. Soltész, A. Umedaly, E. Reimer, and J. M. Ansermino (2013). "Robust closed-loop control of induction and maintenance of propofol anesthesia in children". *Pediatric Anesthesia* **23** (8), pp. 712–719.

The clinical details of the study, upon which Papers II, IV and VII are based, are presented in this paper.

N. West was the main contributor to this publication. K. Soltész took part during some of the clinical cases and assisted in preparing the manuscript – particularly the controller related section.

Paper VII van Heusden, K., J. M. Ansermino, K. Soltész, S. Khosravi, N. West, and G. A. Dumont (2013b). "Quantification of the variability in response to propofol administration in children". *IEEE Transactions on Biomedical Engineering*. In press.

This paper presents the model structures and system identification methods used to obtain the models, which were used in tuning the controllers described in Papers II, IV and VI.

The paper was written foremost by K. van Heusden. K. Soltész characterized the unidentifiability problem, caused by the lack of sufficient input signal excitation, and proposed the introduction of low (first) order models. He also assisted in assembling the manuscript.

Paper VIII Soltész, K., G. A. Dumont, and J. M. Ansermino (2013a). "Assessing control performance in closed-loop anesthesia". In: *21st Mediterranean Conference on Control and Automation (MED13)*. Platanias-Chania, Greece, pp. 191–196.

Recently, several control systems for closed-loop anesthesia have been demonstrated both in simulation and clinical studies. A set of performance measures, proposed by Varvel et al., have constituted the standard means of comparing such systems. This paper debates the adequacy of the Varvel measures, as applied to closed-loop anesthesia, and proposes an alternative set of measures. Key features of the proposed measures are: wide acceptance within the control community; reflection of clinical feasibility; separate measures for induction and maintenance of anesthesia; separation of outliers detection and performance evaluation. The proposed measures are descriptive, few, and easy to compute.

K. Soltész constructed the examples and wrote the manuscript. G. A. Dumont and J. M. Ansermino provided useful comments on engineering and clinical aspects, respectively.

Unpublished Work

Apart from the enlisted papers, the thesis contains contributions, which have not yet been published. A deeper discussion on what the challenges and objectives of modeling and controlling anesthesia in humans is provided. A variation of the identification scheme in Paper VII is proposed, together with a related discussion on model structure. Integrator anti-windup and a possible way to handle temporary loss of measurement signal are discussed. Finally, an up to date survey of prior art in closed-loop controlled hypnosis (using propofol) and analgesia (using remifentanil) is given.

Outline

Chapter 1 provides an introduction to clinical anesthesia from an automatic control perspective. This involves a review of the functional components and temporal phases of anesthesia and an introduction to the anesthetic drugs considered in the thesis. Different drug dosing regimens and clinical monitors are presented. Finally, models commonly used in the literature are introduced.

Chapter 2 reveals identification issues related to the models introduced in Chapter 1. Previous and current attempts to approach these issues are presented. A model structure and identification procedure with the aim of producing safe models in the absence of adequate input excitation is proposed and demonstrated on clinical data. The resulting models are subsequently used throughout the thesis.

Chapter 3 deals with control of the hypnotic and analgesic components of anesthesia, defined in Chapter 1. Goals for a hypnotic depth closed-loop control system are established. A controller structure and tuning method, based on the models revealed in Chapter 2, for meeting these goals are introduced. The outcome of a clinical study, implementing some of the proposed techniques and justifying the remaining, is presented. Chapter 3 also proposes a simple soft-sensor based technique to control analgesia by means of remifentanil infusion. The analgesia controller is intended to be used alongside the hypnotic depth controller, with no changes made to the structure or tuning of the latter. Its functionality and performance is demonstrated in a realistic simulation scenario.

Chapter 4 is divided into two parts. The first part summarizes the thesis and the second part proposes future research directions and activities.

1

Introduction

1.1 Clinical Anesthesia

The thesis deals with automation within clinical anesthesia. The aim is to make the text self-supporting, which is why the first chapter contains an introduction to clinical anesthesia, from the viewpoint of a control systems engineer. This introduces the minimum of information needed to support the remaining text, assuming no medical knowledge on top of what is provided in the high school curriculum. (Medical terms, with which the engineer might not be familiar, are explained in footnotes.) The interested reader might therefore wish to consult a text book, e.g. [Miller and Pardo, 2011] or [Barash et al., 2009], to obtain a broader introduction to the field of clinical anesthesia. A historical perspective is provided in [Keys, 1978] or the more recent [Diaz et al., 2001].

Functional Components

Although anesthetic drugs are used in several contexts, the intended target application in the thesis is elective general surgery. Within this application, anesthesia can be conveniently classified into three functional components, each associated with a corresponding class of drugs [Barash et al., 2009]. These functional components are shown in Figure 1.1 and presented below.

Hypnosis The main functional component of anesthesia is hypnosis, or the rendering of drug-induced unconsciousness. Its purpose is to take the patient to a state which inhibits the perception and recall of noxious stimuli[1].

Analgesia Although an adequate hypnotic state prevents the patient from perceiving or recalling noxious stimuli, their presence can still affect the hemodynamic[2] state of the patient, respiration and hormonal secretion. This

[1] Noxious stimulus: an actually or potentially tissue damaging event.
[2] Hemodynamics: the study of blood flow and circulation.

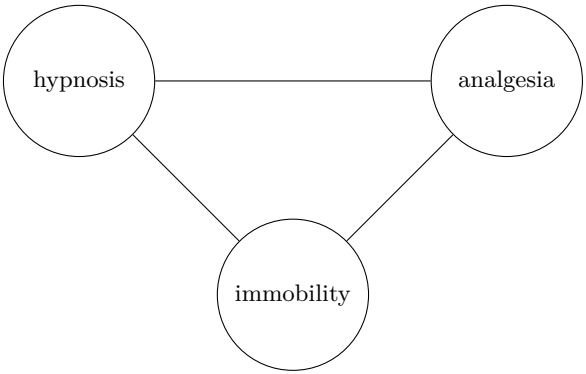

Figure 1.1 The three functional components of clinical anesthesia: hypnosis, analgesia and immobility.

can be prevented by analgesic[3] drugs which compromise the sympathetic and parasympathetic nervous systems.

Immobility Certain muscles, particularly abdominal[4] ones, exhibit reflex activity. This activity is typically not blocked in an adequate hypnotic and analgesic state, which motivates the use of paralyzing drugs, establishing a neuromuscular blockade, during some surgical procedures. The resulting immobility component of anesthesia is completely decoupled from hypnosis and analgesia, which allows separate treatment from a control perspective. The thesis focuses entirely on control of the hypnotic and analgesic patient states and there will consequently be no emphasis on the immobility component of anesthesia.

Anesthetic Drugs

This section discusses some aspects of drugs used to provide an adequate hypnotic and analgesic state during surgical procedures. Furthermore, the two drugs used throughout the remainder of the thesis are introduced.

Hypnotic Drugs – Propofol A drug of which the main purpose is to control the hypnotic state of the patient is referred to as a hypnotic drug. There exist a multitude of known hypnotic drugs, several of which are no longer used in clinical practice. See [Barash et al., 2009] for an extensive pharmacopedia. Hypnotic drugs can be classified by means of administration; inhalation or intravenous infusion.

[3] Analgesia: the absence of sensibility to pain.

[4] Abdomen: the part of the body that lies between the thorax and the pelvis and encloses the stomach, intestines, liver, spleen, and pancreas.

The routinely used inhaled volatile drugs[5] (nitrous oxide, isoflurane, desflurane and sevoflurane) are not purely hypnotic, but also provide analgesia to some extent. By means of real-time mass spectroscopy it is possible to measure the alveoal[6] uptake, by comparing drug concentration in inhaled and exhaled gas.

Routinely used intravenous drugs (propofol, ketamine, etomidate, midazolam, diazepam, lorazepam and thiopental) are pure hypnotic drugs, with the exception of ketamine which also provides analgesia to some extent. Propofol is a relatively new addition to this group, introduced in the 1990s. It has both fast redistribution and metabolism [Cummings et al., 1984] and does not accumulate in tissues unlike some of the other drugs. Particularly due to these properties, propofol has become widely accepted and the standard drug of choice for intravenous anesthesia. Throughout the remainder of the thesis, propofol will be the hypnotic drug of consideration.

Unlike inhaled drugs, it is not possible to measure the effect site (brain) concentration of propofol in real-time. This disadvantage is outweighed by the fast redistribution and metabolism of the drug, its lack of accumulation and the possibility of precise titration by means of electronically controlled intravenous infusion pumps. Besides, it is common practice to predict the effect site drug concentration using mathematical patient models, introduced in Section 1.3.

A major advantage of propofol, as compared to inhaled drugs, is that it is a pure hypnotic. This allows for decoupled control of the hypnotic and analgesic components of analgesia. It should be mentioned that this decoupling is, however, somewhat complicated by a synergistic interaction between propofol and several analgesic drugs. A model of this synergy is introduced in Section 1.3.

Another reason for the increasing popularity of propofol is that its use is associated with low incidence of postoperative nausea and vomiting compared to other hypnotic drugs [Borgeat et al., 1992], [Sebel and Lowdon, 1989]. This decreases the duration of postoperative care and ultimately patient mortality. Furthermore, propofol lacks the strong hypotensive[7] action common to inhaled drugs.

Analgesic Drugs – Remifentanil The fact that inhaled hypnotic drugs have analgesic properties enable their stand-alone use during surgical procedures involving limited noxious stimulation. During more stimulating procedures, or whenever the hypnotic drug of choice does not possess analgesic

[5] Volatile drug: a drug that can be readily vaporized and administered by inhalation or mechanical ventilation.

[6] (Pulmonary) alveolus: the blood–breathing gas interface site for oxygen and carbon dioxide.

[7] Hypotensive: causing a reduction in blood pressure.

effect, an analgesic drug is co-administered with the hypnotic one.

The most frequently used analgesic drugs are from the family of opioids (remifentanil, sufentanil, alfentanil, fentanyl, morphine and hydromorphine). In doses representative for clinical anesthesia, opioids do not exhibit hypnotic properties. However, there exists a synergistic effect between opioids and several of the hypnotic drugs, including propofol [Kern et al., 2004], [Minto et al., 2000]. This synergy enforces both the effect of the hypnotic and analgesic drug and plays a key role when the drugs are co-administered.

Remifentanil is the most recent addition to the opioid family. It is characterized by its very fast redistribution and metabolism; remifentanil is the fastest-acting of the opioids and its dynamics are of an order of magnitude faster than those of propofol. This makes remifentanil well suited for closed-loop controlled anesthesia and at the same time somewhat harder to manually titrate than the other opioids. The explanation of its fast metabolism is that remifentanil is metabolized by esterases[8] in the blood plasma, while the metabolism of other opioids rely on hepatic[9] biotransformation and renal[10] excretion. This motivates the use of remifentanil in patients with liver or kidney conditions.

The Anesthetic State

In the context of this work, providing adequate anesthesia is equated to controlling the anesthetic state of the patient undergoing general surgery. The anesthetic state is here defined as the combination of the hypnotic and analgesic states. The means of affecting this state (the control signals) are the intravenous infusion rates of propofol and remifentanil, respectively.

Depth of Hypnosis The hypnotic state can be adequately quantified by a scalar variable, referred to as the depth of hypnosis (DOH). The DOH measurement variable is defined in Section 2.1. As described later in this section, there exist real-time DOH monitors, enabling feedback control of the DOH. Modeling the influence of propofol infusion rate on the DOH is the topic of Section 1.3 and Chapter 2. For now, it is sufficient to mention that DOH is, in stationarity, monotonically dependent on the propofol infusion rate. Noxious stimulation decreases the DOH, see Section 2.2.

Depth of Analgesia The analgesic state of the patient can also be quantified by a scalar; the depth of analgesia (DOA[11]). However, to date there

[8] Esterase: any enzyme which catalyzes the hydrolysis of an ester into its alcohol and acid.
[9] Hepatic: pertaining to the liver.
[10] Renal: pertaining to the kidney.
[11] In some literature DOA is used to denote depth of anesthesia, which is used analogously with DOH.

exist no reliable, clinically available, (real-time) DOA monitors. This is confirmed in the introduction of several works proposing novel candidates e.g. [Brouse et al., 2011] and [Liley et al., 2010].

State Estimation There exists no single device, which accurately measures or estimates the anesthetic state of the patient. However, the anesthetic state is reflected in patient signs (which are relatively hard to artificially measure) and biological signals (which are generally relatively easy to measure).

Patient signs reflecting the anesthetic state involve response to speech, eyelash reflex, miosis[12], grimacing (and other movement), breathing pattern, lachrimation[13] and perspiration; see [Barash et al., 2009] for a more extensive description. With the partial exception of breathing pattern, all mentioned signs indicate an excessively low DOH or DOA. Since both remifentanil and propofol depress spontaneous breathing and additionally act in a synergistic fashion on both the DOH and DOA, it is hard to draw correct conclusions about the anesthetic state from the patient breathing pattern alone.

A more informed estimate of the anesthetic state can be made if measurement of heart rate, blood pressure, blood oxygen saturation and blood or end-tidal[14] carbon dioxide concentrations are available. These are easily measurable scalar entities, monitored in every modern operating room. For instance, noxious stimulation increases blood pressure and heart rate when the DOA is inadequately low. In the aware state, the respiratory reflex is triggered by an increasing blood carbon dioxide concentration. Since remifentanil depresses the respiratory reflex, monitoring the blood or end-tidal carbon dioxide concentrations provide surrogate measures of the DOA. If the anesthetic state of the patient remains unaltered and no mechanical ventilation is provided, a high carbon dioxide concentration is likely to be proceeded by a decline in blood oxygen saturation, which can rapidly evolve into a critical state.

The DOH is reflected in the brain activity of the patient and it has been shown to correlate well with certain features of the cortical electroencephalogram (EEG), see e.g. [Liu et al., 1997] and [Bibian et al., 2010]. To date there exist several clinical DOH monitors based on this finding, including the Bispectral Index (BIS) monitor [Johansen and Sebel, 2000], the Spectral Entropy (SE) monitor [Viertö-Oja et al., 2004], the NeuroSense monitor [Bibian et al., 2010], the Cerebral State Index (CSI) monitor [Jensen et al., 2006], the Index of Consciousness (IoC) monitor [Revuelta et al., 2008], the Narcotrend monitor [Kreuer et al., 2001] and the A-line monitor [Litvan et al., 2002]. All these monitors compute a scalar DOH estimate based on the

[12] Miosis: the constriction of the pupil of the eye, resulting from a normal response to an increase in light.
[13] lachrimation: tear production.
[14] End-tidal: at the end of a normal exhalation.

EEG spectrum, which is obtained non-intrusively by means of electrodes on the forehead of the patient. The A-line monitor is different from the others in that it makes use of the auditory evoked potential (AEP)[15] resulting from the introduction of a certain sound signal by means of earphones, to determine the DOH of the patient.

The BIS monitor is the one of the mentioned devices which is by far the clinically most wide-spread. However, both clinical and simulation parts of the thesis make use of the NeuroSense monitor, for reasons explained in Section 2.1.

As mentioned, there exist no reliable, clinically available DOA monitors to date. There are, however, several ongoing studies with the aim of developing such devices. Some examples include the Surgical Stress Index (SSI) [Huiku et al., 2007] based on heart rate variability, blood pressure and plethysmographic[16] pulse wave amplitude, the PhysioDoloris monitor [Jeanne et al., 2009] based on heart rate variability, the MedStorm monitor [Choo et al., 2010] based on skin conductance variability, the Analgoscore monitor [Hemmerling et al., 2009] based on mean arterial pressure (MAP) and heart rate, a measure [Liley et al., 2010] based on EEG characteristics and another measure [Brouse et al., 2011] based on heart rate variability. For the context of the thesis it is assumed that direct DOA measurements are not available.

Regardless of the presence of monitoring devices, human experience plays a key role in assessing the anesthetic state of the patient. In current practice, drug doses are determined by the anesthesiologist as described in Section 1.2.

The Reference State Assuming the anesthetic state has been properly quantified and can be estimated in real-time, it remains to define a reference anesthetic state in order to provide adequate anesthesia. This reference is influenced by several factors, of which the type of surgical procedure is the dominant one. The magnitude and persistence of noxious stimulation plays a key role. Procedures involving moderate amounts of noxious stimulation can be conducted under a low DOH, referred to as sedation, with or without the co-administration of analgesic drugs.

Higher DOH and DOA are required in the presence of noxious stimulation. However, a high DOH or DOA depresses the respiratory system, resulting in apnea[17] [Barash et al., 2009]. During some surgical procedures this is anticipated and the patient is mechanically ventilated through an artificial

[15] Auditory evoked potential: a component of the EEG arising when the brain processes sound information.

[16] Plethysmogram: the output of a pulse oximeter; a device usually attached to a fingertip, optically measuring oxygen saturation of arterial blood.

[17] Apnea: the cessation of breathing.

airway such as a tracheal[18] tube or laryngeal mask airway[19]. Other surgical procedures, particularly ones requiring airway access, dictate spontaneously breathing patients. During these procedures it is crucial to limit the DOH and DOA in order to avoid apnea in the patient.

If the DOH is too low, awareness can occur during the surgical procedure. This can be particularly problematic if neuromuscularly blocking drugs are co-administered, in which case the patient can be totally aware but unable to communicate due to the immobility caused by the neuromuscular blockade. Depending on the analgesic state the patient might or might not perceive nociceptive[20] signals. The most serious cases of awareness are those which the patient is able to recall after the surgical procedure [Liu et al., 1991]. Furthermore, it is desirable to minimize drug use in order to facilitate postoperative recovery [Gan et al., 1997] and decrease long-term postoperative mortality [Monk et al., 2005]. It should also be noted that the hypnotic–opioid synergy, mentioned above and further explained in Section 1.3, provides several control signal (propofol and remifentanil infusion rate) combinations resulting in the same DOH, but with different associated DOA.

As indicated in this section there are several considerations to take into account when determining the reference anesthetic state. They will be revisited below and in Section 3.1 as they play an important role when synthesizing clinically adequate controllers for the anesthetic state.

Temporal Phases of Anesthesia

Section 1.2 reviews possible dosing regimens, which in the control framework correspond to manual, open-loop feed-forward and closed-loop techniques, respectively. Regardless of which paradigm is used, the administration of anesthesia during general surgery can be divided into three distinct temporal phases, described below.

Induction The induction phase of anesthesia (or simply induction) is a transient phase during which the patient is transitioned from consciousness to an adequate anesthetic state. Induction is routinely conducted by administering bolus[21] doses of propofol and remifentanil followed by essentially constant rate infusions of the two drugs. The typical duration of induction is a few minutes.

Noxious stimulation is moderate during induction, with the exception of intubation[22] toward the end of the induction phase during procedures

[18] Trachea: Cartilaginous tube descending from the larynx (the part of the respiratory tract containing the vocal chords), carrying air to the lungs. Also known as windpipe.
[19] Laryneal mask: An airway tube with a cuff which is inserted between the vocal chords.
[20] Nociception: the neural processes of encoding and processing noxious stimuli.
[21] Bolus: A single, relatively large dose of a drug.
[22] Intubation: the insertion of a tracheal tube.

requiring mechanical ventilation. The control challenge during induction of anesthesia is therefore that of fast reference tracking. This is foremost complicated by the presence of a large inter-patient variability in the sensitivity to propofol and remifentanil, combined with uncertain parameter values obtained for each individual, further described in Section 2.1.

An aggressive control strategy in combination with a patient–model mismatch often results in an overshoot of the measurement signal. In cases requiring spontaneously breathing patients, a DOH or DOA overshoot may result in an apneic period, which needs to be resolved before continuing with the procedure. A high DOH might also result in hypotension, which is of particular concern in fragile patients such as the elderly. On the other hand, an overly defensive control strategy will result in an induction of long duration, prolonging the surgical procedure, which ultimately influences the queuing time of the operating room. This is particularly a concern during short routine surgeries, where the duration of the entire procedure is on the same time scale as that of induction of anesthesia.

Propofol infusion is perceived as painful by several patients while the DOH and DOA are still low [Tan and Onsiong, 1998]. This is particularly true in young children [Cameron et al., 1992]. It was suggested in [Scott et al., 1988] that the perceived pain increases with decreased propofol infusion rate. Although the pain can be partially alleviated by adequate premedication, it is desirable to avoid an overly defensive drug dosing strategy at the beginning of induction.

Ultimately, a trade-off between expected induction duration and model error sensitivity has to be wisely made in the process of synthesizing a control strategy for the anesthetic state.

Maintenance Reaching the desired anesthetic state marks the transition from the induction to the maintenance phase. See Section 2.2 for a possible definition of the boundary between the two phases.

The main focus during maintenance of anesthesia is attenuation of the influence of noxious stimuli on the anesthetic state, further considered in Section 2.2. The control objective during maintenance is therefore that of output disturbance rejection subject to model uncertainty. As explained in Section 3.1, the reference DOH can be regarded as an interval rather than a scalar value, further motivating this focus. Similar to that during induction, a trade-off between performance and robustness needs to be made when synthesizing a control strategy.

Anesthetic reference state changes may be issued during the maintenance phase if the reference anesthetic state is deemed insufficient. It might be motivated to decrease the DOH or DOA reference toward the end of the procedure, to shorten the duration of the emergence phase. This also decreases the total use of drug.

Emergence The transition between maintenance and emergence is marked by the halting of anesthetic drug administration. This is sometimes done in the presence of moderate noxious stimulation, typically from skin closure. The influence of this stimulation on the DOH shortens the time it takes for the patient to return to consciousness, ultimately influencing the queuing time of the operating room.

The emergence phase is uninteresting from a control perspective as the control signals (drug infusion rates) are disabled. However, according to the models discussed in Chapter 2, drug dosing during maintenance (and induction) can affect the duration of the maintenance phase, which should be taken into consideration.

1.2 Drug Dosing Regimens

As mentioned in Section 1.1, this work considers procedures during which propofol is used as the hypnotic drug and remifentanil as the analgesic one. Both propofol and remifentanil are administered by means of intravenous boluses or infusions. This setting, in which all anesthetic drugs are administered intravenously is known as total intravenous anesthesia (TIVA) [Absalom and Struys, 2007]. From a control point of view, TIVA can be provided using either of the three dosing regimens described below. It should be noted that it is not necessary to use the same regiment for all co-administered drugs. Different administration regimens may also be used for induction and maintenance or even within the same temporal phase of anesthesia.

Manual Control

This is the current standard practice of providing anesthesia. The anesthesiologist assesses the anesthetic state of the patient and adjusts drug dosage accordingly. In the current context, this corresponds to setting the flow rates of one propofol and one remifentanil infusion pump. If the hypnotic or analgesic state of the patient is deemed insufficient, the anesthesiologist might provide bolus doses by means of the pump interface. The role of the anesthesiologist can here be viewed as that of a sophisticated state estimator and feedback controller.

In the presence of expected changes in surgical stimulation, or other circumstances leading to an expected change of the anesthetic state, the anesthesiologist can decide to change drug infusion rates or issue a bolus dose of either drug. Furthermore, drug doses are sometimes decreased to reduce emergence time, as mentioned in Section 1.1.

To summarize, the anesthesiologist has the combined role of state estimator, feedback controller and feed-forward (from foreseeable disturbances

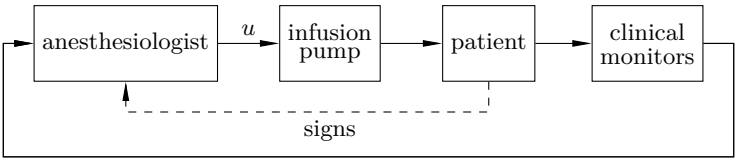

(a) Manual control.

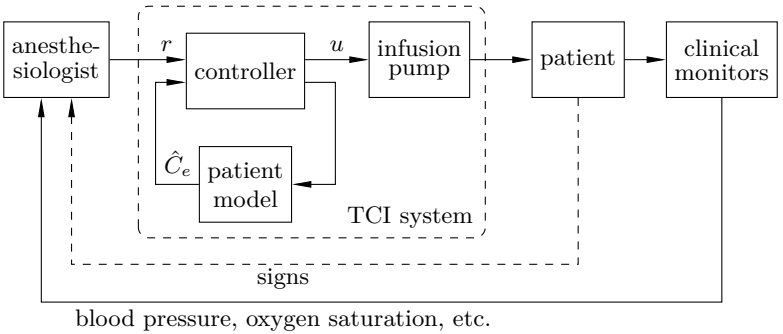

(b) Open-loop feed-forward control, also known as TCI.

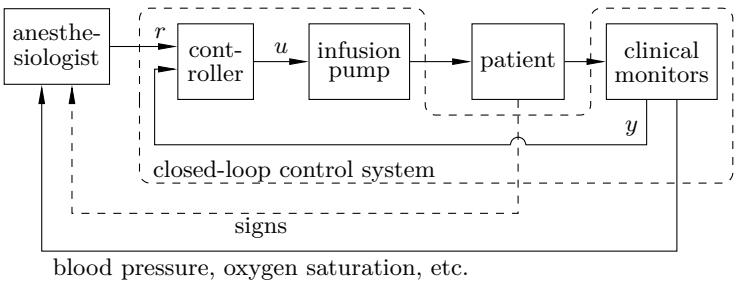

(c) Closed-loop control.

Figure 1.2 Schematic overview of drug dosing regimens used in clinical anesthesia.

and reference) controller. A schematic sketch illustrating the manual dosing regimen is shown in Figure 1.2(a).

Open-loop Feed-Forward Control

A step toward automated anesthesia was taken through the introduction of Target controlled infusion (TCI) systems [Absalom and Struys, 2007]. A TCI system is an open-loop feed-forward controller. Rather than setting an infusion rate, the anesthesiologist sets a target drug concentration. Depending on the TCI system, this is either a blood plasma or effect site (brain) drug concentration [Pouke et al., 2004]. The TCI system then relies on a patient model, see Section 1.3, to compute an adequate infusion profile, which is subsequently delivered to the patient intravenously by means of a computer controlled infusion pump.

From the above description it is clear that TCI systems are sensitive to model error and lack a mechanism to counteract disturbances. The role of the anesthesiologist is consequently similar to the one during manual drug dosing. A frequent assessment of the anesthetic state, see Section 1.1, is made and the target concentration is adjusted accordingly. In doing so, the anesthesiologist essentially introduces integral action to the control scheme. This is indeed needed in order to attenuate disturbances and handle model error. Feed-forward from anticipated disturbances and reference changes are handled in the same way as during manual drug dosing. A schematic sketch illustrating TCI drug dosing is shown in Figure 1.2(b), in which $\hat{C}_e$ denotes the estimated effect site drug concentration.

So far, several similarities between manual dosing and TCI have been described. There are, however, two distinct differences between the two drug dosing regimens. Firstly, the anesthesiologist thinks in terms of target concentrations rather than drug infusion rates when using a TCI system. This is merely a matter of scaling the input signal, but can be convenient as anesthetic drugs are available in several dose concentrations. Propofol is e.g. marketed both as 5 mg/ml and 10 mg/ml solutions. Secondly, and more importantly, manual and TCI drug dosing exhibit different behaviors when infusion rate and target concentration, respectively, are changed by the anesthesiologist. Upon a target concentration change, a TCI system computes an optimal infusion profile to transition between the currently estimated drug concentration and the new reference. There are slight differences between existing TCI systems in how optimality is defined in this context. A representative definition, used in [Shafer and Gregg, 1992] corresponds to reaching the target without overshoot in minimal time.

TCI systems are commercially available on several markets apart from the USA, where the dosing regimen has not yet obtained FDA[23] approval.

[23] FDA: The United States Food and Drug Administration.

The oldest and commercially dominating TCI system is the Diprifusor [Glen, 1998], which provides TCI of propofol. The Stanpump TCI algorithm [Shafer and Gregg, 1992] is available as open source software and has consequently been adopted by several research studies. TCI systems for remifentanil have also been suggested and clinically evaluated, see e.g. [Moerman et al., 2009]. However, the very fast redistribution and metabolism of remifentanil limits the benefit of these systems.

It should be kept in mind that all TCI systems rely wholly on open-loop patient models. Steady state and low frequency model errors can efficiently be handled by the anesthesiologist as described above. However, meeting the optimality condition upon target concentration (reference) changes can only be guaranteed when the patient model is accurate. Currently available patient models, described in Section 1.3, are based on biometric parameters such as age and body mass. Large inter-patient variability in drug sensitivity limits the accuracy of these models.

TCI and manual dosing of propofol have been compared in several studies, with varied conclusions. It was reported in [Servin, 1998] that the TCI test group on average were subject to lower doses of propofol early during the cases, while [Breslin et al., 2004] and [Russell et al., 1995] report the opposite. During later parts of the cases [Servin, 1998] and [Breslin et al., 2004] report comparable propofol use in both test groups, while substantially higher propofol doses for the TCI test group were reported in [Russell et al., 1995]. Since both the manual and TCI dosing regimens dictate manual interaction and due to other potential differences it is hard to draw a clear conclusion from these studies, in favor of either drug dosing regimen. However, both [Servin, 1998] and [Russell et al., 1995] report that a clear majority of the involved anesthesiologist prefer the TCI over manual dosing. (No mention of clinician preference is made in [Breslin et al., 2004].)

Closed-loop Control

In the closed-loop control regimen drug dosing is based on feedback from a measure of clinical effect, as explained in the overviews [Bibian et al., 2005] and [Absalom et al., 2011]. Two types of controllers are commonly reported in the literature and schematically depicted in Figure 1.3; one in which the controller sets the infusion rate of a computer controlled infusion pump directly, shown in Figure 1.3(a), and one where the controller sets the target of a TCI system around which it is cascaded, shown in Figure 1.3(b). The latter architecture is de facto a limiting special case of the first and there appears to be no clear advantage of being restricted to the augmented process dynamics which the presence of the inner TCI system results in.

The anesthesiologist still plays an important role when a closed-loop controlled drug dosing strategy is used. As closed-loop controllers are purely

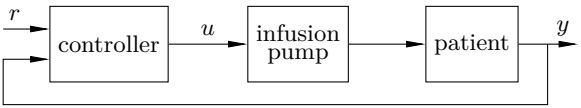

(a) Direct control of the infusion rate.

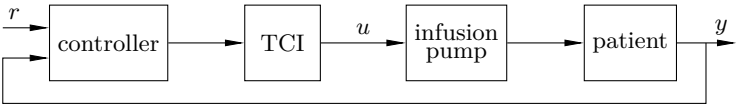

(b) Cascaded control of a TCI system.

Figure 1.3 Two commonly used closed-loop control architectures in anesthesia drug delivery.

reactive, the feed-forward paths from planned setpoint changes and anticipated disturbances described previously are not present. This can be readily solved by introducing a manually controlled feed-forward term in the control signal (infusion rate or target concentration, depending on system).

A schematic sketch illustrating the closed-loop controlled dosing regimen is shown in Figure 1.2(c). In this regimen, the controlling role of the anesthesiologist, frequently adjusting the infusion profile or target concentration, is handled by a feedback controller. However, the expertise of the anesthesiologist is still needed e.g. to predict and counteract disturbances.

There exists a large inter-patient variability in the sensitivity to anesthetic drugs. There is also a significant intra-patient variability. For instance, loss of blood may alter the sensitivity to anesthetic drugs. A robust closed-loop controller can handle all these issues to some extent, but there will always be outlier cases, requiring manual attention. There is also the possibility that manual attention is needed to resolve complications originating either from the surgery or the anesthesia itself, or from equipment failure.

To conclude, providing adequate anesthesia is a complex topic and it would be naive to propose the replacement of a highly competent anesthesiologist with a simple closed-loop controller. However, the controller can be used to shift the focus of the anesthesiologist toward critical events.

The prospect of closed-loop controlled anesthesia, based on EEG measurements, was introduced in the 1950s. This work was pioneered by a group led by Bickford. Clinical trials making use of volatile anesthetics were conducted on rabbits, cats, monkeys and humans, see e.g. [Soltero et al., 1951]. Several clinical closed-loop studies involving human patients, volatile anesthetics and EEG measurements have been conducted since. From an engineering viewpoint the group led by Morari [Gentilini et al., 2001] has arguably been the

most influential. Although outside the scope of this work, it should be mentioned that closed-loop controlled administration of neuromuscular blockades have recently received significant attention; see e.g. [Mendonça et al., 2004].

In the TIVA setting, the use of EEG monitoring (BIS) as the measurement for closed-loop control was assessed in [Morley et al., 2000] with the conclusion that the BIS variable was a suitable signal for closed-loop control of DOH. Performance of closed-loop controlled propofol infusion systems guided by EEG have been reported clinically acceptable in e.g. [Absalom and Kenny, 2003]. Such a system was compared to manual dosing in [Liu et al., 2006]. The conclusion was that "automatic control of consciousness using the BIS is clinically feasible and outperforms manual control". Examples of other comparison studies are [Struys et al., 2001] in which the closed-loop controlled dosing was deemed clinically acceptable and resulted in an induction of longer duration, but less overshoot in the measured variable (BIS) and [Puri et al., 2007] which reports adequate closed-loop anesthesia with lower drug use as opposed to manual practice. A relatively recent addition to this list of reports is [Hemmerling et al., 2010], concluding that "the closed-loop system for propofol administration showed better clinical and control system performance than manual administration of propofol". Lately, closed-loop co-administration of propofol and remifentanil has drawn significant research attention. The clinical feasibility of a SIMO control approach was evaluated in [Liu et al., 2012], which concluded that "automated control of hypnosis and analgesia guided by M-Entropy is clinically feasible and more precise than skilled manual control". Due to the lack of reliable DOA sensors, most studies to date are, however, focused on the control of DOH.

A selection of studies featuring clinically evaluated closed-loop controllers for DOH using propofol, DOA using remifentanil or both, combined with EEG monitoring, is presented in Appendix C.1. The reader is referred to [Manberg et al., 2008] and [Bibian, 2006] for a historical survey of closed-loop control studies not limited to the use of propofol and remifentanil for controlling DOH and DOA, respectively. An up to date review of closed-loop anesthesia, with a TIVA emphasis, is found in [Dumont, 2012].

Apart from reported clinical studies, there exist a multitude of publications evaluating the feasibility of various controller architectures in the EEG-guided closed-loop controlled TIVA setting, utilizing propofol or remifentanil. A selection of such simulation work is presented in Appendix C.2. Proposed control strategies range from PI to NMPC to fuzzy.

Despite numerous clinical studies and a multitude of publications showcasing simulations, closed-loop controlled anesthesia is yet awaiting broad clinical acceptance. One legitimate reason for this is the concern of patient safety. The safe functionality of any candidate system needs to be demonstrated, preferably both in theory and practice, before it is made widely available. This dictates a validation of models used in the synthesis of the

control system and a quantifiable measure of robustness of the resulting system together with a clinical study verifying the design. Furthermore, the user interface of the device implementing the closed-loop controller is of great importance since automation aims to decrease the workload of the anesthesiologist, not the other way around. Developing a system with the mentioned properties is a challenge dictating the collaboration between several professional groups including anesthesiologists, control system engineers and human-machine interface designers. Another aspect, not to be overlooked, is the involvement of regulatory agencies [Manberg et al., 2008], which in most countries is a prerequisite to clinical evaluation of medical systems. Finally, once a prototype has been developed and successfully demonstrated, there is the need of a substantial capital investment to turn it into a product and reach broad clinical acceptance.

1.3 The Traditional Patient Model

As described in Section 1.2, both the TCI and closed-loop controlled drug dosing regimens rely on patient models; TCI directly relies on a model while the closed-loop approach relies on a model either indirectly to tune the controller or directly if MPC, IMC or similar control techniques are pursued. This section is dedicated to introduce the by far most common model structure used to describe the redistribution, elimination and effect of anesthetic drugs. This model structure can be decomposed into a series connection of a pharmacokinetic (PK) model relating drug infusion, distribution and elimination and a pharmacodynamic (PD) model, relating effect site concentration[24] to clinical effect. The combined model is referred to as a PKPD model. A comprehensive introduction to PKPD modeling is provided in the review [Derendorf and Meibohm, 1999].

Pharmacokinetic (PK) Models

The pharmacokinetic (PK) model describes what the body does to the drug; how it is redistributed and eliminated.

Model Structure The traditional model structure used to describe the PK is the mammillary compartment model. For propofol and remifentanil it is customary to use models with three, or sometimes two, compartments. The basic idea behind the compartment model is to cluster tissues with similar properties into compartments and model the drug flow between them, alongside elimination and addition of drug. A schematic block diagram of

[24] In some literature the PD model is defined as relating blood plasma, rather than effect site, concentration to clinical effect.

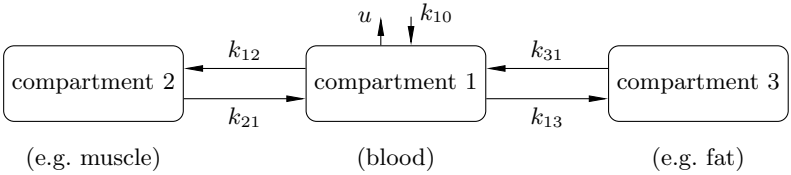

Figure 1.4 A mammillary compartment model with three compartments.

such a model with three compartments is shown in Figure 1.4. The notation used in Figure 1.4 is explained throughout the remainder of this section.

Drug mass in compartment i is denoted $m_i \geq 0$ and the per time proportion of drug migrating from compartment i to compartment j is described by the rate constant $k_{ij} \geq 0$:

$$\dot{m}_i = \sum_{j=1}^{n} k_{ji} m_j - \sum_{j=0}^{n} k_{ij} m_i + u_i, \tag{1.1}$$

where n is the number of compartments in the model. The compartment corresponding to $i = 0$ is the environment and k_{j0} models elimination of drug from compartment j. The per time mass of drug introduced into compartment i from the environment is described by $u_i \geq 0$. From (1.1) it is evident that the compartmental model is a delay-free linear time-invariant (LTI) system.

In the context of anesthesia the central compartment is supposed to model the blood plasma, which is where drug is added in TIVA. Consequently, $u_i = 0 \ \forall i \neq 1$ and it is natural to introduce $u = u_1$. The peripheral compartments only exchange drug with each other indirectly through the central compartment. Furthermore, drug is assumed only to be eliminated from the central compartment, mainly by metabolism and excretion, rendering $k_{i0} = 0 \ \forall i \neq 1$. For the $n = 3$ compartment case, the application of these constraints results in the state space representation

$$\dot{m} = \begin{bmatrix} -(k_{10} + k_{12} + k_{13}) & k_{21} & k_{31} \\ k_{12} & -k_{21} & 0 \\ k_{13} & 0 & -k_{31} \end{bmatrix} m + \begin{bmatrix} 1 \\ 0 \\ 0 \end{bmatrix} u. \tag{1.2}$$

The dynamics of some anesthetic drugs, e.g. remifentanil, are commonly described using only two compartments. The two compartment model is a special case of (1.2) and its state space representation is therefore not explicitly given here.

In order for (1.2) to be a realistic model, it is necessary that there is no net flow between compartments i and j, whenever they hold the same drug

concentration, i.e., $x_i = x_j$, where

$$x_i = \frac{m_i}{v_i}. \tag{1.3}$$

Here x_i is the drug concentration in compartment i, which has volume v_i. Note that the compartment volumes, also referred to as volumes of distribution, are a theoretical construct and should not be thought of in terms of a physiological volume. The mentioned net flow constraint can now be stated, assuming equal concentrations $x_i = x_j$:

$$k_{ji}m_j = k_{ij}m_i \Leftrightarrow k_{ji}v_jx_i = k_{ij}v_ix_j \Leftrightarrow k_{ji}v_j = k_{ij}v_i. \tag{1.4}$$

Combining (1.1) and (1.4) yields

$$\begin{aligned} \frac{1}{v_i}\dot{m}_i &= \sum_{j=1}^{n} \frac{v_j}{v_i}k_{ji}\frac{m_j}{v_j} - \sum_{j=0}^{n} k_{ij}\frac{m_i}{v_i} + \frac{1}{v_i}u_i \\ \Leftrightarrow \dot{x}_i &= \sum_{j=1}^{n} \frac{v_j}{v_i}k_{ji}x_j - \sum_{j=0}^{n} k_{ij}x_i + \frac{1}{v_i}u_i \\ \Leftrightarrow \dot{x}_i &= \sum_{j=1}^{n} k_{ij}(x_j - x_i) - k_{i0}x_i + \frac{1}{v_i}u_i. \end{aligned} \tag{1.5}$$

Note that the compartment volumes only enter (1.5) as an input scaling. Consequently, the model (1.5) is fully parameterized by k_{10}, k_{12}, k_{13}, k_{21}, k_{31} k_{10} and v_1 (7 parameters) in the three compartment case and by k_{10}, k_{12}, k_{21} and v_1 (4 parameters) in the two compartment case. The state space representation corresponding to (1.2) becomes:

$$\dot{x} = \begin{bmatrix} -(k_{10}+k_{12}+k_{13}) & k_{12} & k_{13} \\ k_{21} & -k_{21} & 0 \\ k_{31} & 0 & -k_{31} \end{bmatrix} x + \begin{bmatrix} \frac{1}{v_1} \\ 0 \\ 0 \end{bmatrix} u. \tag{1.6}$$

It could be noted here that (1.2) and (1.6) are both positive systems, since their system matrices are Metzler. However, due to (1.4), only (1.6) is guaranteed to describe a compartmental system [Luenberger, 1979].

Assuming the plasma concentration $C_p = x_1$ is the output of (1.6), the system has the following transfer function representation:

$$G_{C_p,u}(s) = \frac{1}{v_1}\frac{(s+k_{21})(s+k_{31})}{(s+p_1)(s+p_2)(s+p_3)}. \tag{1.7}$$

The poles $-p_i$ solve the characteristic equation

$$\begin{cases} p_1 + p_2 + p_3 = k_{12} + k_{13} + k_{21} + k_{31} \\ p_1p_2 + p_1p_3 + p_2p_3 = k_{10}(k_{21} + k_{31}) + k_{31}(k_{12} + k_{21}) + k_{13}k_{21} \\ p_1p_2p_3 = k_{10}k_{21}k_{31}. \end{cases} \tag{1.8}$$

In some literature, the PK model is parameterized in terms of the clearances c_i, describing the drug volume per time, migrating from a specific compartment. The clearances for the system (1.6) are:

$$\begin{cases} c_1 = v_1k_{10} \\ c_2 = v_2k_{21} = v_1k_{12} \\ c_3 = v_3k_{31} = v_1k_{13}, \end{cases} \tag{1.9}$$

where the rightmost equalities follow from (1.4).

Effect Dynamics It is possible to measure C_p in (1.7) by means of drawing blood samples, which are subsequently analyzed. The achievable bandwidth is not high enough for control purposes, but useful for identification of the PK model parameters. When comparing the measured blood plasma concentration from such blood samples to DOH measurements from an EEG monitor, it has been observed that the monitor response lags the blood plasma concentration. A contributing reason to this is that the dynamics between the blood plasma and the effect site, which for propofol is the cerebellar cortex[25], are not modeled. It was suggested in [Sheiner et al., 1979] that the PK model (1.7) should be augmented by the series connected lag link

$$G_{C_p,C_e}(s) = \frac{k_{e0}}{s + k_{e0}}, \tag{1.10}$$

where C_e is referred to as the effect site concentration of the drug. Introducing the notation $x_e = C_e$ for the effect site concentration, the state space representation of (1.10) becomes

$$\dot{x}_e = -k_{e0}x_e + k_{e0}x_1, \tag{1.11}$$

where x_1 is the primary compartment drug concentration. From the notation of (1.11) it appears as if x_e is the drug concentration in a compartment, which is fed by the central compartment, and from which drug is eliminated to the environment by rate constant k_{e0}. Assuming this "effect compartment" holds drug mass m_e and has a volume v_e, its dynamics are described by

$$\begin{aligned} \dot{m}_e &= -k_{e0}m_e + k_{1e}m_1 \\ \Leftrightarrow \frac{1}{v_e}\dot{m}_e &= -k_{e0}\frac{m_e}{v_e} + \frac{v_1}{v_e}k_{1e}\frac{m_1}{v_1} \\ \Leftrightarrow \dot{x}_e &= -k_{e0}x_e + k_{e1}x_1, \end{aligned} \tag{1.12}$$

[25] Cerebellar cortex: The convoluted layer of superficial grey substance in the brain.

where the last equivalence follows from (1.4). Equating (1.11) with (1.12) yields $k_{e0} = k_{e1}$. However, to fit into the compartment framework, a term $-k_{1e}x_1$, describing the drug flow from the central compartment to the effect compartment, would have to be added to the dynamics of $\dot{x}_1$ in (1.6). Since $k_{1e} = v_e/v_1 \cdot k_{e1}$, it follows that $k_{1e} \approx 0$ when $v_e \ll v_1$. Consequently, the effect site model (1.10) fits into the compartment framework under the realistic assumption that the effect compartment has negligible volume compared to the central compartment. Under this assumption it also becomes irrelevant whether the term $-k_{e0}x_e$ in (1.11) corresponds to elimination of drug to the environment or reflux to the central compartment. The latter would add the influx term $k_{1e}x_e$ to the dynamics of $\dot{x}_1$ in (1.6), which is negligible if $k_{e1} \approx 0$.

In the literature, the effect dynamics are typically considered part of the pharmacodynamics, described in the next section, rather than the PK. This distinction is only semantic. However, in order to avoid confusion, it is pointed out that the effect dynamics (1.10) are considered part of the PK in the thesis. This choice is supported by the compartment model interpretation given above. When referring to a two- or three compartment model, the effect compartment is not counted toward this number. This omission is made to be consistent with the literature.

It was suggested in [Bibian, 2006] that (1.10) possibly under-models the true effect site dynamics, motivating the introduction of the model structure

$$G_{C_e,C_p}(s) = \frac{k_{e0}}{s + k_{e0}} e^{-sL}. \tag{1.13}$$

Furthermore, it was argued that the effect dynamics could possibly be of higher order than (1.13), but that the C_p profiles available for identification were not persistently exciting of an order permitting identification of additional parameters. To justify the structure of (1.13), analysis of residuals obtained when using (1.10) and (1.13), respectively, to identify effect dynamics from clinical data were conducted. Residuals obtained with (1.13) were significantly smaller and their distribution whiter.

Connecting (1.7) and the effect dynamics (1.13) yields the combined PK model structure

$$G_{C_e,u}(s) = \frac{k_{e0}}{v_1} \frac{(s + k_{21})(s + k_{31})}{(s + p_1)(s + p_2)(s + p_3)(s + k_{e0})} e^{-sL}. \tag{1.14}$$

This structure, possibly without the delay L, will be referred to as the traditional PK model. Some previously published alternatives to this structure as well as their motivations are mentioned in Section 2.2. For now, let it suffice to note that (1.14) has a total of nine parameters in the three compartment case and seven parameters in the two compartment case.

Pharmacodynamic (PD) Models

The pharmacodynamic (PD) model describes what the drug does to the body; how the clinical effect is related to the drug concentration at the effect site. The common definition is that the PD describes the relation between blood plasma drug concentration C_p and clinical effect. As mentioned previously, the effect dynamics are considered part of the PK in the thesis. Consequently, the role of the PD becomes to describe the relation between the effect site concentration C_e in (1.14) and the clinical effect E. For convenience the effect is scaled so that $E = 0$ in the absence of drug and $E = 1$ is the maximal achievable effect. The plasma concentration corresponding to $E = 1/2$ is described by the parameter $C_{e,50}$. It is convenient to normalize the C_e with respect to $C_{e,50}$, by introducing

$$v = \frac{C_e}{C_{e,50}}. \tag{1.15}$$

Clearly $v = 0$ in the absence of drug and $v = 1$ when the effect site concentration is $C_e = C_{e,50}$.

The PD is typically modeled as a monotone continuous function

$$E = E(v), \tag{1.16}$$

with the properties $E(0) = 0$, $E(1) = 1/2$ and $E(v) \to 1$ as $v \to \infty$. The default choice for the structure of $E(v)$ in the literature is the Hill function (also known as the sigmoidal Emax function):

$$E = 1 - \frac{1}{1 + v^\gamma}, \ \gamma \geq 1. \tag{1.17}$$

The parameter γ is referred to as the Hill parameter or Hill degree. The Hill function, for three values of γ, is shown in Figure 1.5.

When using a clinical monitor to obtain a measure y of E, it typically holds that $E_0 = y(0)$ has a value $0 \leq E_0 \ll 1/2$ and that $y \to E_\infty$, where $1/2 \ll E_\infty \leq 1$, as $v \to \infty$. I.e., for a particular patient, the range of measurements is confined to (E_0, E_∞) which fits inside $(0, 1)$. In most literature the bounds E_0 and E_∞ are attributed to the PD. However, it is more appropriate to view them as a characteristic of the monitor. This is merely a semantic difference but explains the absence of E_0 and E_∞ as parameters in (1.17).

From clinical data it is hard to argue that there is no model structure better suited for the task than (1.17). However, the Hill function is simple and features characteristics which are observed in clinical practice; it has a linear region around $v = 1$ and a saturating effect as v increases beyond the linear region. Furthermore, (1.17) complies with receptor theory[26] [Derendorf and

[26] Receptor theory: the application of receptor models to explain drug behavior.

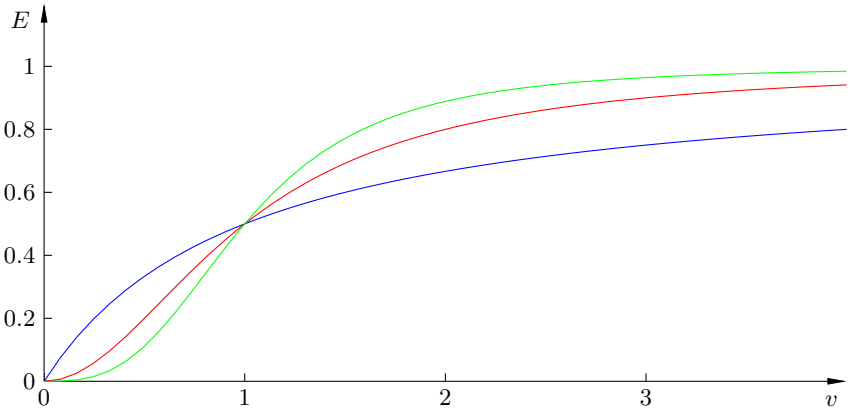

Figure 1.5 The Hill curve, parameterized in γ, defines the clinical effect E in terms of normalized effect site concentration v. Here curves for $\gamma = 1$ (blue), $\gamma = 2$ (red) and $\gamma = 3$ (green) are shown.

Meibohm, 1999]. The Hill function will be further discussed and analyzed in Section 2.2.

Drug Interaction Models

Both the hypnotic drug propofol and analgesic drug remifentanil are commonly modeled within the above described framework. When the two drugs are co-administered, they act synergistically on both hypnosis and analgesia. It was concluded in [Bouillon et al., 2002] that the PK of propofol is not affected by remifentanil co-administration and that the effect of propofol on the remifentanil PK is only relevant when propofol is administered as boluses. Consequently, the synergy is attributed to the PD and modeled as a generalization of the Hill function to a surface. I.e., the hypnotic effect E_h is a function of the normalized propofol and remifentanil effect site concentrations:

$$E_h = E_h(v_p, v_r), \tag{1.18}$$

where v_r is defined in the same way as $v = v_p$ was in (1.15). While (1.18) describes the PD interaction towards hypnosis, there exists a similar function E_a of the same arguments, describing the PD interaction towards analgesia. The thesis will only consider the interaction towards hypnosis, and consequently the subscript will be omitted:

$$E = E(v_p, v_r). \tag{1.19}$$

Different parameterizations have been suggested for the interaction surface $E(\cdot)$. The most common one found in the literature is the one presented in

[Minto et al., 2000]:

$$E(v_p, v_r) = 1 - \frac{1}{1 - \left(\frac{v_p + v_r}{v_{50}(\theta)}\right)^{\gamma(\theta)}}, \tag{1.20}$$

where θ is the relative concentration of v_r:

$$\theta = \frac{v_r}{v_p + v_r}. \tag{1.21}$$

An interpretation of this parameterization is that $v_p + v_r$ is the concentration of a virtual drug with $C_{e,50}$-value $v_{50}(\theta)$. This virtual drug has a Hill-like PD, where the Hill coefficient γ depends on the relative concentration of propofol and remifentanil. It was suggested in [Minto et al., 2000] that a forth order polynomial be used to model $v_{50}(\cdot)$ and a second order one for $\gamma(\cdot)$. The interaction surface is defined through the coefficients of these polynomials, which are to be identified from clinical data.

An interaction plane, being a local linearization of the interaction surface (1.20), was proposed in [Ionescu et al., 2011a] and used in the synthesis of an MPC controller.

Another parameterization for the interaction surface was proposed in [Kern et al., 2004]. It is an extension of (1.17), where v denotes the virtual drug

$$v = v_p + v_r + \alpha v_p v_r. \tag{1.22}$$

This structure has only one parameter α, where $\alpha > 0$ corresponds to a synergistic interaction. Another appealing feature, apart from the low number of parameters, is that the interaction model exactly corresponds to the propofol PD in the absence of remifentanil ($v_r = 0 \Rightarrow v = v_p + v_r + \alpha v_p v_r = v_p$). Values of α towards different effects, identified in a rigorous study, have been published in [Kern et al., 2004].

Parameter Values

Assuming that the PK model structure (1.14) adequately describes the dynamic relation between drug infusion u and effect site concentration C_e, it remains to identify a total of nine or seven parameters, depending on the number of model compartments. Since remifentanil is rapidly metabolized and redistributed as compared to propofol, several published PK models for remifentanil make use of only two compartments, while three compartments seem to be the choice of preference for propofol PK models.

Timed measurements of the central compartment concentration x_1 can be obtained by drawing blood samples, which in practice results in sparsely, and often non-uniformly, sampled identification data. The peripheral compartments do not correspond to any particular tissues. Rather, the second

compartment is usually designated to model vascular[27] tissues, which equilibrate rapidly, while the third compartment models non-vascular tissues, which equilibrate slowly. A result of this approximative nature of these compartments is that their respective concentrations x_2 and x_3 cannot be directly measured. Consequently, parameter identification relies solely on blood sample data.

Even if an effort is made to device experimental conditions with an input (infusion profile) u which persistently excites the dynamics (1.6) and the output x_1 is sampled frequently enough to resolve the dynamic response, the obtained model is only valid for the patient under current investigation. The most common strategy to address inter-patient variability in identified model parameters is to introduce a parameterization

$$(k_{10}, k_{12}, k_{13}, k_{21}, k_{31}, v_1) = f(\text{biometric parameters}), \tag{1.23}$$

and minimize a monotonous function of the prediction error over the population, when (1.6) is parameterized using (1.23). Here, the biometric parameters can for instance be patient age, height, (lean body) mass and gender. There exists customized computer software, such as NONOMEM [Sheiner and Beal, 1980] to perform the typically extensive computations, which are needed to establish the possibly nonlinear function $f(\cdot)$ in (1.23). With the large degree of freedom given by the many parameters and possible choices of $f(\cdot)$ in (1.23), care must be taken not to over-fit the data.

A possible indicator of the combined large inter-patient variability and over-parametrization in the propofol case is the existence of numerous published candidates for $f(\cdot)$ in (1.23). Each such candidate is here referred to as a PK model. For children, nine named PK models are enlisted in [Coppens et al., 2011] and it is demonstrated, using clinical data, that they generally perform poorly as predictors. Corresponding models for adults include the ones proposed in [Schüttler and Ihmsen, 2000], and [Schnider et al., 1998].

The number of available PK models for remifentanil is smaller. One natural reason for this is that controlling analgesia using remifentanil TCI has received considerably less attention than the corresponding control of hypnosis using propofol. Another contributing reason would be the very fast time scales of remifentanil PK dynamics, which makes it hard to identify dynamics beyond steady state using sparsely collected blood samples. Arguably the most common remifentanil PK models are one with three compartments for adults proposed in [Minto et al., 1997] and one with two compartments for children proposed in [Rigby-Jones et al., 2007]. It was concluded in [Soltész et al., 2012a] that these two models are similar in terms of primary compartment volumes and clearance rates.

[27] Vascular: indicative of a copious blood supply.

A survey of five studies presenting values for the half-effect concentration $C_{e,50}$ for propofol were presented in [Bibian, 2006] and it was concluded that values vary significantly between studies. Similarly it was concluded that variation in values of γ identified for each of the patients in one of the studies vary significantly.

It was reported in [Dumont et al., 2009] that identification based on data from 44 adult patients resulted in propofol γ-values in the range $1.1 \leq \gamma \leq 4.7$, with only one occurrence of $\gamma > 3$. In [Coppens et al., 2011] γ was identified using nine previously published propofol PK models, using clinical data from 28 children. The result was $1.02 \leq \gamma \leq 2.07$. It was also concluded that using these PK models may not have provided accurate estimates. Additional published reports generally confirm $1 \leq \gamma < 3$ for propofol. This supports the choice of γ-values in Figure 1.5.

Values of γ for remifentanil (towards analgesia) are not explicitly considered in the thesis.

Although not providing a complete reference to published traditional PK and PD models for propofol and remifentanil, the current section has served to give an overview and indicate that the use of these models is not completely uncontroversial. A further discussion of possible reasons for the variation in published parameter values as well as the validity and adequacy of the traditional model structure is given in Section 2.2.

2

Models for Control

2.1 Equipment Models

Section 1.3 of the previous chapter presented the traditional PKPD models, used to describe the uptake, redistribution, elimination and clinical effect of anesthetic drugs. These models describe the patient or, in automatic control terms, the process. Any closed-loop control system has two additional components, which need to be considered in modeling: the actuators and the sensors. In this context, the sensor is the clinical DOH monitor and the actuator is the intravenous infusion pump. While the patient model is the main topic of this chapter, the first section is dedicated to modeling of the actuator and sensor.

The Clinical Monitor

The BIS Monitor As mentioned in Section 1.1, there exist several commercially available DOH monitors. The by far most wide-spread one is the Bispectral Index (BIS) monitor (Aspect Medical Systems, Inc., Newton, USA) [Johansen and Sebel, 2000]. The output of the BIS monitor, often referred to as the BIS variable, the BIS value or simply the BIS, is a scalar between 0 and 100. A BIS value of 0 corresponds to an iso-electric EEG, indicating the highest possible DOH, also referred to as the fully anesthetized state. In the absence of clinical effect, the monitor outputs a value close to 100, corresponding to the fully aware state. The mean BIS value in the absence of clinical effect varies slightly between patients, but typically lies in the 90–100 range.

The BIS monitor employs a proprietary algorithm, resulting in time-varying dynamic behavior. In particular, it features a piecewise constant, but switching, output delay. The varying delay introduces an uncertainty in the dynamics to be controlled and consequently dictates a more robust and hence conservative controller tuning. A possible approach to forego this

Figure 2.1 Photograph showing the NeuroSense NS-701 monitor and its self-adhesive sensor. Image courtesy of NeroWave Systems Inc.

problem was suggested in [Ionescu et al., 2011b], where a real-time delay estimator is used in a Smith predictor[1] scheme.

The NeuroSense Monitor The NeuroSense NS-701 monitor (NeuroWave Systems Inc., Cleveland Heights, USA) [Bibian et al., 2010], shown in Figure 2.1, was developed with closed-loop controlled anesthesia in mind. It provides one surrogate DOH measure per cerebral hemisphere[2] based on a wavelet transform of the raw EEG, collected using a non-intrusive self-adhesive sensor mounted on the forehead of the patient. The output of the NeuroSense monitor is termed the wavelet-based anesthesia value for central nervous system, abbreviated WAV_{CNS} and further explained in [Bibian, 2006]. In terms of scale the WAV_{CNS} is compatible with the BIS monitor output, and the two monitors have equal steady state behavior [Zikov et al., 2006]. For the sake of simplified notation, the WAV_{CNS} measurements can be affinely scaled to conform with (1.17). I.e., the measured effect $y = E_0 \approx 0$, where $E_0 \geq 0$, corresponds to the fully aware state and $y = E_\infty = 1$ corresponds to the fully anesthetized state. It could be noted that E_0 and E_∞ are properties of the patient rather than the monitor. However, in the total absence of drug, the clinical effect was defined to be $E = 0$ in (1.17) and hence it becomes natural to introduce E_0 as a patient specific property of the monitor.

It is assumed throughout the thesis, unless otherwise explicitly stated, that the WAV_{CNS} signals – both raw and filtered versions – have been affinely scaled to the interval $(0, 1)$ such that zero corresponds to the 0 or E_0 level[3], and one corresponds to the maximal clinical effect $E_\infty = 1$.

[1] The Smith predictor is a delay compensating controller structure proposed in [Smith, 1959].

[2] Cerebral hemisphere: Either of the two symmetrical halves of the brain.

[3] It should be clear from the context which of the two values are used at different occasions throughout the thesis.

The NeuroSense monitor provides its two synchronized raw WAV_{CNS} signals uniformly sampled at 1 Hz. Modeling this behavior by a 1 s delay provides a model with a negative phase shift exceeding that of the actual monitor. This is a sound model with closed-loop control in mind as it enforces additional robustness of the controller. As the raw WAV_{CNS} signals contain high frequency noise at significant power, the NeuroSense monitor employs an output low-pass filter, which is the zero-order hold sampled equivalent of $1/(\frac{4}{15}T_r s+1)^2$. The parameter T_r is, with a slight abuse of notation, referred to as the trending rate and chosen from $\{5, 10, 15, 30, 60\}$ s, either by the user or automatically. The conversion factor between the trending rate and second-order filter time constant ($T = \frac{4}{15}T_r$) stems from the approximation of a rectangular window FIR filter with width T_r by a second-order low-pass filter with time constant T. In fact, the filter implementation in the monitor introduces an additional unit delay. The dynamic relation between the effect E in (1.17) and the NeuroSense monitor output y are hence described by the zero-order hold sampled equivalent of the linear time-invariant (LTI) relation

$$y(s) = E_0 + (1 - E_0)\frac{1}{(sT + 1)^2}e^{-2s}E(s). \tag{2.1}$$

(Note that there is no distinction, apart from context, between time- and Laplace domain signals in the thesis.)

The NeuroSense monitor implements algorithms for artifact removal and reconstruction of missing episodes of the measurement signal. These algorithms depend on the trending rate and the developer of the monitor claims that a trending rate of $T_r = 60$ s in (2.1) enables reconstruction of missing data episodes up to 20 s, which rarely occur. Conversely, if the trending rate is $T_r = 5$ s, it is enough with a 2 s artifact presence to create a gap in the monitor output y. It was further recommended by the developer that the $T_r = 30$ s option should be chosen for the closed-loop control application described in Appendix B.2, as it provides adequate low-pass filtering without excessive negative phase shift, while enabling reconstruction of most expected corrupted measurement signal episodes. Consequently, the clinical closed-loop controlled study reported in [van Heusden et al., 2013b], [van Heusden et al., 2013a] and [West et al., 2013] and simulations leading up to it, employed the monitor model of (2.1) with $T_r = 30$ s.

It could be argued that the use of the raw WAV_{CNS} signal

$$y_{\text{raw}}(s) = E_0 + (1 - E_0)e^{-s}E(s). \tag{2.2}$$

would provide larger flexibility in the controller design. Tailoring the measurement signal filter would allow for a conscious trade-off between noise suppression and negative phase shift. Furthermore, the Wiener structure[4] of

[4] Wiener system: An LTI system connected in series with a static output nonlinearity.

the traditional patient model described in Section 1.3 would not be broken by adding the LTI dynamics (2.2) in series after the output nonlinearity, since the delay of (2.2) and the static nonlinearity do commute. However, in order to omit filtering in the monitor, a replacement method for handling corrupted measurement signal episodes needs to be implemented. Such a method is proposed, and demonstrated in simulation, in Section 3.3.

As mentioned above, the NeuroSense monitor provides one WAV_{CNS} signal per hemisphere. Let y_l and y_r denote the left and right hemisphere WAV_{CNS} signals, respectively. These signals are accompanied by signal quality indices (SQI), where the reliability ranges from 0 (unreliable) to 100 (reliable). In the thesis a linear scaling of the SQI is adopted, mapping the SQI $(0, 100) \rightarrow (0, 1)$. Let SQI_l and SQI_r denote the left and right SQI signals, respectively. The NeuroSense monitor also outputs a per hemisphere signal describing the suppression ratio (SR), defined as the percentage of time during the past 5 minutes that the corresponding EEG signal has had an amplitude of less than 5 μV. Let SR_l and SR_r describe the left and right suppression ratios, respectively. The iControl system described in Appendix B lets y be either y_l or y_r, based on the switching heuristic of Algorithm 2.1.

```
if  (SQI_curr < .6) && (SQI_alt > .6) {
  switch to alt
} else {
  if ( SQI_curr > .6 ) && (SQI_alt > .6) {
    choose side based on biggest SR value
  }
}
```

Algorithm 2.1 The iControl hemisphere selection heuristic.

In Algorithm 2.1, `SQI_curr` and `SQI_alt` denote the currently selected hemisphere and the alternative hemisphere, respectively. As the switching might lead to discontinuities, the following scheme for constructing y is proposed:

$$\begin{aligned} y &= \frac{w_l y_l + w_r y_r}{w_l + w_r}, \\ w_l &= \text{SQI}_l(1 - \text{SR}_l), \\ w_r &= \text{SQI}_r(1 - \text{SR}_r). \end{aligned} \tag{2.3}$$

The scheme in (2.3) is continuous in y_l and y_r as well as in the weights w_l and w_r. It should, however, be noted that the particular weighting proposed by (2.3) is also a heuristic with no direct clinical motivation.

The monitor setup used in the clinical study outlined in Appendix B is the combination of (2.1) and the hemisphere selection heuristics of Algorithm 2.1,

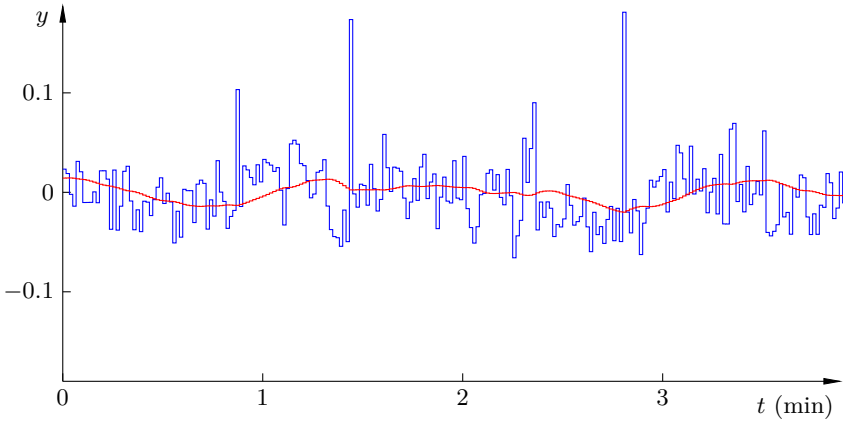

Figure 2.2 Representative raw (blue) and $T_r = 30$ s trended (red) WAV_{CNS} measurement noise, recorded prior to propofol infusion.

while all simulations and identification examples reported in the thesis are based on a combination of (2.2) and (2.3).

The raw WAV_{CNS} signal has a high measurement noise content. Figure 2.2 shows a representative raw WAV_{CNS} signal from one of the cases in the iControl study described in Appendix B. The signal was recorded before the beginning of propofol infusion and its mean has been subtracted to better illustrate the measurement noise. The corresponding $T_r = 30$ s trended signal with subtracted mean is shown in red in the same figure. Representative raw WAV_{CNS} sequences from the iControl study, collected prior to propofol infusion, with means subtracted, such as the blue one shown in Figure 2.2, were concatenated to form a sequence with a temporal duration of 1 h. The power spectrum of this sequence is shown i Figure 2.3.

The power spectrum shown in Figure 2.3 is essentially white, corresponding to a signal obtained by drawing samples from a normal distribution with standard deviation $\sigma = 9 \cdot 10^{-2}$. I.e., the raw WAV_{CNS} measurement noise is essentially white with a variance $\sigma^2 = 8 \cdot 10^{-3}$. This white signal will serve the purpose of monitor noise model in simulations throughout the thesis.

The Infusion Pump

The iControl system outlined in Appendix B.2 operates at a 5 s sampling period, with zero-order hold behavior of the actuator. Due to the time scale of the dynamics, disclosed in Section 2.2, there is no advantage in pursuing faster actuation. Within the corresponding bandwidth, transients in dynamic response and jitter of commercially available infusion pumps, such as the Alaris used in iControl, are negligible. For this reason, no dynamic model for

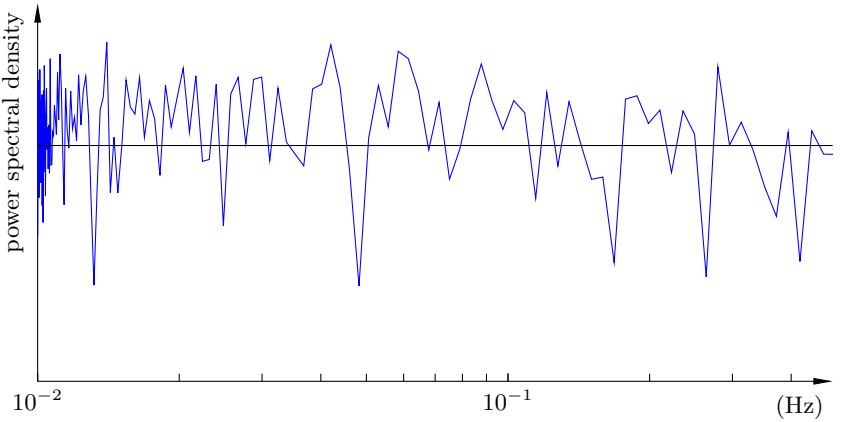

Figure 2.3 Power spectrum of concatenated raw WAV_{CNS} signals with means subtracted. The black line indicates the power spectral density of the white noise model.

the actuator, i.e. the infusion pump, needs to be considered in the design and analysis of closed-loop controlled anesthesia systems.

2.2 Propofol Patient Model

The Purpose of Modeling

Before attempting any modeling of the patient response to propofol, it is important to specify how the model will be used, which in terms specifies which characteristics of the behavior should be well-explained by the model. The models proposed in this section are intended to be used as a basis for the synthesis and evaluation of closed-loop DOH control systems, guided by the output of the NeuroSense monitor explained in Section 2.1. The purpose of modeling is therefore that of the PKPD models presented in Section 1.3, i.e., to describe the dynamics between propofol infusion and clinical effect.

The complex nature of the human body makes it fair to assume that the use of the traditional PKPD model structure corresponds to some extent of under-modeling. Meanwhile, as explained below in this section, the available input signal for identification is not capable of fully exciting the dynamics of even a severely simplified model. Furthermore, it is well-known that there exists a large inter-patient variability in the response to propofol, further discussed in this section. This combination of under-modeling and insufficient excitation for identifying model parameters dictates conservatism with the aim to devise models upon which it is safe to base the design of a closed-loop controller.

The compartmental nature of the PK model is physiologically motivated. Compartmental systems are positive; they have maximal gain at the zero frequency, and they lack oscillatory modes. The exact value of the steady state gain is not critical if the controller employs integral action. Likewise, the high frequency fidelity of the model is of limited importance due to the lack of oscillatory modes and the low high-frequency gain of the underlying system. Instead, the modeling effort should focus on yielding a model which is accurate around the intended cross-over frequency of the closed-loop system. Since the system is safety critical, it is motivated to identify models which over-estimate the negative phase shift of the system to be controlled.

Only induction phase data has been used for the identification of models in the thesis and the publications listed in the preface, for reasons explained further below. The success of this approach relies on that the model identified from induction phase data is valid also during maintenance of anesthesia. This assumption has not been thoroughly researched, but the traditional PKPD models imply the assumption to be true.

The control objective during induction of anesthesia is essentially to track a reference step. It can therefore be expected that models identified from data sets which were obtained during closed-loop controlled induction of anesthesia are suitable for synthesis of control systems similar to those used to produce the identification data sets, despite the under-modeling mentioned earlier [Anderson, 2002], [Lecchini et al., 2006].

Identifiability

Unmeasurable Disturbances From Section 1.1 it is evident that DOH measurements collected once surgery has begun are corrupted by unmeasurable disturbances caused by the surgical stimulation. Without special caution to assure the absence of, or compensate for, surgical stimulation, it is therefore not possible to obtain unbiased model parameter estimates later than during the induction phase of anesthesia. Furthermore, relying on data sets with input excitation beyond what the traditional drug dosing regimen produces would not allow for system identification from data sets collected in previously conducted clinical trials.

Persistence of Excitation As mentioned in Section 1.3, the clinical response to propofol is typically characterized using a PKPD model. The structure of the traditional PKPD model is that of a Wiener system. In this context the LTI system is compartmental and can be represented by the transfer function (1.14) with an additional linear scaling (1.15). The output nonlinearity has the parameterization (1.17). In the below discussion it will be assumed that the clinical monitor has unit dynamics. Even in the resulting absence of monitor parameters E_0, E_∞ and those of the monitor dynam-

ics (2.1) or (2.2), this representation requires at least 8 parameters for its characterization.

During TIVA with propofol it is customary for the anesthesiologist to dose the drug as a nominal steady rate infusion, upon which drug boluses can be superimposed. Typically, the procedure is initiated with such a bolus in order to limit duration of the induction phase of anesthesia, for reasons explained in Section 1.1. Consequent boluses are given in connection to sudden increases in surgical stimulation, either proactively or reactively. Step-wise changes in the nominal infusion rate are made if the anesthesiologist deems the DOH to be inadequate. Data from a representative manually controlled induction of anesthesia from the open-loop study described in Appendix B.1 is shown in blue in Figure 2.4. The propofol infusion profile is shown in Figure 2.4(b) and its resulting response in the DOH, as measured using the NeuroSense monitor, with trending $T_r = 30$ s in (2.1), is shown in Figure 2.4(a). Note that the infusion unit is mg/kg/min, i.e., normalized with respect to patient mass. This is one of two customary units in which propofol infusion rates are reported, the other being ml/h, which needs to be complemented with the drug dose concentration in units of mg/ml.

In order to limit the duration of the induction phase of anesthesia, closed-loop DOH control systems, such as iControl explained in Appendix B.2, typically mimic the manual control behavior in that induction of anesthesia is initiated by a bolus followed by a slowly varying infusion rate. A representative induction phase data set from the iControl study is shown in red in Figure 2.4. Although TCI data is not considered for identification in the thesis, it can be mentioned that TCI inductions of anesthesia have similar characteristics to manual and closed-loop controlled ones in that the input is essentially a propofol bolus followed by a slowly varying steady infusion.

Since only induction phase data is available for modeling, the input profile is essentially the sum of an impulse (the bolus) and a step (the continuous rate infusion).

The degree of persistent excitation provides an estimate of how many model parameters can be consistently identified using a certain input signal [Åström and Wittenmark, 2008]. The impulse has degree of persistent excitation zero, while the corresponding degree is one for the step. It is therefore unlikely that even the 7 parameters of the LTI part of the patient dynamics can be successfully identified from induction phase data.

An obvious approach to facilitate identifiability would be to alter the input signal in order to better excite the dynamics to be identified. For an open-loop system this can be achieved by a tailored infusion profile. In the TCI and closed-loop control paradigms a custom reference profile, other than a step, could be employed during the induction phase of anesthesia. In the absence of major disturbances, an additional possibility for the closed-loop case would be to conduct a low-amplitude relay feedback experiment [Häg-

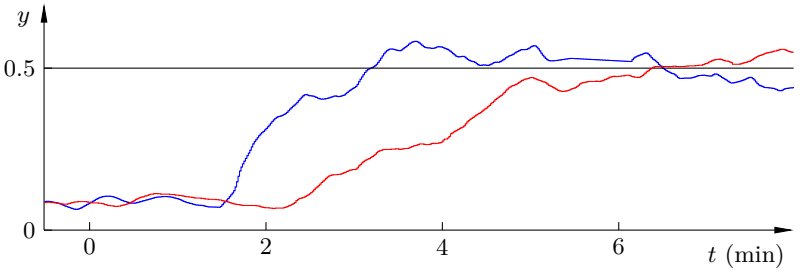

(a) DOH measurement y.

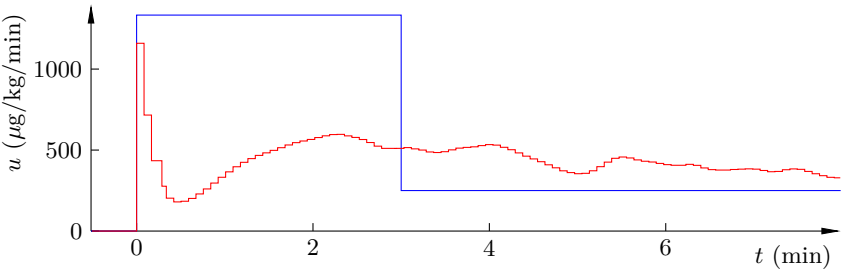

(b) Propofol infusion rate u.

Figure 2.4 Representative induction profile for one manually controlled case (blue) and one closed-loop controlled case (red). The black line marks the DOH setpoint.

glund and Åström, 2002], [Soltész et al., 2010] during the maintenance phase of anesthesia. This would yield the $-180°$ phase shift angular frequency and corresponding gain of the system, which would be valuable in the controller synthesis. Although increasing the input excitation has obvious advantages from an engineering perspective, it is not straightforward due to patient safety and ethics concerns. An increased excitation of the patient dynamics may well lead to changes in hemodynamic stability, with related adverse effects [Monk et al., 2005]. Deviations from the traditional drug dosing protocol would also need to be explained to the anesthesiologist who is supervising the procedure. Studying similar supervised automated systems have suggested that misconceptions regarding the intended behavior of the control system are likely to cause the operator to switch the system to manual mode [Dzindolet et al., 2003].

The lack of sufficiently exciting input signal has previously seen several approaches. In [Soltész et al., 2013b] previously published formulas of the form (1.23) are used to yield PK model parameters, based on biometric parameters, such as patient age and body mass, as explained in Section 1.3. The

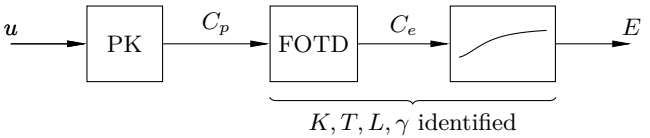

(a) Fixed PK dynamics.

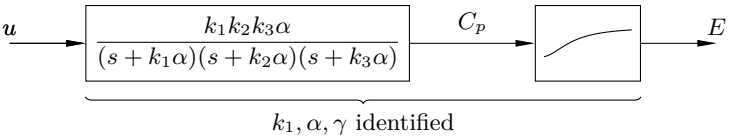

(b) Fixed pole ratio.

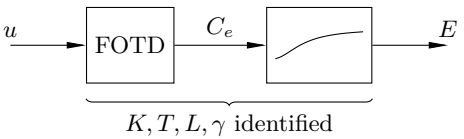

(c) FOTD structure.

Figure 2.5 Block diagrams showing different approaches to overcome the lack of identifiability.

resulting PK model is driven by the recorded infusion profile to produce an estimated plasma concentration C_p. The FOTD dynamics between this C_p and the measured clinical effect are subsequently identified. A block diagram illustrating this fixed PK approach is shown in Figure 2.5(a). The FOTD system can only provide negative phase shift. As a consequence, the approach fails if the PK model obtained by (1.23) is slower than the PK dynamics of the actual patient. Another approach, explained in [da Silva et al., 2010] and shown in Figure 2.5(b) is to use a third-order LTI system with fixed pole ratios to model the PK. This requires only the identification of the dominant pole, steady state gain and nonlinearity parameter γ. A third approach, evaluated in [van Heusden et al., 2013b] and shown in Figure 2.5(c), is to approximate the PK model (1.14) with a FOTD system. In this approach, the delay models the negative phase shift corresponding to the unmodeled poles of (1.14).

Of the mentioned approaches, that in which the PK dynamics are modeled by a FOTD system is clearly the one of lowest complexity. It is therefore remarkable that full identification of its parameters from representative in-

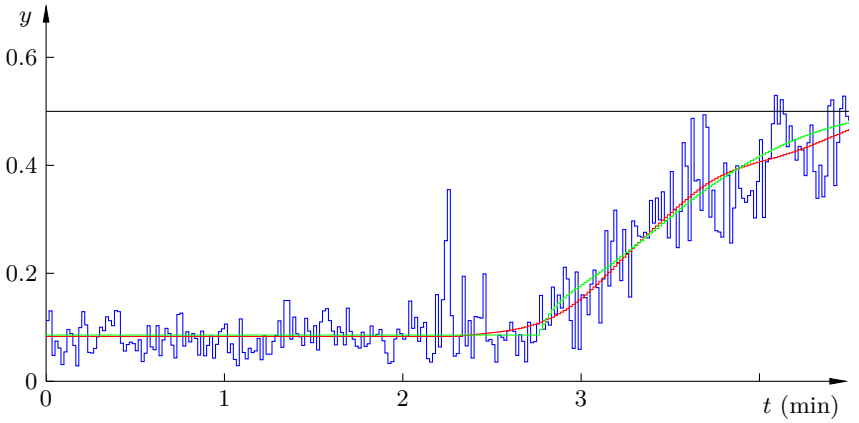

Figure 2.6 Representative raw WAV_{CNS} profile y_{raw} from closed-loop controlled induction of anesthesia (blue) together with the responses $\hat{y}_{\text{raw}}$ of identified models (red, green) and setpoint (black).

duction phase data is not possible, even when the clinical monitor is assumed to hold unit dynamics. To illustrate this, assume that the full model dynamics are characterized by the parameter set $\{K, T, L, \gamma\}$, as shown in Figure 2.5(c). A representative induction phase DOH measurement series from the iControl study described in Appendix B.2 is shown in blue in Figure 2.6. Here, the unfiltered WAV_{CNS} profile y_{raw}, corresponding to the monitor model (2.2) is shown. The time $t = 0$ min marks the beginning of propofol infusion. The relative timing of the DOH and propofol infusion profiles has been adjusted to eliminate the delay of the monitor model (2.2) and the monitor parameter E_0 was manually identified. Consequently, the unit monitor dynamics assumption holds for this example.

The parameter space spanned by $\{K, T, L, \gamma\}$ was gridded and the model corresponding to each grid point was driven by the propofol infusion profile resulting in the blue DOH profile shown in Figure 2.6. Subsequently, the $\mathcal{L}_2$-norm difference between the measured and simulated DOH profiles was computed. Figure 2.7 shows this difference for a section of $\{L, \gamma\}$ space. (The values of K and T at each grid point were chosen as those minimizing the error at that grid point.) The figure shows that there is a deep and essentially flat valley in this cost landscape. Two points are marked along the bottom of this valley and the correspondingly colored simulated DOH profiles are shown in Figure 2.6. The red point corresponds to a big value of γ and a small value of L, while the green point corresponds to a small value of γ and a big value of L. The relative output error $\mathcal{L}_2$-norm difference between the two marked points is merely 0.8 %, while the monitor measurement noise model presented previously in the thesis, typically results in relative output

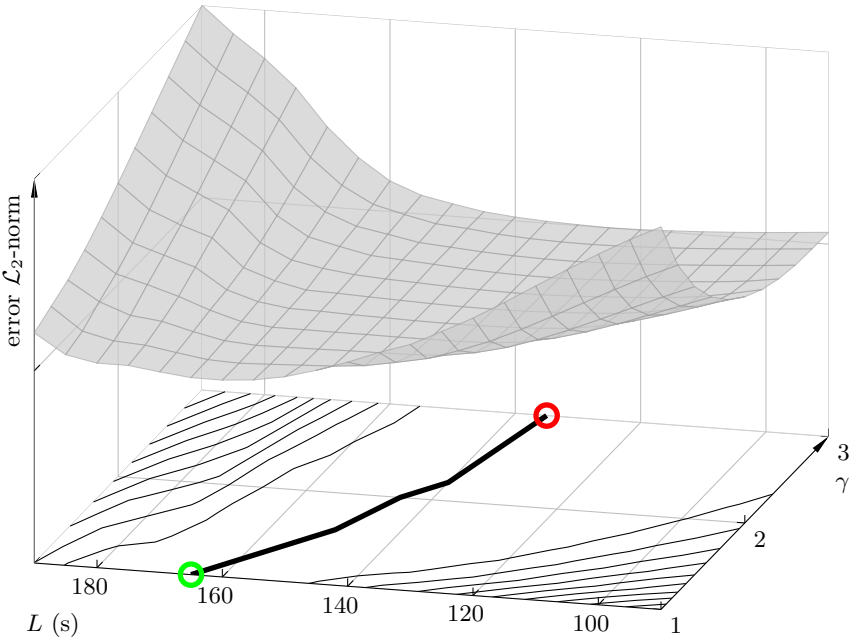

Figure 2.7 Minimal output error $\mathcal{L}_2$-norm between the induction phase DOH profile in Figure 2.6 (blue) and simulations using FOTD–Hill models at differnet points in $\{L, \gamma\}$ space.

error $\mathcal{L}_2$-norm fluctuations of 5 %. It is therefore not possible to decide upon a specific $\{L, \gamma\}$ pair along the valley of Figure 2.7, based on a representative DOH profile y_{raw} such as the one shown in blue in Figure 2.6.

The unidentifiability along a path in $\{L, \gamma\}$ space is not unexpected. Figure 1.5 shows the Hill function (1.17) for three values of its parameter γ. The clinical effect E at low normalized drug concentrations v decreases as the value of γ increases. The normalized drug concentration v is initially low during induction of anesthesia, and consequently it is hard to determine whether the delayed clinical response is caused by the delay L or the static nonlinearity (1.17) with a large value of its parameter γ.

Due to the transient nature of the induction phase and its limited duration, it is not possible to confidently determine the steady state gain K of the FOTD model. Particularily, there exists an ambiguity in $\{K, T\}$ space, similar to that in $\{L, \gamma\}$ space; a small steady state gain cannot be entirely distinguished from a slow time constant.

It should also be pointed out that there is typically no availability of validation data, as only one induction of anesthesia is expected per patient during any one particular procedure.

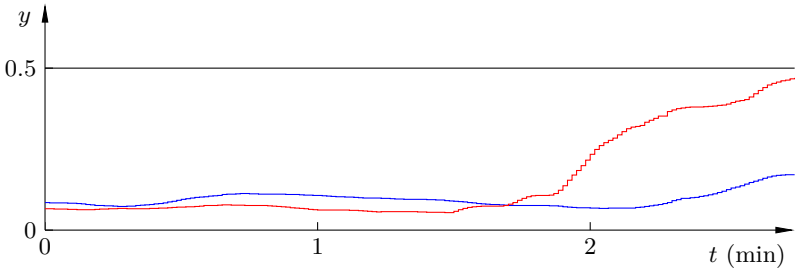

(a) DOH measurement y.

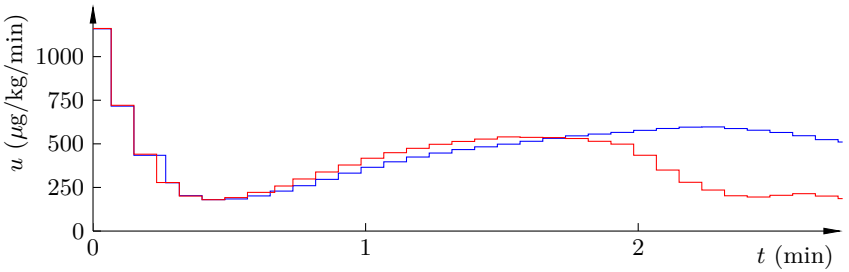

(b) Propofol infusion rate u.

Figure 2.8 Two closed-loop controlled infuion profiles (blue, red), together with setpoint (black), illustrating inter-patient variability in the sensitivity to propofol.

Inter-Patient Variability

There exists a large inter-patient variability in the sensitivity to propofol [Bibian et al., 2006]. This particularly hold true for children [Coppens et al., 2011], [van Heusden et al., 2013b], for which the iControl system has been evaluated as described in Appendix B.2. To illustrate this point, Figure 2.8 shows two inductions of anesthesia using propofol. Both cases are female patients. The blue case is from an 8 year old, 31 kg, 135 cm patient while the red case is from a 10 year old, 41 kg, 151 cm patient. Infusion rates of propofol for each of the two cases are shown in Figure 2.8(b) and the corresponding DOH profiles, using the $T_r = 30$ s trending option of the NeuroSense monitor, are shown in Figure 2.8(a). The infusion rates are given in units of μg/kg/min, i.e. normalized with respect to body mass. Despite similar biometric parameters and infusion profiles, the patient responses differ significantly. This behavior is representative and poses a challenge in controller synthesis. Possible approaches to handle this variability are discussed in Section 3.3.

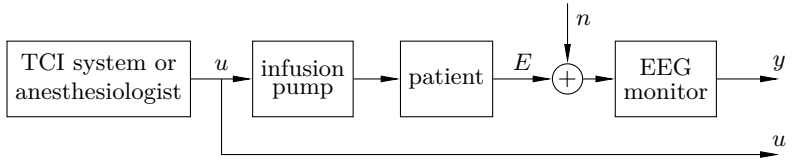

(a) Open-loop identification scenario.

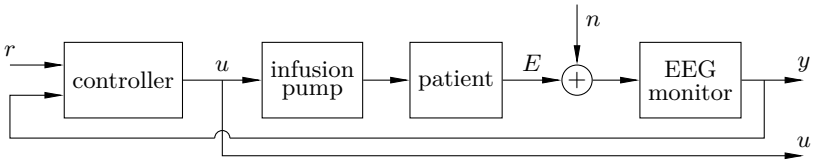

(b) Closed-loop identification scenario.

Figure 2.9 The input u is unaffected by measurement noise n in the open-loop scenario, but not in the closed-loop one.

Closed-Loop Bias

When model parameters are identified from induction phase data collected during manually or TCI dosed anestheisa, the noise at the input and output are not expected to be correlated. This is evident from the block diagram in Figure 2.9(a). Under closed-loop control, the input–output signal pair can no longer be considered uncorrelated in terms of noise, since there now exists a path for noise through the controller as shown in Figure 2.9(b).

There are three main approaches to closed-loop identification, discussed in [Forssell and Ljung, 1998]. The direct approach does not take the feedback path into account, and is therefore succeptible to the aforementioned bias. In the indirect approach, a model of the feedback path is used to obtain the corresponding open-loop process parameters. Finally, the joint input–output approach considers a system with the closed-loop reference and measurement noise as inpupts, while the control signal and measurement signal are considered outputs.

All models presented in the thesis and its underlying publications were obtained using the direct approach in an output-error framework. This is motivated by the simplicity of the direct approach relative to that of the indirect and joint input–output ones. Furthermore, the direct approach does not require knowledge of the closed-loop controller dynamics used during the identification experiment. For the current application, use of the direct approach was deemed valid since the process parameters to be identified are determined by the low-frequency dynamics, which are on the time scale of minutes. The influence of the aforementioned monitor noise model is therefore negligible.

Nonlinearity

The output nonlinearity model reported in essentally all publications describing PD models for anesthesia is the Hill function (1.17). The Hill function is obtained in receptor theory as the solution of a statistical ligand–receptor binding problem [Phillips et al., 2012]. As such, the Hill function is a concentration-dependent binding curve with essentially linear behavior for low concentrations and a saturation effect as the concentration increases. The mentioned receptor theory background has led to the adoption of the Hill function to model the PD behavior of a multitide of clinical drugs, including anesthetic ones.

The receptor theory problem yeilding the Hill function as its solution is most likely a severe simplification of the effect site mechanics of propofol and other anesthetic drugs. In the absence of the monitor dynamics (2.1), it would therefore be desirable to model the dynamics between propofol infusion and measured clinical effect by a more general Wiener system. A popular approach to Wiener system identification is to represent the static output nonlinearity by the coefficients of a truncated Volterra series and simultaniously identify these and the parameters of the LTI dynamics [Hunter and Korenberg, 1986]. It has already been demonstrated that simultaneous identification of LTI PK parameters and the parameter γ of the Hill nonlinearity (1.17) is problematic. The additional parameters introduced by the truncated Volterra series approach would contribute to further loss of identifiability. Consequently, the Hill function representation of the patient model output nonlinearity is adopted throughout the thesis; mostly for historic reasons and due to the lack of a motivated alternative.

The presence of the Hill nonlinearity complicates the use of linear controller synthesis and analysis methods. At least two methods to circumvent this have been reported in the literature; exact and local linearization. Since the Hill nonlinearity (1.17) is a monotone function of the normalized effect site concentration v, it has an inverse:

$$v(E;\gamma) = \left(\frac{E}{1-E}\right)^{1/\gamma}. \tag{2.4}$$

It was suggested in [da Silva et al., 2012] and [Ionescu et al., 2008] that (2.4) could be implemented in the controller as illustrated by the block diagram in Figure 2.10. Here γ is the nonlinearity parameter of the patient, while $\hat{\gamma}$ is the parameter assumed by the controller. The strategy is termed exact linearization, as it completely cancels the nonlinearity (1.17) when $\hat{\gamma} = \gamma$. The exactly linearizing controller aims at controlling the estimated normalized drug concentration $\hat{v}(y;\hat{\gamma})$, which is straight forward, using a linear controller.

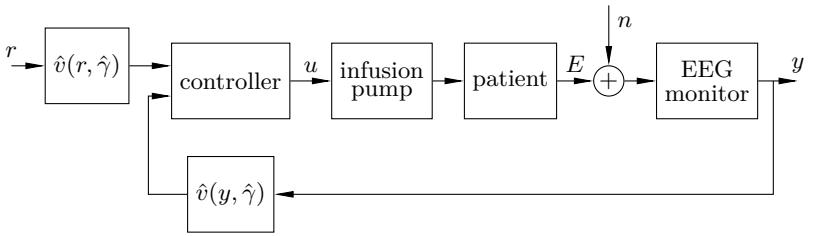

Figure 2.10 Block diagram showing an exactly linearizing closed-loop controller.

Assuming that the measured and actual clinical effect are identical, i.e. $y = E$, the error in the controlled variable $\hat{v}$ becomes

$$\tilde{v} = v - \hat{v} = v - v^{\gamma/\hat{\gamma}}. \tag{2.5}$$

As illustrated by Figure 2.7, there is no guarantee that $\hat{\gamma}$ is close to γ, and consequently it is hard to guarantee performance using the exact linearization approach.

An alternative to exact linearization is local linearization, see e.g. [Dumont et al., 2009]. In the vicinity of a stationary operating point, represented by the normalized effect site concentration v_o, the Hill function (1.17) can be well approximated by its linearization:

$$E(v) \approx E_o + \left.\frac{\partial E(v;\gamma)}{\partial v}\right|_{v=v_o} \Delta v, \tag{2.6}$$

$$E_o = E(v_o;\gamma) = 1 - \frac{1}{1+v_o^\gamma}, \tag{2.7}$$

$$\left.\frac{\partial E(v;\gamma)}{\partial v}\right|_{v=v_o} = \frac{\gamma v_o^{\gamma-1}}{(1+v_o^\gamma)^2}, \tag{2.8}$$

$$\Delta v = v - v_o. \tag{2.9}$$

Note that the local and exact linearization approaches are identical at the operating point defined by E_o, which corresponds to $v_o = 1$. When using the local linearization approach, the most common alternative has been to choose the operating point corresponding to $E_o = 1/2$ and synthesize only one controller based on the corresponding local linearization. This is the method used in essentially all publications where linear control strategies such as (linear) MPC or PID are evaluated in the anesthesia context. The choice $E_o = 1/2$ is motivated by $E = 1/2$ being the by far most common reference in DOH control systems.

One possible alternative would be to use several linearization points with corresponding controllers. A method which resembles this approach is pre-

sented in [Lin et al., 2004], where one set of linear models is used for the DOH range $E \leq 0.3$ and another set of models for the DOH range $E > 0.3$.

If the drug dosing control scheme implements integral action, it is feasible to locally model the nonlinearity as the gain $\partial E/\partial v$. The bias term E_o in (2.6) is successfully compensated for by the integrator in the controller. This is the case reported in most publications, including [Dumont et al., 2009].

In the thesis and its underlying publications, all controllers have been synthesized for the operating point corresponding to $(v_o = 1, E_o = 1/2)$. I.e., the Hill function has been replaced by the series gain

$$\left.\frac{\partial E}{\partial v}\right|_{v=1} = \frac{\gamma}{4}, \tag{2.10}$$

in the patient model used for control synthesis and the integrator of the controller has been responsible to correct the bias E_o. However, the full nonlinear models have been used in all simulations conducted to evaluate controller performance.

When $v > 1$ it holds that

$$\frac{\gamma}{4} > \frac{\gamma v_o^{\gamma-1}}{(1+v_o^{\gamma})^2}, \ \forall \gamma > 1. \tag{2.11}$$

Hence, the model (2.10), used for controller synthesis, underestimates the process gain in the region corresponding to a large DOH. In addition, zero gain results from local linearization at $E_o = 0$ for $\gamma > 1$ and as $E_o \to 1$. These low gain regions will make the closed-loop controller act restrictively when $v > 1$ and when $v \approx 0$. This mitigates the risk of overdosing due to the unavailability of a negative valued control signal. Loss of stability due to under-actuation is not a major concern, since the uncontrolled process is inherently stable.

In the region $0 \leq v_o \leq 1$, which is traversed during induction of anesthesia, the gain is initially zero at $E_o = 0$, then increases to reach its maximal value at

$$v_o = \left(\frac{\gamma-1}{\gamma+1}\right)^{1/\gamma}. \tag{2.12}$$

Evaluating (2.10) at $\gamma = 1.5$ gives the series gain 0.38. The corresponding gain at $v_o = 0.34$ from (2.12) is 0.61. This means that the local linearization results in a 61 % (the relative difference between 0.38 and 0.61) worst case under-estimation of the process gain. Closed-loop controllers for induction of anesthesia designed using the local linearization approach need to take this gain "uncertainty" into account.

Note that the parameter E_0, describing the measured effect in absence of drug, has been omitted in this section. This has been done to simplify notation. However, since $E_0 > 0$ merely corresponds to an affine scaling of the measurement, this has resulted in no loss of generality.

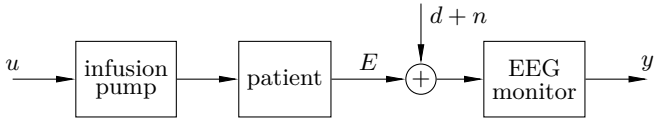

Figure 2.11 Block diagram illustrating the path through which surgical stimulation d affects the DOH.

Surgical Disturbance Model

In order to evaluate prospective controllers in simulation, it is of importance to realistically mimic the disturbances arising from surgical stimulation. As mentioned in Chapter 1, surgical stimulation mainly acts as an additive output disturbance, lowering the DOH. It is hence introduced through the same path as the measurement noise described in Section 2.1 and illustrated in Figure 2.11. Two disturbance profiles, describing surgical procedures, have been proposed previously in the literature. They are briefly explained below and a third, simpler profile is proposed and subsequently used throughout the thesis.

The surgical stimulation profile shown in Figure 2.12(a) was suggested in [Struys et al., 2004]. The negative spikes from left to right are explained to represent: arousal due to laryngoscopy[5] or intubation, incision[6] followed by a period of no stimulation, abrupt stimulation and short-lasting larger stimulation (three occurrences). The base-level step represents the onset of continuous normal surgical stimulation.

The surgical stimulation profile shown in Figure 2.12(b) was proposed in [Dumont et al., 2009]. It consists of an initial step, representing the arousal caused by incision. The subsequent decaying exponential represents how the offset slowly decreases and settles to a level at which normal surgical stimulation might occur. Eventually, the stimulation is withdrawn altogether, which is represented by the second decaying exponential.

In the thesis the simple output disturbance profile shown in Figure 2.12(c) is used to evaluate controllers in simulation. It consists of a double step, which allows the system to settle and gives a picture of the closed-loop reaction which is easy to characterize in automatic control terms such as overshoot and settling time. From its response it is also possible to anticipate how the system would react to the previously published profiles.

Models used in the iControl Study

The iControl study made use of patient models which were identified from data collected during open- and closed-loop controlled anesthesia. This model

[5] Laryngoscope: a tubular endoscope that is inserted into the larynx through the mouth.
[6] Incision: a cut into a body tissue or an organ.

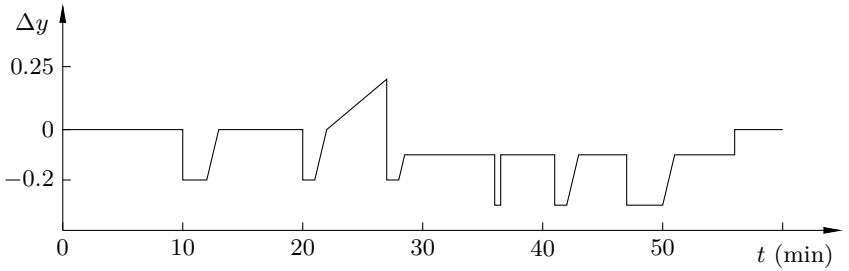

(a) Profile suggested in [Struys et al., 2004].

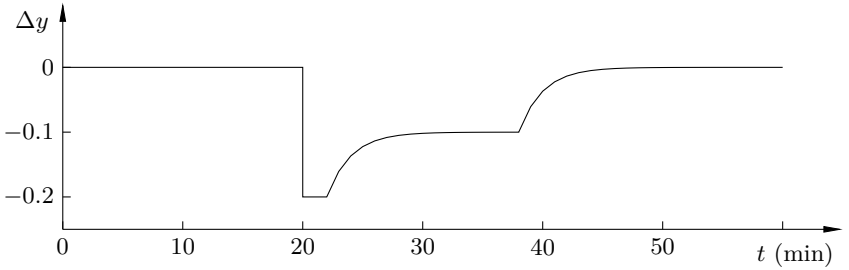

(b) Profile suggested in [Dumont et al., 2009].

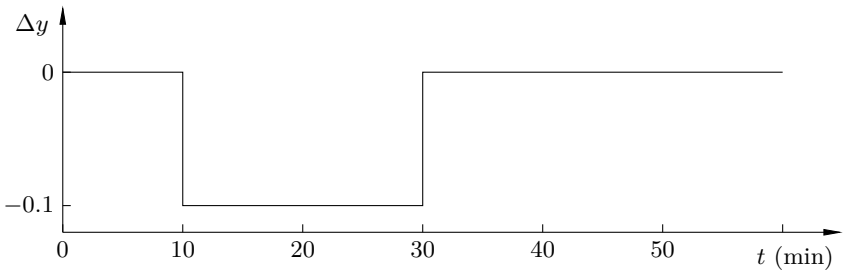

(c) Profile used in the thesis.

Figure 2.12 Additive output disturbance profiles used to evaluate closed-loop DOH controllers in simulation.

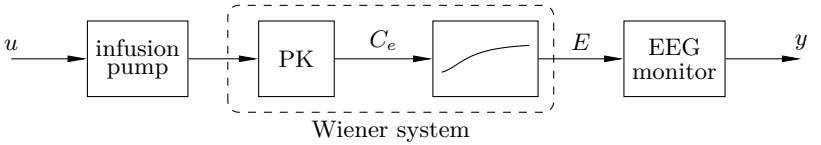

Figure 2.13 The LTI monitor dynamics break the Wiener structure of the model to be controlled.

development work was foremost conducted by Klaske van Heusden at The University of British Columbia, Vancouver, Canada, with partial involvement of the author. Essential characteristics of these models and their identification is presented here, whereupon a slightly modified identification approach is described.

Details on the clinical protocol under which data was collected are given in Appendix B and [van Heusden et al., 2013b]. Only data from the initial 10 min after the start of propofol infusion were used for identification, since nociceptive stimulation is typically present during the subsequent maintenance phase of anesthesia. A manual procedure was used to discard data sets showing signs of disturbances during these initial 10 min, which could not be related to the input using the proposed model structures.

The measurements used for identification were filtered with the $T_r = 30$ s trending option of the NeuroSense monitor. The trended signal was used in order to utilize the artifact removal algorithm of the NeuroSense monitor, see Section 2.1. The Wiener model structure consisting of LTI PK dynamics with a static output nonlinearity was consequently broken, as shown in Figure 2.13. The fact that the nonlinearity (1.17) and the LTI monitor dynamics (2.1) do not commute, was disregarded and the monitor dynamics were partially compensated for by filtering the identification input signal, i.e. the propofol infusion rate, with (2.1).

Identification was subsequently conducted using the output-error framework in a direct approach. The identifiability issue was tackled by initially identifying an LTI model between input and measurement and subsequently fit the Hill function parameter γ to minimize the residual. This approach tends to over-estimate the delay L (negative phase shift) and under-estimate the Hill parameterγ (output dependent gain), which is sound from a control synthesis perspective as it eventually results in more conservative controllers.

Two identification approaches were considered; the fixed PK dynamics approach illustrated in Figure 2.5(a) and the FOTD approach shown in Figure 2.5(c). Both approaches are explained in [van Heusden et al., 2013b] and it was concluded that the two approaches produce equally satisfactory results when applied to the available data.

A Simplistic Approach to Modeling

This section presents an identification procedure similar to the one in [van Heusden et al., 2013b], but not requiring manual data processing. Developing such a scheme is fundamental in order to automate tuning of the closed-loop controller. While the ideas behind the proposed identification scheme are motivated, the resulting models have not yet been verified to the extent of those presented in [van Heusden et al., 2013b].

It was concluded in [van Heusden et al., 2013b] that the FOTD model structure shown in Figure 2.5(c) did perform as well as other evaluated structures. Consequently, it is chosen here for its simplicity in terms of its few parameters: E_0, K, T, L and γ.

The parameter E_0, describing the clinical effect in absence of drug, was estimated by $\hat{E}_0$, defined as the mean value of the measurement signal between the beginning of the measurement series and the start of propofol infusion. The $T_r = 30$ s trending option of the NeuroSense monitor, explained in Section 2.1, was enabled to utilize the artifact removal properties of the monitor.

As previously discussed, the pair $\{L, \gamma\}$ is not identifiable using representative induction phase data. It has also been pointed out that it is desirable to under-estimate γ in order to simultaneously over-estimation of L, which in terms yields a more conservative controller tuning. The nonlinearity parameter γ from (1.17) was therefore fixed to its smallest possible value $\gamma = 1$, yielding the output nonlinearity

$$E = 1 - \frac{1 - E_0}{1 + v}, \tag{2.13}$$

shown, for $E_0 = 0$, in blue in Figure 1.5.

Rather than using the initial 10 min following the beginning of propofol infusion for identification, the definition of induction phase duration from [Liu et al., 2006] was adopted. Identification was consequently performed on data collected during the time elapsed from the start of propofol infusion to the moment when the trended measurement signal y rises to and remains above 80 % of its setpoint for 30 s.

The raw NeuroSense output y_{raw} (cf. blue signal in Figure 2.2) is filtered through the inverse of (2.13),

$$\hat{v} = \frac{1 - \hat{E}_0}{1 - y_{\text{raw}}} - 1, \tag{2.14}$$

to obtain the estimate $\hat{v}$ of v.

Note that the expression in (2.14) is only valid for $y_{\text{raw}} \geq \hat{E}_0$. This and similar aspects, such as potential division by zero in (2.3), require attention when producing code for simulation or clinical studies, but are not explicitly addressed in the presentation of the thesis.

The $\{L, T\}$ parameter space is gridded, with a resolution[7] equal to the sample time of the system, which is 1 s. The lower bound for the delay parameter estimate $\hat{L}$ was chosen to be 0 s, whereas the upper bound was set to the time at which the measurement y rises to and remains above 20 % of the setpoint for 30 s. The corresponding limits for the time constant $\hat{T}$ were chosen as 1 s (the sample time of the system) and half the duration of the considered data set, respectively.

At each grid point a 1 s zero-order hold discretization of $e^{-\hat{L}s}/(s\hat{T} + 1)$ is driven by the recorded propofol infusion profile u to produce $\hat{v}'$. The optimal parameter value of the gain $\hat{K}$ for the grid point is subsequently determined by least squares applied to $\hat{v}$ and $\hat{v}'$. The obtained gain is used to construct $\hat{v} = \hat{K}\hat{v}'$. Applying the output scaling defined through $\hat{E}_0$ and the nonlinearity (2.13), the model output

$$\hat{y}_{\text{raw}} = 1 - \frac{1 - \hat{E}_0}{1 + \hat{v}} \tag{2.15}$$

is obtained. It would now be possible to select the grid point minimizing the output error between $\hat{y}_{\text{raw}}$ and y_{raw}. However, this would not utilize the artifact removal algorithm of the NeuroSense monitor, mentioned in Section 2.1. Instead, $\hat{y}_{\text{raw}}$ is filtered by the $T_r = 30$ s linear trending filter used in the NeuroSense monitor to produce $\hat{y}$. The error, here defined by the $\mathcal{L}_2$-norm[8] of $y - \hat{y}$ is computed at each grid point and the parameters set $\{\hat{K}, \hat{T}, \hat{L}\}$ corresponding to the minimum is selected. One example of the involved signals is shown in Figure 2.14.

The outlined identification procedure was applied to data from the 94 closed-loop controlled cases further described in Section 3.2. (Profiles from 23 of these cases are shown in Figure 3.12. The remaining 71 profiles are shown in Figure 3.15.)

Rather than manually selecting data sets for inclusion or exclusion, the decision was based on reliability of the identified model, as outlined below.

Only the part of the data set corresponding to the time after the identified delay $\hat{L}$ is actively used in the identification of the time constant $\hat{T}$. Hence, identified values $\hat{T}$, which are large compared to the duration of this part of the data set indicate that either the experiment duration or input excitation was insufficient. Consequently, models identified from data sets with duration t_{ind} were discarded if $t_{\text{ind}} - \hat{L} < \hat{T}$. This resulted in the exclusion of 24 models. For the same reason, models where $\hat{T}$ was found to be optimal at its upper grid bound were removed, resulting in the exclusion of an additional 14 cases.

[7] The actual implementation exploits local smoothness of the cost function to iteratively refine the grid and hence speed up the identification.

[8] The norm is scaled by the reciprocal square root of the data set duration, in order not to favor short data sets.

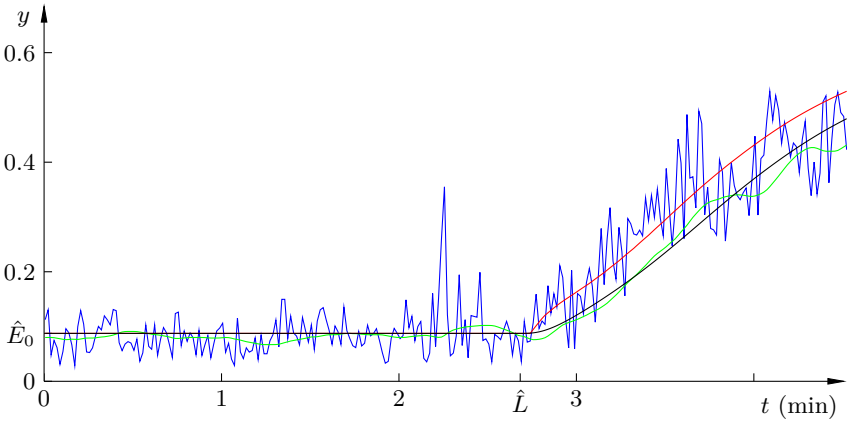

Figure 2.14 Signals involved in process model identification: y_{raw} (blue), $\hat{y}_{\text{raw}}$ (red), y (green) and $\hat{y}$ (black).

The presence of artifacts in y_{raw} or of disturbances caused by surgical stimulation in y both increase the output error. Consequently, models resulting in an output error above a heuristically determined threshold were discarded. Both the $\mathcal{L}_1$ and $\mathcal{L}_2$ norms of the difference between y and $\hat{y}$ were thresholded in order to capture both average and worst-case deviations. The threshold values were adjusted based on the first 47 data sets and the adequacy of the resulting values was confirmed by application on the remaining 47 data sets. The established thresholds corresponded to the exclusion of cases with maximal and root means square error exceeding 7 % and 15 %, respectively. The thresholds resulted in exclusion of 4 and 11 cases, respectively. Parameter values of the remaining 41 models are enlisted in Appendix A while histograms showing their distribution are shown in Figure 2.15.

As can be seen in Figure 2.15, there exists a large inter-model variability in the parameter values. With the given data it is hard to tell whether this entirely reflects the inter-patient variability of the underlying dynamics or if parts of it are caused by insufficient excitation during the identification experiment.

The described identification scheme could be used to individualize the closed-loop controller tuning upon induction of anesthesia in cases where a valid model is identified. For the existing 94 data sets, this would have been possible in 41 cases, i.e., in 44 % of all cases. The topic of individualized control is further discussed in [Soltész et al., 2013b] and Section 3.3.

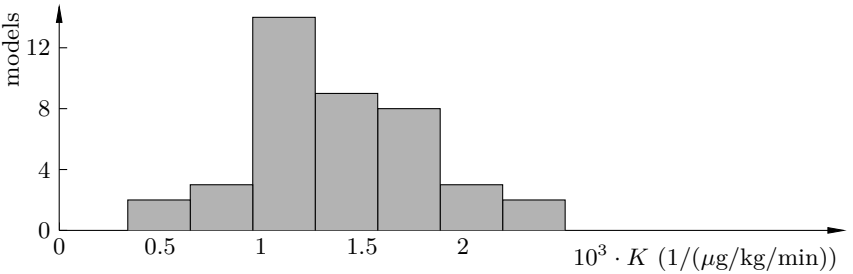

(a) Gain K.

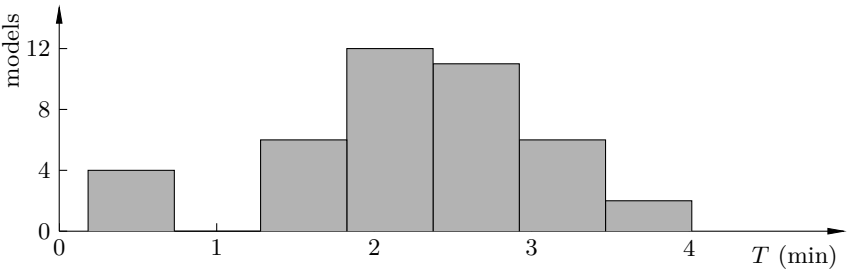

(b) Time constant T.

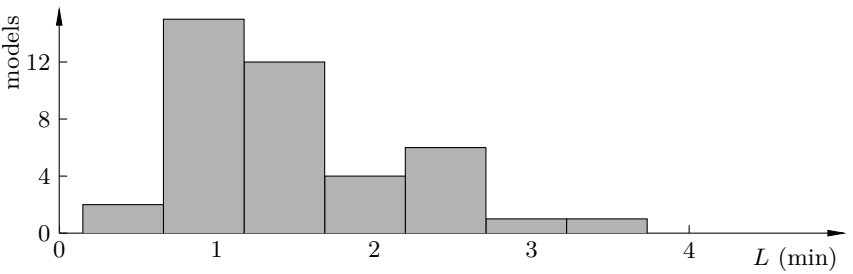

(c) Delay L.

Figure 2.15 Distribution of identified model parameters.

2.3 Remifentanil Patient Model

As mentioned in Section 1.1, there exist no reliable method to directly measure the DOA. However, the DOA and DOH are related as described in Section 1.3.

Pharmacokinetic interaction between propofol and remifentanil has been investigated in healthy adults [Bouillon et al., 2002]. It was concluded that the pharmacokinetics of propofol are not changed by remifentanil, that the central compartment clearance and elimination rate of remifentanil are decreased in the presence of propofol and that the effect of propofol on the concentration–time course of remifentanil is only clinically relevant when bolus doses of remifentanil are administered. No similar study has been conducted in children. The approach taken in the thesis and in previous closed-loop controlled studies, see Appendix C, is to neglect any PK interaction between the two drugs.

There exist several published compartment models, describing the pharmacokinetics of remifentanil in terms of biometric parameters, as explained in Section 1.3 and illustrated in (1.23). The work leading up to the thesis has not considered identification of custom remifentanil PK models. The reasons for this are foremost the mentioned absence of reliable DOA monitors, in combination with the insufficient input signal excitation resulting from the clinical remifentanil dosing protocol of the iControl study, described in Appendix B.2. The model used for simulations in the underlying work [Soltész et al., 2012a] is a remifentanil PK model for children, originally published in [Rigby-Jones et al., 2007][9]. Similar models for the adult population include [Minto et al., 1997] and [Egan et al., 1996].

Comparing the speed (e.g. rise time) of the identified propofol patient models of Section 2.2 or previously published counterparts, with those of published remifentanil PK models show that the dynamics of remifentanil are an order of magnitude faster than those of propofol. The comparatively instantaneous dynamics of remifentanil makes the drug easier to dose in closed-loop. Particularly, the absence of a prolonged lag allows for more aggressive controller design in the presence of representative inter-patient variability.

One aspect, which cannot be overlooked, is the documented PD interaction between propofol and remifentanil, described in Section 1.3. In fact, it is this synergistic interaction that enables joint control of the DOH and the DOA, in the absence of a DOA monitor, as explained in Section 1.1. The thesis utilizes the interaction model originally published in [Kern et al., 2004] and explained in Section 1.3. The interaction parameter in (1.22) is assumed to be $\alpha = 5.1$ as reported in [Kern et al., 2004]. Similarly a plasma

[9] Several models are presented in [Rigby-Jones et al., 2007]. The one used in [Soltész et al., 2012a] is the Rigby-Jones model with patient weight as its only biometric parameter.

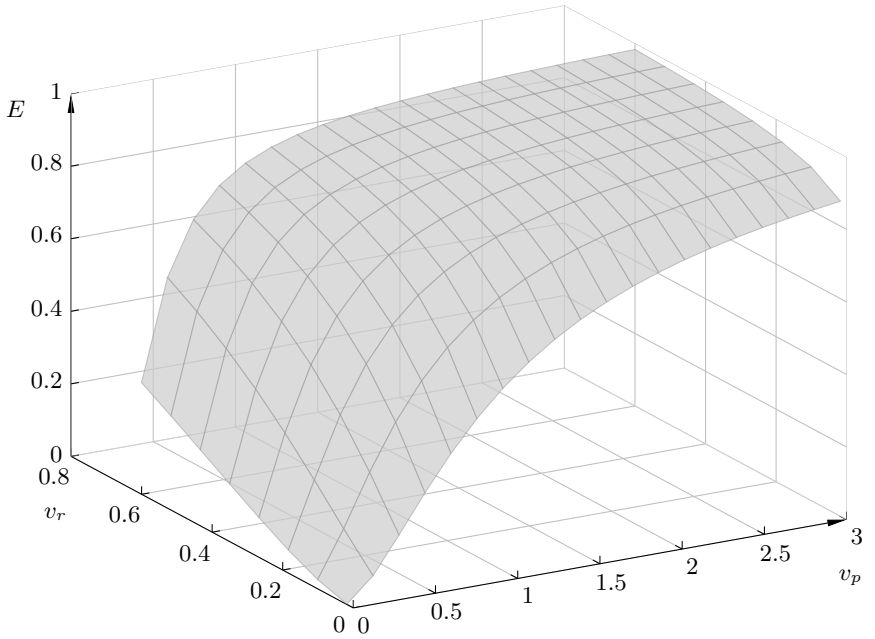

Figure 2.16 PD interaction surface relating the normalized effect site concentrations v_p and v_r to the clinical effect towards DOH, E.

concentration of $C^r_{e,50} = 12.5$ ng/ml is used to compute v_r. Note that this C_e value is with respect to DOH, rather than DOA. Values for the parameter γ are adopted from the propofol model. This makes the PD interaction surface model (1.22) collapse into the Hill PD for propofol (1.17) in the absence of remifentanil, i.e., when $v = v_p$. An example of the PD interaction surface arising from combining (1.22) and (1.17) is shown in Figure 2.16 for clinically relevant ranges of v_p and v_r and $\gamma = 1.5$.

3

Control of Anesthesia

3.1 Performance Measures

The control objective being discussed in this chapter is setpoint tracking of the DOH, in the presence of model uncertainties and disturbances, which were described in Chapter 2.

The current practice for performance assessment of EEG-guided DOH control systems is the computation of four measures introduced in [Varvel et al., 1992]. These *Varvel* measures were proposed to evaluate the performance of anesthesia systems, however not the EEG-guided variety outlined in Section 1.2. Despite this, they have become the gold standard in clinical evaluation as is evident from several studies in which DOH measures derived from the EEG were used to control hypnotic drug infusion rate, see Appendix C.1.

This chapter will begin with a discussion of how to evaluate closed-loop controlled anesthesia system, before moving on to clinical and simulation results as well as possible extensions of an existing system towards control of the DOA.

Objectives

The rationale behind introducing performance measures is to map the n-dimensional DOH error vector, where n is the number of available samples, to an m-dimensional ($m \ll n$) space in which each dimension has a distinct interpretation, strongly coupled to the performance of the system. As mentioned above, $m = 4$ for the Varvel measures. Ultimately it would be desirable to set $m = 1$ and describe performance of the control system by only one scalar. This was attempted in [Liu et al., 2006] by introducing the *global score*, discussed further below.

The control objectives differ between temporal phases of anesthesia, which suggests the use of different performance measures for each temporal phase and calls for a systematic method to determine the transition between subsequent phases.

The clinical objective during induction of anesthesia is to make a fast transition to the DOH setpoint, with limited overshoot and short settling time, as discussed in Section 1.1. Limiting the induction phase duration is particularly motivated for anxious patients. A more rapid induction of anesthesia may also alleviate the discomfort associated with the infusion of propofol in conscious patients. Furthermore, limiting the duration of the induction phase results in an increased availability of the operating room and its staff. Meanwhile, limiting the overshoot is critical during maintenance of procedures which require spontaneous breathing, since a high DOH generally results in apnea. Avoiding a DOH overshoot is also critical in some patient groups such as the elderly, in order to avoid the associated potential for hypotension.

During maintenance of anesthesia, it has been recommended that the DOH measurement y, introduced in Section 2.1, should lie in the $(0.4, 0.6)$ range, with a setpoint of $r = 0.5$ [Kelly, 2003], [Agrawal et al., 2010]. Too large an y could result in awareness with recall [Liu et al., 1991], which is likely to cause the patient considerable psychological stress, while excessively low DOH values result in hypotension and an increase in long-term mortality [Monk et al., 2005]. Furthermore, variability in the DOH, which induces significant changes in blood pressure, are potentially harmful for the patient. In order to maintain hemodynamic stability, it is therefore of interest to quantify such variability.

Finally, it is desirable to minimize the duration of the emergence phase of anesthesia, resulting in faster recovery for the patient and increased availability of the operating room. Since no control signal is available during the emergence phase, it is only possible to affect its duration by control actions taken during the maintenance phase of anesthesia. The possibility to do so relies on individual control of propofol and remifentanil (or another drug pair with similar interaction properties). E.g., an increase of analgesic drug and corresponding decrease of hypnotic drug toward the end of the maintenance phase of anesthesia will achieve a decrease in emergence duration, while increasing the DOA.

The Varvel Measures

The Varvel measures were introduced to assess the estimation performance of TCI systems. Their intended purpose is to describe the fit between measured (blood sample) and estimated (PK model) plasma concentrations. This can be conducted either for an individual or a population. The individual case will be considered next.

The Varvel measures are based on the *median* of the relative error and its modulus, respectively. The original motivation for use of the median rather than the mean was the asymmetric appearance of data sets available to the authors of [Varvel et al., 1992]; most PK estimation errors were close to

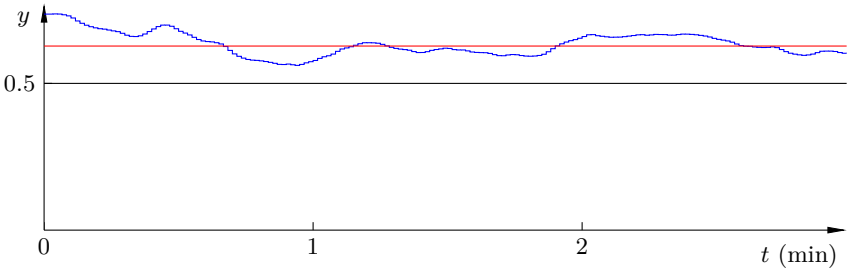

(a) Systematic small error.

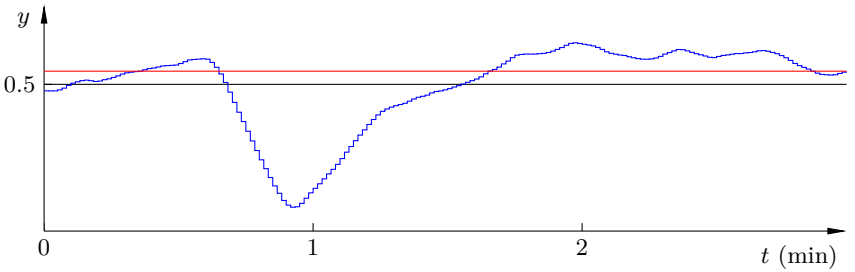

(b) Sporadic large error.

Figure 3.1 Two tentative maintenance phase DOH profiles (blue), with corresponding setpoint (black) and resulting median error (red).

the median, with few but distant outliers. This motivation, justified in the intended context, results in an unfortunate choice when adopted for EEG-guided DOH control. As mentioned above, $y \in (0.4, 0.6)$ is considered adequate. This suggests that a maintenance phase like the one in Figure 3.1(a) should be desirable to the one in Figure 3.1(b), while basing the error metric on the median has the opposite outcome. It can be argued that median-based measures provide inherent filtering and artifact removal. However, they make no distinction between artifacts, noise and momentary large errors which indeed reflect the DOH of the patient.

The Varvel performance measures are MDPE, MDAPE, divergence and wobble. They are defined, explained and discussed below. Denote by C_m the sample vector of measured plasma concentrations and by C_p, the corresponding estimates. The times corresponding to entries of C_m and C_p are in t and in the unit of hours. All vectors hold N elements.

The (relative) percentage performance error (PE) is defined as

$$\mathrm{PE} = 100\frac{C_m - C_p}{C_p}. \tag{3.1}$$

The division in (3.1) is to be interpreted as element-wise, making PE a vector quantity. PE is not reported as one of the Varvel measures, but rather used as the basis for their computation.

The definition (3.1) has been applied to EEG-guided DOH control in numerous publications by exchanging C_m for y and C_p for r. Some of these publications are listed in Appendix C. Such previous publications have made use of the BIS DOH scale, where the fully aware state corresponds to a value of 100 and the fully anesthetized state corresponds to a value of 0. This results in less error penalty whenever the DOH setpoint is closer to the fully aware state. However, the risk of the patient becoming aware requires particularly tight control in this region.

The median performance error (MDPE) is the median value of the PE between all samples:

$$\text{MDPE} = \text{median}(\text{PE}). \tag{3.2}$$

As such it captures the bias of the estimator, but not its variability.

The median absolute performance error (MDAPE) is defined as

$$\text{MDAPE} = \text{median}(|\text{PE}|). \tag{3.3}$$

As opposed to the MDPE, the MDAPE does not convey information regarding the error bias, but rather the representative error magnitude.

Divergence is the slope of the linear regression of |PE| against t:

$$\text{divergence} = \frac{t^T|\text{PE}| - N\bar{t}|\overline{\text{PE}}|}{t^T t - N\bar{t}^2}, \tag{3.4}$$

where the bars denote the mean operator. The unit of divergence is percent per hour and the measure aims at describing whether the error increases or decreases over time. An unstable control system will result in a positive divergence. Beyond concluding instability, the divergence is of little practical use. Three different y-profiles are plotted in solid together with a common setpoint of $r = 0.5$ in Figure 3.2. The respective divergences of these profiles are -26, -2 and 32 percent per hour, proportional to the slopes of the dashed lines. It is of arguable clinical significance when during the maintenance phase the error spike occurs, yet its temporal location strongly affects the divergence, while leaving all other of the Varvel measures unaffected.

Wobble is the last of the Varvel measures. It was introduced to capture variability in the estimator. Wobble is defined as the median absolute deviation between PE and MDPE:

$$\text{wobble} = \text{median}(|\text{PE} - \text{MDPE}|). \tag{3.5}$$

Wobble measures variability in the DOH. As such it is strongly affected by filtering of the measurement signal. In order to compare systems in terms

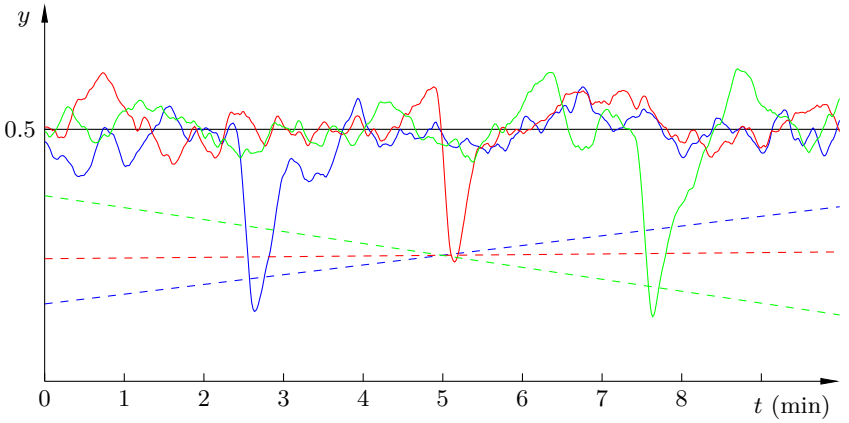

Figure 3.2 The solid lines show tentative DOH profiles, with the horizontal black line as setpoint. The divergence for each of these profiles is proportional to the slope of the correspondingly colored dashed line.

of wobble it is therefore essential that the same filtering is used. This is problematic when using the BIS monitor, as it uses a proprietary filtering algorithm and switches between several filters [Ionescu et al., 2011b].

The global score (GS) is not one of the Varvel measures, but was introduced in [Liu et al., 2006] as an attempt to score EEG-guided DOH control systems with one scalar:

$$\mathrm{GS} = \frac{\mathrm{MDAPE} + \mathrm{wobble}}{\text{fraction of time } y \in (0.4, 0.6)}. \tag{3.6}$$

Apart from characterizing performance by means of a singe scalar, the GS takes the clinical feasibility bounds from [Kelly, 2003] into account. Expanding the numerator of (3.6) results in

$$\mathrm{median}|\mathrm{PE}| + \mathrm{median}|\mathrm{PE} - \mathrm{median}(\mathrm{PE})|. \tag{3.7}$$

While the idea of one scalar performance measure is appealing, it is hard to intuitively interpret (3.7) and the clinical relevance of the GS has never been established.

It was concluded in [Varvel et al., 1992] that the population distribution of individually computed MDPEs and divergences are quite symmetric, while the corresponding MDAPEs and wobbles are slightly asymmetric. Consequently, different approaches for combining the individual measures to correspond to populations were discussed. The two-stage approach defines the population measures as the mean values taken over the population. A modification of the two-stage approach is the pooled-data approach, where

each individual is weighted by the reciprocal number of available samples. This is further elaborated in the variance-weighted approach, in which individuals are weighted by the reciprocals of the variances of the measures. Details of these pooling strategies are found in [Varvel et al., 1992], in which the authors recommend the variance-weighted approach but conclude that all approaches yield similar results.

Proposed Performance Measures

Below, performance measures more adequate for the evaluation of EEG-guided DOH control than the Varvel ones are proposed. As suggested above, it is relevant to use different measures of performance during the induction and maintenance phases of anesthesia. In fact, most closed-loop studies reporting the Varvel measures do so for maintenance phase data only.

Here it will be assumed that a vector Y, holding N DOH measurements, is available, together with the corresponding setpoint vector R. The not necessarily uniformly sampled time stamps of entries in Y and R are stored in T (unit: s). The vectors are assumed to be adjusted so that the first sample in T corresponds to the start of hypnotic drug administration. To simplify notation, the sections of $\{T, R, Y\}$ corresponding to the temporal phases of anesthesia being considered will be denoted $\{t, r, y\}$, each holding n elements.

Induction Phase Measures Two performance measures, reflecting the objectives outlined above, are proposed below.

Induction Duration (ID) is adopted from [Liu et al., 2006], where it was defined as the time elapsed from the start of hypnotic drug administration to the first moment when y rises to and remains above 0.4 for 30 consecutive seconds. This definition does not punish large drug boluses which rapidly achieve the desired goal but result in excessive overshoots. Furthermore, it only considers the setpoint $r = 0.5$, To account for this, staying above 0.4 is replaced by staying within $r \pm 0.1$ and an additional measure for characterizing overshoot is introduced.

The overshoot (OS) is defined as

$$\mathrm{OS} = 100 \cdot \max_k \frac{y_k - r_k}{1 - r_k}. \tag{3.8}$$

I.e., an overshoot of 100 % corresponds to $y = 0$, while an overshoot of 0 % corresponds to $y = r$. It is possible that the maximum overshoot occurs after the end of induction, as defined by ID. This can for instance be the case if there is a slow integrator in the controller, which builds up during the induction phase. It seems hard to device a robust, control system independent, rule to decide how much of the maintenance phase should be included in the evaluation of (3.8). The conservative approach in the thesis has therefore been to include the entire maintenance phase. As a consequence, OS is not

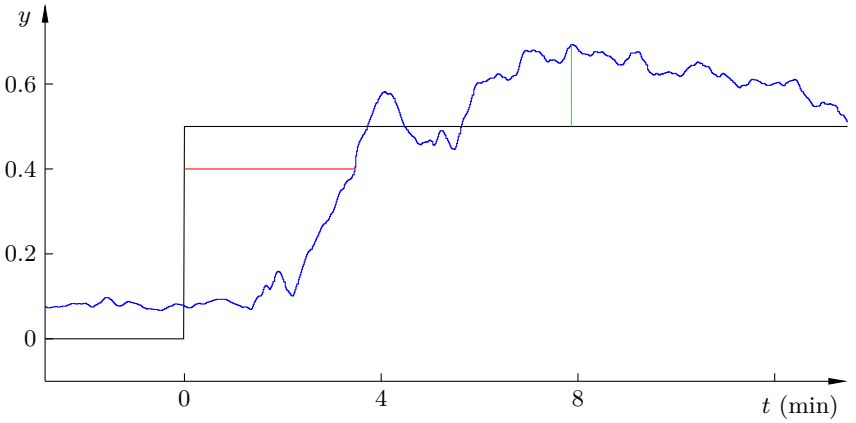

Figure 3.3 Graphical illustration of induction duration ID (red) and overshoot OS (green) using clinical DOH data (blue) with setpoint in black.

an induction phase specific measure. However, for most cases the maximum overshoot occurs during, or shortly after, the induction phase.

The definitions of ID and OS are illustrated in Figure 3.3 on clinical data from the iControl study described in Appendix B.2.

Maintenance Phase Measures The trapezoidal approximation of the integrated error (IE) is introduced to replace MDPE:

$$\mathrm{IE} = \sum_{k=1}^{n-1} \frac{t_{k+1} - t_k}{t_n - t_1} \frac{(r_{k+1} - y_{k+1}) + (r_k - y_k)}{2}. \tag{3.9}$$

The IE is normalized with respect to the maintenance phase duration. As opposed to the median, the IE punishes outliers (linearly). Furthermore, it is used as minimization criterion in existing controller synthesis strategies, of which [Garpinger and Hägglund, 2008] presents one example within PID control.

Since the IE only conveys information about the average error, its sole use as performance measure can be misleading; an error distribution which is balanced with respect to zero results in a small IE. This can be the case when e.g. the closed-loop system exhibits oscillatory behavior due to poor tuning. A measure replacing the MDAPE is therefore needed and readily obtained by taking the modulus of the sample-wise error in (3.9), yielding the integrated absolute error (IAE):

$$\mathrm{IAE} = \sum_{k=1}^{n-1} \frac{t_{k+1} - t_k}{t_n - t_1} \frac{|r_{k+1} - y_{k+1}| + |r_k - y_k|}{2}. \tag{3.10}$$

Variability in y can be quantified by the relative difference between the IAE and the IE. This is done by introducing the variability index (VI):

$$\mathrm{VI} = \frac{\mathrm{IAE} - \mathrm{IE}}{\mathrm{IAE}}. \tag{3.11}$$

The VI does not need to be explicitly reported as it is readily computable from the reported IE and IAE.

It is of interest to report how well the system manages to keep y within the clinically feasible range, i.e. within $r \pm 0.1$. Since the sign of the error is of clinical significance (when the error exceeds ± 0.1), it is justified to give separate measures for the percentage of time during maintenance that the error $e = r - y$ exceeds $+0.1$ (E^+) and falls below -0.1 (E^-), respectively. In case of sparse or nonuniform sampling, linear interpolation between consecutive samples can be used to determine the time instants when the maintenance phase control error crosses ± 0.1. respectively.

Emergence Phase Measure The emergence phase of anesthesia is defined to begin when administration of the hypnotic drug is terminated, see Section 1.1. The duration of the emergence phase can be robustly quantified by introducing the emergence phase rise time (ER), here defined as the 63 %, or $1 - e^{-1}$ rise time, commonly reported in other control applications. Note that the standard control nomenclature is somewhat confusing as the measurement signal is actually *decreasing* during the *rise* time.

This time is defined as that between end of hypnotic drug administration, at which instance the DOH setpoint was r_1 and the first time at which y crosses $r_1 - (1 - e^{-1})(r_1 - E_0)$. If the awake baseline level E_0 is not known, the default $E_0 = 0$ may be used. The ER is illustrated in Figure 3.4.

Population Measures Since all the proposed performance measures are unaffected by the duration, in terms of time or samples, of the underlying data, it becomes natural to weight each case equally in the population statistic.

Which statistic to use depends on the clinical aim. The *median* of each measure is adequate if the aim is to evaluate a system which should perform well in the majority of cases, but where a few cases of poorer performance are acceptable. At the other end of the scale, the *worst case* of each measure could be reported. In terms of conservatism, the *mean* lies between these two.

In order to produce comparability between studies it is suggested that at least the population mean $\pm$ standard deviation of ID, OS, IE, IAE, $\mathrm{E}^{\pm}$ and ER be reported. A convenient way to report these statistics together with worst case and median is the use of the modified box plot shown in Figure 3.5.

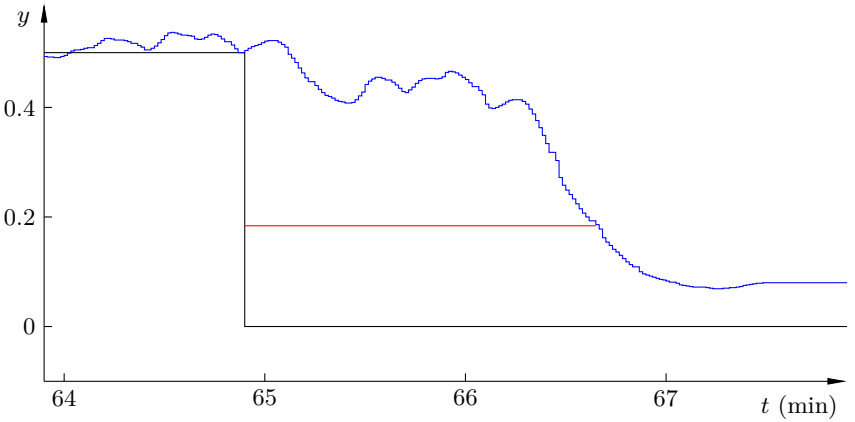

Figure 3.4 The 63 % emergence phase rise time (ER) (red), illustrated using DOH data from the iControl study (blue) with setpoint in black.

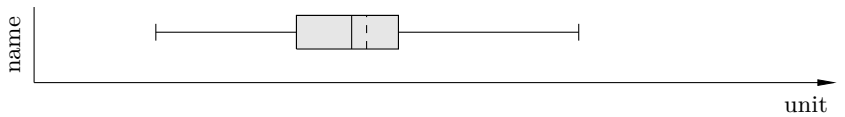

Figure 3.5 This modified box plot shows an example of how the worst case (whisker), standard deviation (box), mean (solid line) and median (dashed line) of ID, OS, IE, IAE, (VI), $E^{\pm}$ and ER can be reported in a comprehensive manner.

Reported Performance Measures

The proposed performance measures are reported in favor of the Varvel ones in connection to simulations presented in the thesis, which have not been previously published. Despite their shortcomings, the Varvel measures have become the gold standard for evaluation of closed-loop controlled anesthesia delivery systems. For this reason, they have been reported in the publications, enlisted in the Preface, upon which the thesis is based.

3.2 The iControl Study

Controller Tuning

This section describes the controller tuning procedure used in the iControl study. Details of the study, such as study population, clinical protocol, controller structure and parameters, are found in Appendix B. A photograph of the iControl closed-loop anesthesia system is shown in Figure 3.6 and a

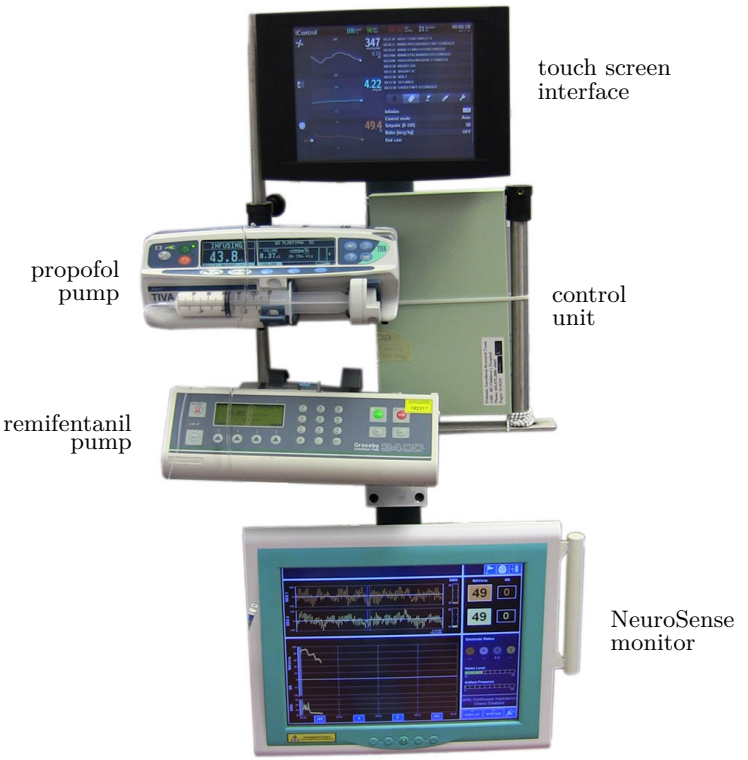

Figure 3.6 The iControl closed-loop anesthesia system.

screen dump of a its touch screen user interface is shown in Figure 3.7. The working environment of the anesthesiologist is shown in Figure 3.8, with the iControl device to the right.

The main challenges in tuning the propofol delivery controller were to provide adequate robustness to handle the inter-patient variability to drug sensitivity and attenuate disturbances caused by surgical stimulation and measurement noise, while maintaining reasonable setpoint tracking performance.

As outlined in Appendix B.2, the study population consisted of children, for which validity of available PKPD models have been debated [Coppens et al., 2011]. Consequently, a system identification study was performed in order to obtain models upon which to base the controller tuning. This study is outlined in Section 2.2 and Appendix B. A full presentation, including listing of model parameters is found in [van Heusden et al., 2013b]. For additional detail on the first part of the study, see [Soltész et al., 2012b].

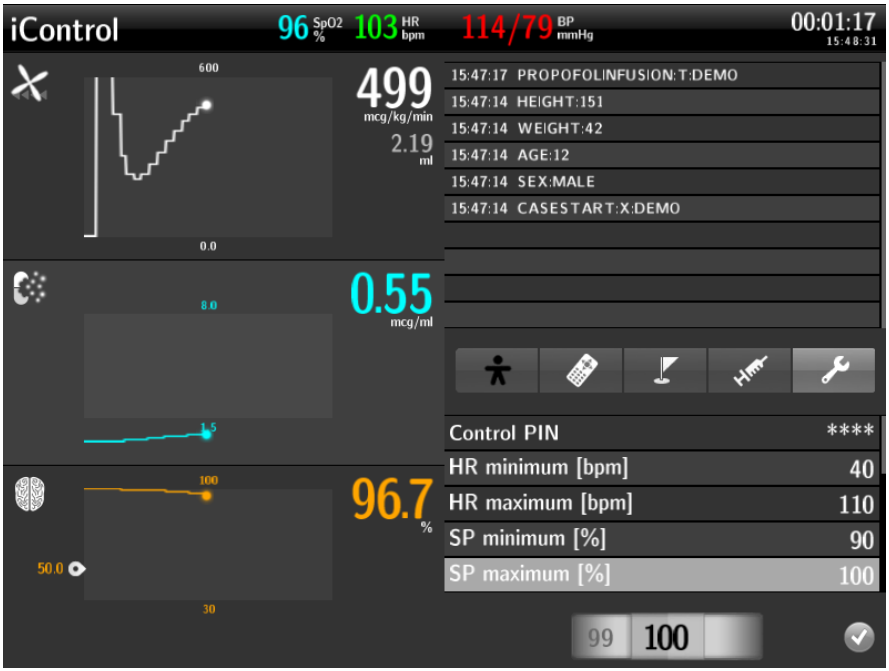

Figure 3.7 The iControl touch screen interface. The screen dump was taken while running in simulation mode.

The initial controller tuning was based on 14 patient models identified from open-loop data obtained during surgeries. Figure 3.9 shows the Bode plots of these models linearized around the nominal setpoint $E_o = r = 0.5$. Tuning of the PID and filter parameters leading to the version used during the initial 23 clinical closed-loop cases was performed based on these models. The robust PID tuning was seeded with the integrated absolute error (IAE) minimizing algorithm described in [Garpinger and Hägglund, 2008] applied to the linearized models. Subsequently, a manual iterative robust tuning procedure was performed. The resulting open-loop Bode plots were drawn for each available model combined with the tentative controller, as shown in Figure 3.10. In parallel, the behavior of the underlying nonlinear system in closed-loop was characterized by simulation, as shown in Figure 3.11. The figure shows simulated y-profiles for the 14 models; simulated induction of anesthesia is shown in Figure 3.11(a), the response to surgical stimulation, modeled by the output disturbance profile of Figure 2.12(c), is shown in Figure 3.11(b). Figure 3.11(c) shows the influence of sensor noise. Note that Figure 3.11(b) also reveals the behavior at setpoint steps as the setpoint and output disturbance signals enter the system at the same location.

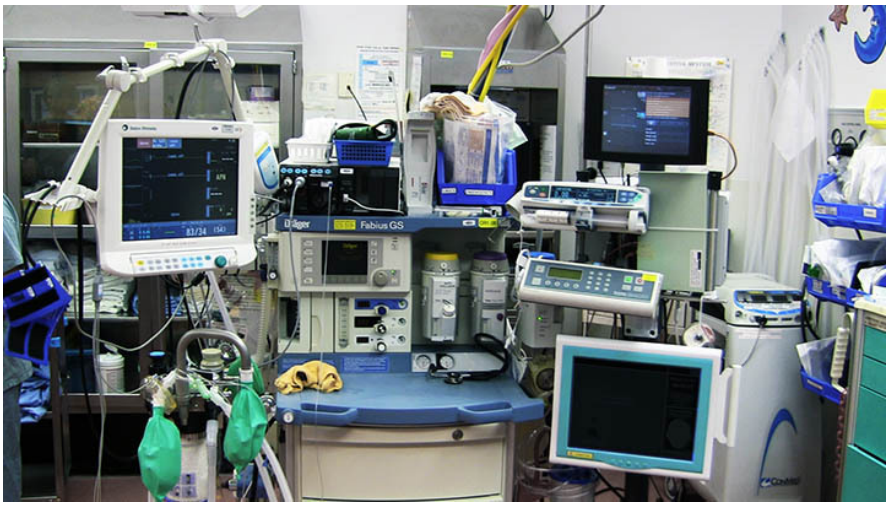

Figure 3.8 The working environment of the anesthesiologist. The photograph is taken in one of the operating rooms of the BC Childrens Hospital, Vancouver, Canada.

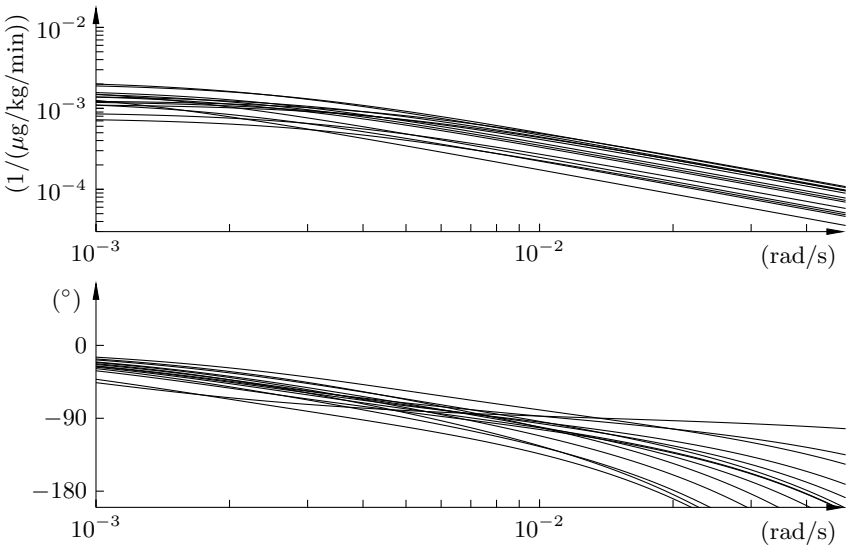

Figure 3.9 Bode plots of patient models obtained from open-loop data, linearized around $E_o = 0.5$. The input and output are propofol infusion (μg/kg/min) and $y \in (0, 1)$, respectively.

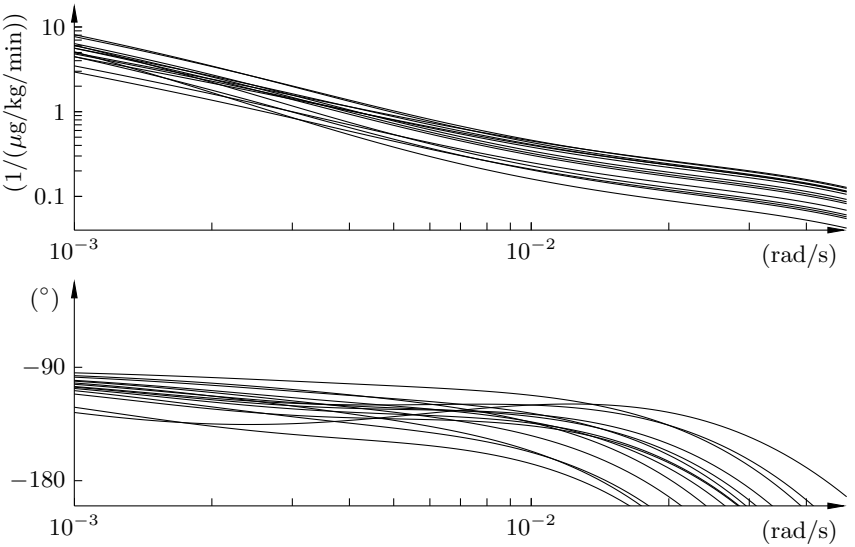

Figure 3.10 Open-loop Bode plots obtained by combining the initial controller tuning from Appendix B.2 with each of the 14 models identified from clinical open-loop data.

Due to the limited number of available models, the initial tuning was deliberately conservative. Gain margins of the linearized system were in the $(4.0, 25.2)$ range, with a mean of 8.3, phase margins were in the $(52°, 72°)$ range, with a mean of 65° and the peak sensitivity M_s was in the $(1.1, 1.5)$ range, with a mean of 1.2. The variation in these robustness measures further indicate the presence of large inter-patient variability in the response dynamics to propofol.

Clinical Outcome – Phase One

The clinical outcome of the initial 23 closed-loop cases of the iControl study are reported in [Soltész et al., 2012b]. Figure 3.12 shows the DOH measurement profiles together with the infusion profiles of these cases. Induction phase data is shown in blue, maintenance phase in red and emergence phase in green. The black triangles mark the beginning and end of of each maintenance phase.

In some cases, the anesthesiologist decreased the DOH setpoint toward the end of the procedure, in order to shorten duration of the emergence phase. This motivates plotting the error e in favor of the measurement signal y. Error profiles corresponding to Figure 3.12 are therefore shown in Figure 3.13.

At some occasions, high amplitude spikes are present in the control signal. Some of these are the result of manually superimposed boluses, which are

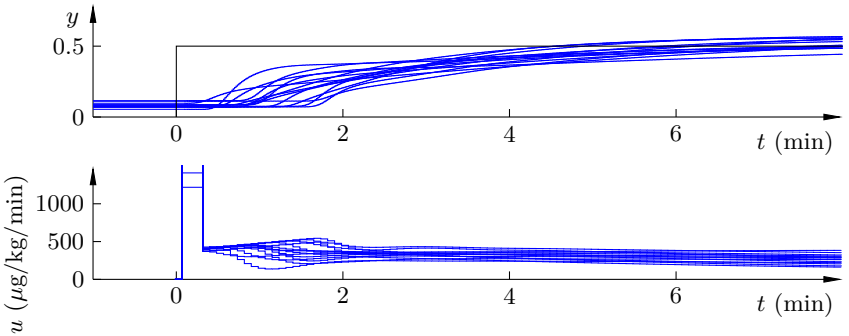

(a) Induction.

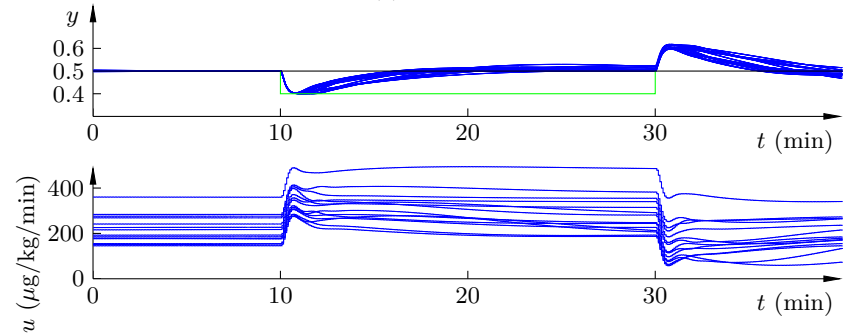

(b) Stimulation.

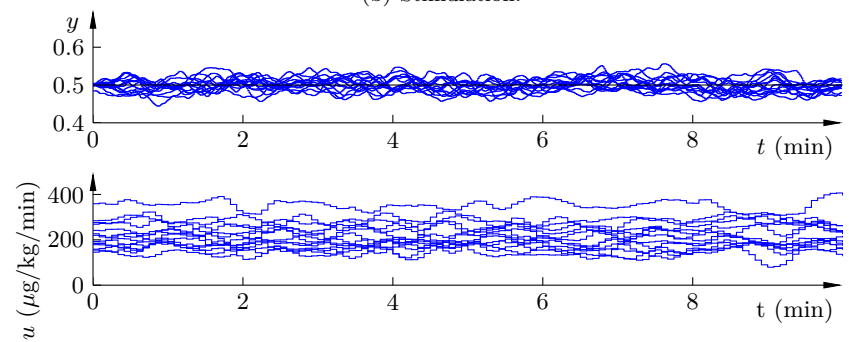

(c) Measurement noise.

Figure 3.11 Simulated closed-loop anesthesia for the 14 available patient models, used in the robust PID tuning procedure (blue). The setpoint and additive output disturbance profiles are shown in black and green, respectively.

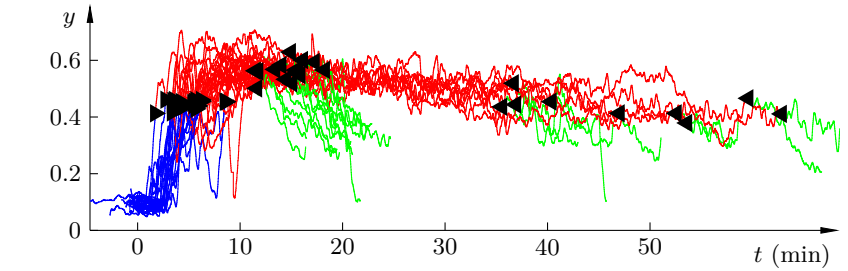

(a) DOH measurement y.

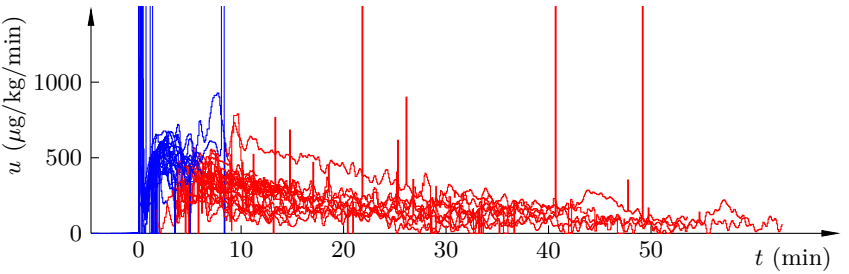

(b) Propofol infusion rate u.

Figure 3.12 Outcome of the initial 23 closed-loop controlled cases. Induction, maintenance and emergence phase data is shown in blue, red and green, respectively. Black triangles mark the beginning and end of each maintenance phase.

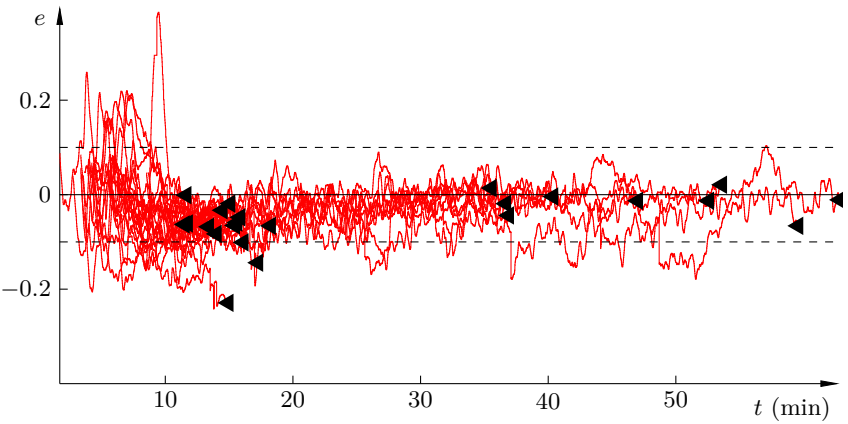

Figure 3.13 Maintenance phase error e during the initial 23 closed-loop controlled cases. The dashed black lines mark the ±0.1 error interval. The end of each data set is marked with a black triangle.

given by the anesthesiologist, who can act as a feed-forward controller from anticipated increases in nociceptive stimulation. The other source for spikes is the switching from closed-loop controlled to TCI mode, which occurs when e.g. the measurement signal quality is below a threshold. A potential strategy for avoiding these spikes is outlined in Section 3.3.

Out of the 23 newly available data sets, 14 were manually deemed suitable for system identification, which extended the available patient model pool size from 14 to 28. Details of the identification of these models are found in [van Heusden et al., 2013b]. The DOH measurements from induction of anesthesia for three of the 14 closed-loop cases used for identification are shown in Figure 3.14(a) (solid) together with the ones obtained through noise-free closed-loop simulations (dashed). Corresponding propofol infusion profiles are shown in Figure 3.14(a). The identified models were driven in closed-loop using the same controller and setpoint profiles as in the corresponding clinical cases. Due to the presence of disturbances it is not feasible to compare such simulations with clinical data beyond induction of anesthesia and there might be slight discrepancies caused by unmodeled disturbances also during the induction phase. As can be seen in Figure 3.14(b), there is a discrepancy between the actual (solid) and simulated (dashed) infusion profiles. The good model fits (similar to the one shown in Figure 2.6) together with the temporal irregularity of the discrepancies suggest that they are due to disturbances rather than model error. Thus, care should be taken when relying on identified models, even when the identification data was collected during induction of anesthesia.

In general, it holds that the clinical and simulated inductions were similar. However, the overshoot upon induction was slightly larger for the clinical cases. This can be attributed to the difference in identification input characteristics, combined with the identifiability issues reported in Section 2.2. I.e., the open-loop cases typically had a higher initial propofol infusion rate, resulting in a fast response.

Controller Re-tuning

With the availability of 14 additional models from the closed-loop study and validated safety of the system, the controller was re-tuned. The tuning procedure was not changed, but now incorporated both the 14 initially available models from open-loop experiments and the additional 14 models from the conducted closed-loop experiments. The tuning objective was to decrease duration of induction while improving disturbance attenuation.

Gain margins with the final re-tuned controller applied to the 28 linearized patient models were in the $(1.9, 16.5)$ range with a mean of 3.6. The phase margins were in the range $(29°, 70°)$ with a mean of 49° and the corresponding values for the maximal sensitivity magnitude were $(1.1, 2.4)$ and 1.5,

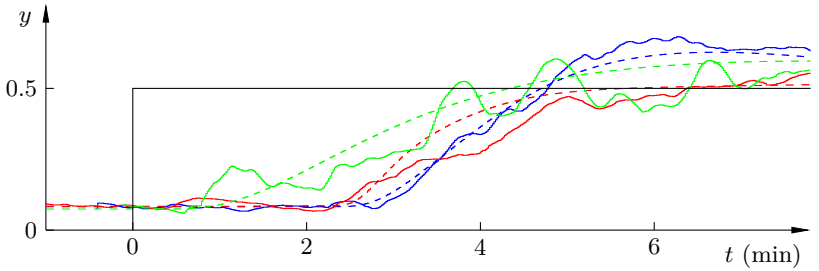

(a) DOH measurement y.

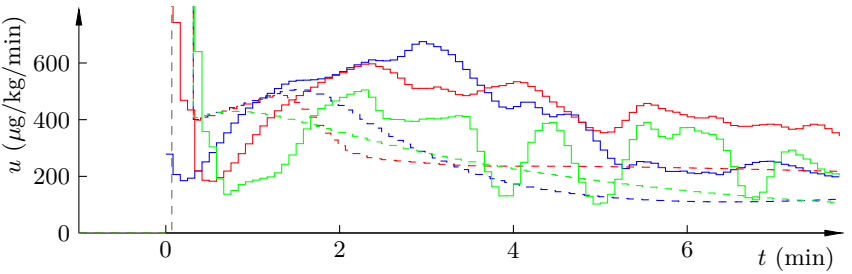

(b) Propofol infusion rate u.

Figure 3.14 Induction phase y-profiles and corresponding infusion rate u-profiles for three of the 14 initially modeled closed-loop cases are shown (solid) together with simulated outcomes (dashed). The common setpoint is shown in black.

respectively. The worst case here was caused by an outlier yielding a notably high value. It was, however, deemed acceptable based on the conservatism inherent from the system identification procedure described in Section 2.2.

In order to compare the old and new tuning, the robustness measures of the new tuning as applied to the initially available 14 models are relevant. These are: gain margin range $(2.1, 25.2)$ with mean 4.6, phase margin range $(38°, 72°)$ with mean $56°$ and maximal sensitivity magnitude range $(1.1, 2.1)$ with mean 1.4.

Clinical Outcome – Phase Two

The re-tuned controller was evaluated in 79 cases, of which 8 cases were conducted with candidate tunings and the remaining 71 with the final version reported in Appendix B.2. Figure 3.15, corresponding to Figure 3.12, shows the measured variable y together with the control signal u, for each of these cases. The maintenance phase errors $e = r - y$ are compiled in Figure 3.16, corresponding to Figure 3.13. Figure 3.17 shows three relatively long last-

ing cases from the set of 71 shown in Figure 3.15. Each case is drawn in a separate color and the correspondingly colored triangle marks the end of the maintenance phase for the case.

Closed-Loop Performance

The combined performance of the cases using the initial and re-tuned controllers described above are reported in terms of the Varvel measures in [van Heusden et al., 2013b]. The same publication also showcases the performance of individual representative cases. The performance measures proposed in Section 3.1 and [Soltész et al., 2013a] have been computed for the 102 closed-loop cases and are reported as modified box plots in Figure 3.18. See [van Heusden et al., 2013a] for a listing of the Varvel measures. Spontaneous breathing was successfully maintained in most cases. During 11 out of the 102 cases, episodes of apnea or airway obstructions were, however, recorded. Details on these cases are found in [West et al., 2013]. Results are further discussed in Chapter 4.

3.3 Simulation Studies

Anesthesia Simulator

The development and verification of the control system described in the thesis relied on the ability to evaluate patient models and controllers in a simulation environment. For this purpose, an application-specific simulator was developed in the Simulink language, tightly integrated with Matlab (The MathWorks Inc., Natwick, USA). The simulator was designed in a modular fashion and allowed for straight forward loading of patient models for propofol and remifentanil, output disturbance and noise models, reference profiles and closed-loop controllers. The top layer of the Simulink model hosting the simulator is shown in Figure 3.19.

In this section, the simulator has been utilized to demonstrate concepts not yet implemented in the iControl system, but with future potential.

Individualized Control

So far, all controllers considered in the thesis have been tuned based on the availability of batches of patient models. It was mentioned in Section 2.2 that parameters of patient models identified from maintenance phase data are likely to be biased by unmeasurable output disturbances. This makes the application of continuously adaptive control schemes potentially riskful due to the possibility of parameter drift caused by such bias. However, it is possible to obtain models from induction phase data, which is often not influenced by such disturbances. This was how the model batches used to

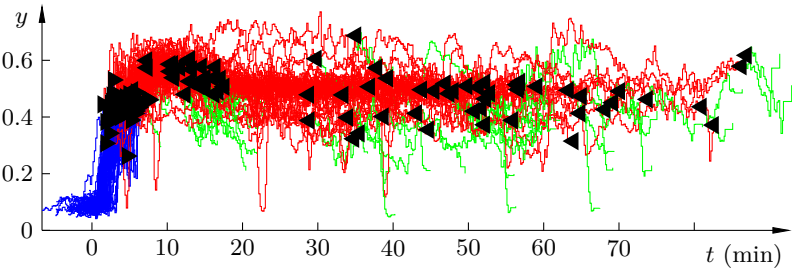

(a) DOH measurement y.

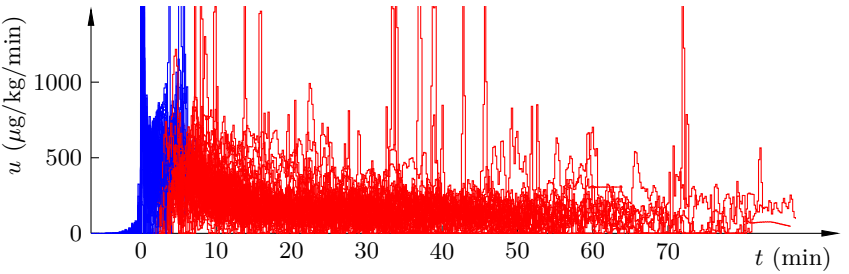

(b) Propofol infusion rate u.

Figure 3.15 Outcome of the 71 closed-loop controlled cases, facilitating the re-tuned controller. Induction, maintenance and emergence phase data is shown in blue, red and green, respectively. Black triangles mark the beginning and end of each maintenance phase.

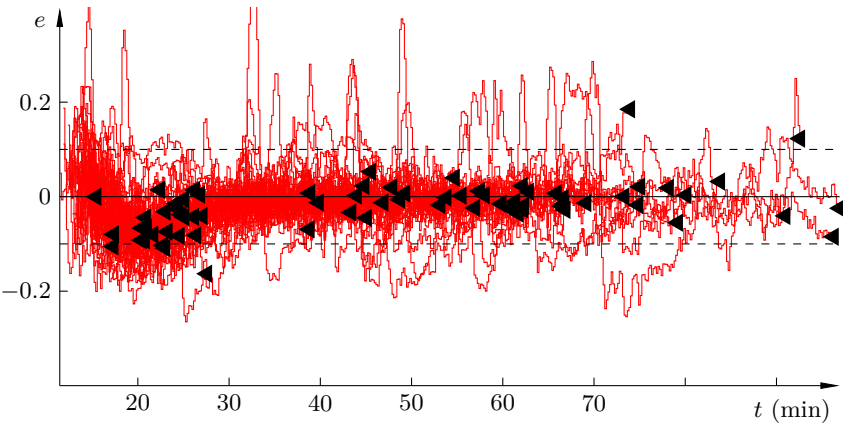

Figure 3.16 Maintenance phase error e during the 71 closed-loop controlled cases, facilitating the re-tuned controller. The dashed black lines mark the ± 0.1 error interval. The end of each data set is marked with a black triangle.

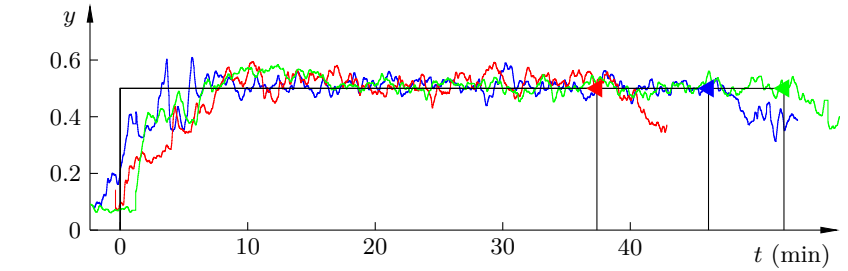

(a) DOH measurement y.

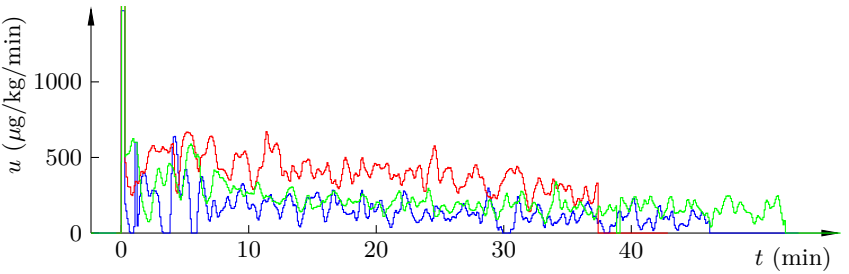

(b) Propofol infusion rate u.

Figure 3.17 Three relative long cases (blue, red, green), from the total of 71 cases shown in Figure 3.15. Correspondingly colored triangles mark the end of each maintenance phase. Setpoint profiles are drawn in black.

tune the iControl system were obtained [van Heusden et al., 2013b]. A similar, but fully automated, identification procedure to that in [van Heusden et al., 2013b] was proposed and demonstrated in Section 2.2. Although a more exciting identification input would be much desired in order to avoid the issues explained in Section 2.2, it is possible to identify at least a subset of the process model parameters based on available data.

The idea briefly presented here, and elaborated in [Soltész et al., 2013b] and [Soltész et al., 2011], is to make use of two controller tunings. The controller used for induction of anesthesia is not different from the ones which have been previously mentioned and discussed. However, if the automated identification method, such as the one proposed in Section 2.2, yields a valid model upon induction of anesthesia, the controller is re-tuned based on this model. This re-tuning of the controller can be automatically conducted, using available robust tuning tools. In [Soltész et al., 2013b] it was done by minimizing the IAE under a maximum sensitivity magnitude constraint.

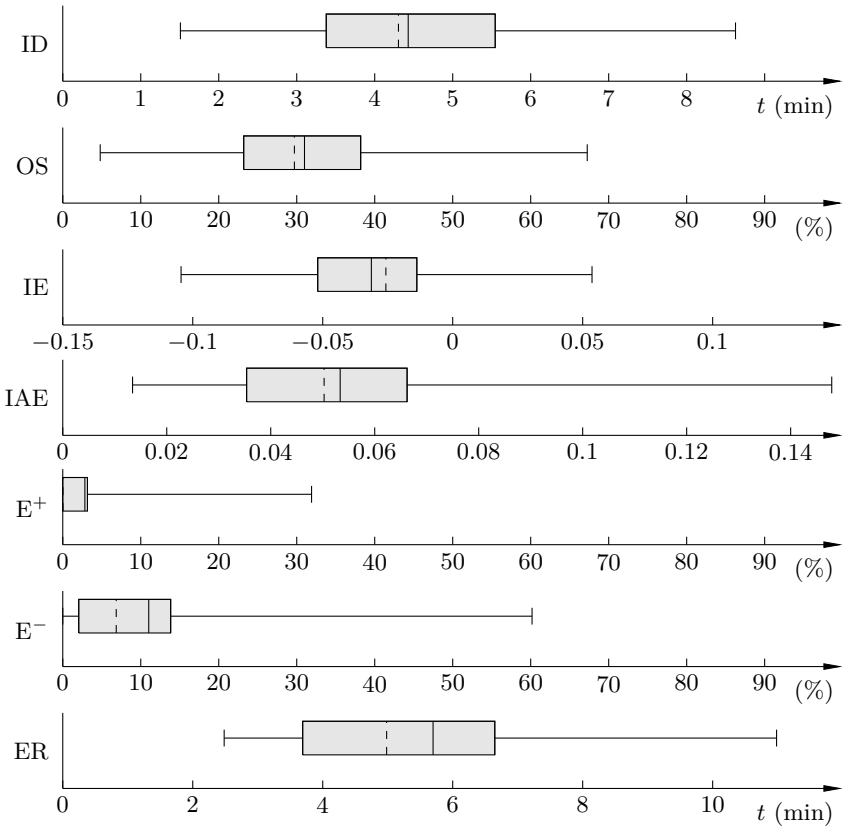

Figure 3.18 Performance of the iControl system during the 102 cases reported in [van Heusden et al., 2013b]. The modified box plots are explained in Figure 3.5.

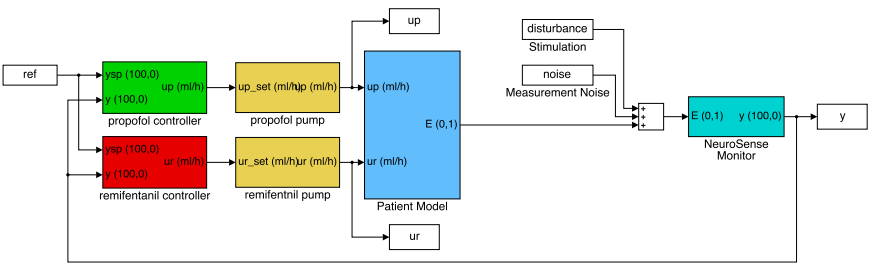

Figure 3.19 Top layer of the Simulink model used to evaluate patient models and controllers in simulation.

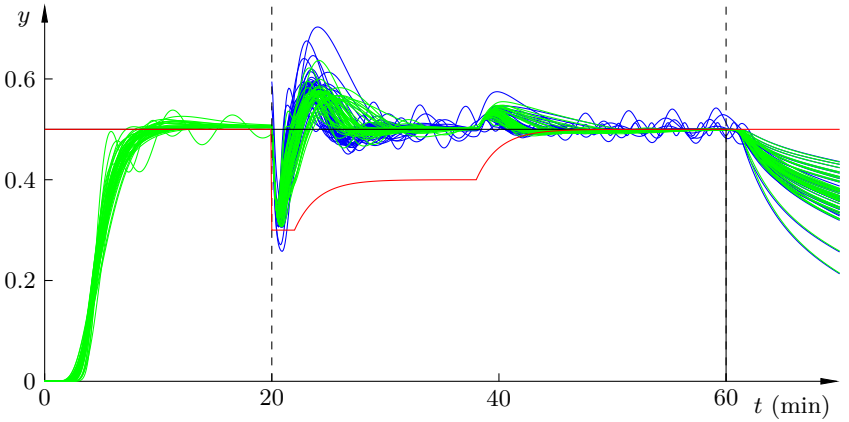

Figure 3.20 Simulations demonstrating the concept of individualized control on 44 PKPD models. Blue and green lines show performance of nominal and individualized controller, respectively. The red line shows the added output disturbance. The setpoint profile is drawn in solid black. Beginning and end of the maintenance phase is marked by vertical dashed black lines.

The re-tuned controller is tailored for the current patient and can therefore be made more aggressive than the induction phase controller, without compromising robustness.

Once the new controller is synthesized it only remains to initiate its state (integrator and measurement signal filter) to obtain a smooth, or bumpless, transfer at the instance of switching.

In [Soltész et al., 2013b] the proposed scheme was demonstrated on a batch of 44 propofol PKPD models, previously published in [Dumont et al., 2009]. The blue lines in Figure 3.20 shows the simulated DOH measurements obtained when using a controller tuned to accommodate the entire batch of 44 models, while the green lines show the outcome from using the proposed individualization scheme. At $t = 20$ min the process model identification and controller re-tuning take place, while an additive output disturbance profile (red) from [Dumont et al., 2009] is applied to mimic a surgical procedure. One can clearly see that the individualized controllers attenuate the disturbance more efficiently. Note that only green lines have been drawn during the induction phase of anesthesia, here defined as up to $t = 20$ min, as there is no difference in tuning between the batch and individualized scheme during this temporal phase.

Although the exact performance gain of the proposed scheme depends highly on the involved models, the simulation result from [van Heusden et al., 2013b] shown in Figure 3.20 gives a clear indication of what can be achieved.

Here the IAE caused by the disturbance profile is decrease on average by 25 %.

Smooth Mode Switches

When switching back and forth between manual, TCI and closed-loop mode, it is desirable to have a smooth transition both in the measurement y and control signal u. One reason for this is that a system with discontinuous behavior can be perceived as irrationally acting by the supervising clinician.

Apart from the possibility of manual mode switches, switching from closed-loop to TCI mode is set to occur automatically in the iControl system if the signal quality falls below a threshold or if the measurement signal is lost altogether. The iControl system defines signal quality in terms of the SQI and the SR, introduced in Section 2.1.

The model on which TCI is based in the iControl system is driven by the infusion rate u, but is not affected by the measurement y even at times when the latter signal is available and reliable. Due to inter-patient variability in propofol sensitivity combined with unmeasurable disturbances, it is therefore likely that the state of the TCI model drifts from the state of the actual patient. Furthermore, the TCI algorithm, adopted from the open source Stanpump TCI [Shafer and Gregg, 1992], is such that it tries to transition the model output to the setpoint in minimum time without overshoot. This essentially corresponds to a bang-bang controller, which yields a bolus at the instance the system is switched from closed-loop or manual mode to TCI if $y < r$. This behavior explains some of the spikes in Figure 3.12(b) and Figure 3.15(b) (in which the remaining spikes represent manually issued boluses).

An alternative proposed here is to let the input–output pair $\{u, y\}$ drive the discretized equivalent of the state observer:

$$\begin{aligned}\dot{\hat{v}}(t) = &-\frac{1}{\hat{T}}\hat{v}(t) + \frac{\hat{K}}{\hat{T}}u(t-\hat{L}) + \\ &K_o\left(\frac{1-\hat{E}_0}{1-y_{\text{raw}}} - 1 - \hat{v}(t)\right)\end{aligned} \tag{3.12}$$

$$\hat{y}_{\text{raw}}(t) = 1 - \frac{1-\hat{E}_0}{1+\hat{v}(t)}. \tag{3.13}$$

The first two terms within the rightmost bracket of (3.12) are the inverse of the Hill function (1.17) with parameter $\gamma = 1$, see (2.14). It was concluded in Section 2.2 that the use of such exact linearization can lead to large errors if there is a mismatch between $\hat{\gamma}$ and γ, see (2.5). However, parameters of the FOTD models used in (3.12) and described in Section 2.2 are obtained

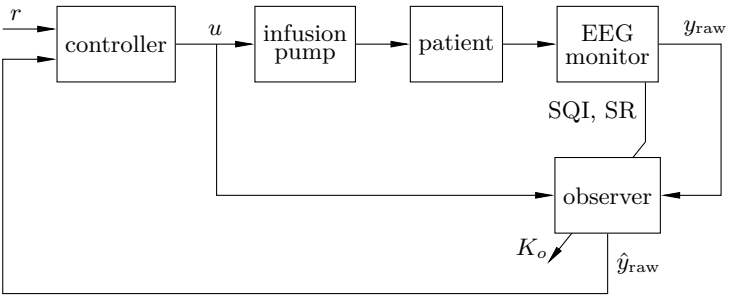

Figure 3.21 Block diagram showing the use of a observer with variable gain, designed to handle signal quality changes and mode switches.

under the structural assumption that $\gamma = 1$, which justifies the inversion of the Hill function in (3.12).

The behavior of the observer is characterized by its gain parameter K_o. When $K_o = 0$, the output $\hat{y}_{\text{raw}}$ depends entirely on the model and does not take the measurement y_{raw} into account. In the other extreme case, when $K_o \to \infty$, it holds that $\hat{y}_{\text{raw}} = y_{\text{raw}}$, i.e. the measurement signal is used as estimate and the model is ignored.

It is convenient to introduce the parameter K'_o:

$$K_o = \frac{1}{K'_o} - 1, \tag{3.14}$$

which, with a slight abuse of notation, maps the K'_o range $(0, 1)$ to the K_o range $(\infty, 0)$.

The idea proposed here is to use $\hat{y}_{\text{raw}}$ as measurement signal for the same controller in both closed-loop and TCI mode, as shown in the block diagram of Figure 3.21. Switching to TCI mode is conducted simply by setting $K'_o = 1$, while pure closed-loop mode corresponds to $K'_o = 0$. Furthermore, it is possible to use values $0 < K'_o < 1$ when in closed-loop mode with limited signal quality. One candidate way of achieving this is to let K'_o be a monotone function of the signal quality indices SQI_l and SQI_r combined with the suppression ratios SR_l and SR_r:

$$K'_o = \left(\frac{\text{SR}_l + \text{SR}_r}{2}\right)\left(1 - \frac{\text{SQI}_l + \text{SQR}_r}{2}\right). \tag{3.15}$$

Figure 3.22 shows an example with clinical data $\{u, y\}$ up to time $t = 30$ min, during which it is assumed that $\text{SQI}_l = \text{SQI}_r = 1$ and $\text{SR}_l = \text{SR}_r = 0$. At time $t = 30$ min, the measurement y_{raw} is assumed to be lost. The observer gain parameter is consequently set to $K'_o = 1$ and the feedback loop is now closed over the patient model characterized by $\{\hat{K}, \hat{T}, \hat{L}\}$. Since

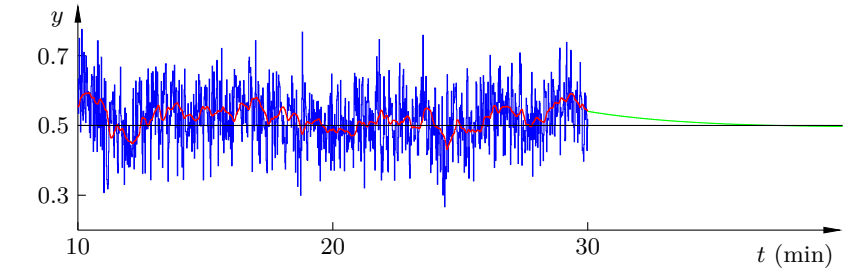

(a) DOH signals y_{raw} (blue), y (red) and $\hat{y}_{\text{raw}}$ (green) with setpoint (black).

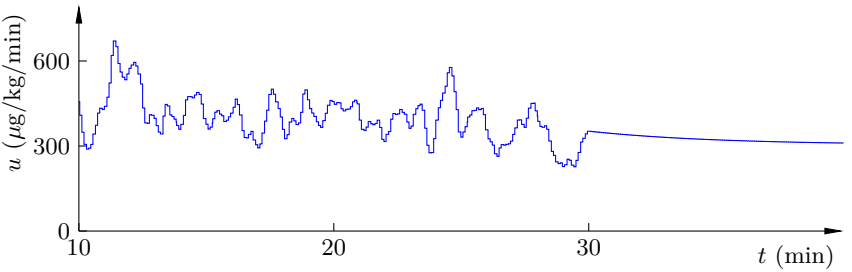

(b) Propofol infusion rate u.

Figure 3.22 The figure shows data form a clinical case until time $t = 30$ min, where the measurement signal is assumed to be lost and is replaced by the observer output.

the scheme has not been clinically evaluated, the result for $t > 30$ min in Figure 3.22 is the outcome of a simulation. The section shown in green in Figure 3.22(a) shows the estimate $\hat{y}_{\text{raw}}$, which explains the lack of noise seen in the measurements y_{raw} (blue) and y (red).

It should be mentioned that the scheme presented in this section has only been conceptually demonstrated. In particular, more effort needs to be put into the investigation of its behavior in the $0 < K'_o < 1$ region, before involving it in a clinical trial.

Integrator Anti-Windup

The clinical results shown in Figure 3.12 and Figure 3.15 indicate a slow settling time of the control error upon induction of anesthesia. A contributing reason to this is that the integrator of the controller builds up during the initial assumed model delay L and the subsequent traversal of the nonlinearity (1.17). This can be seen for one of the clinical cases in Figure 3.23. The measurement y is shown in Figure 3.23(a). The corresponding control signal is shown in Figure 3.23(b) (blue) together with its integrator term (red).

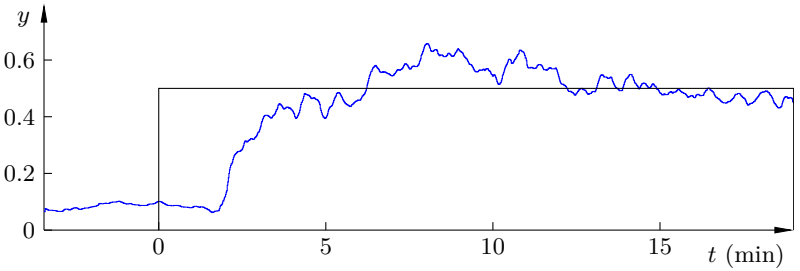

(a) DOH measurement y (blue) with setpoint (black).

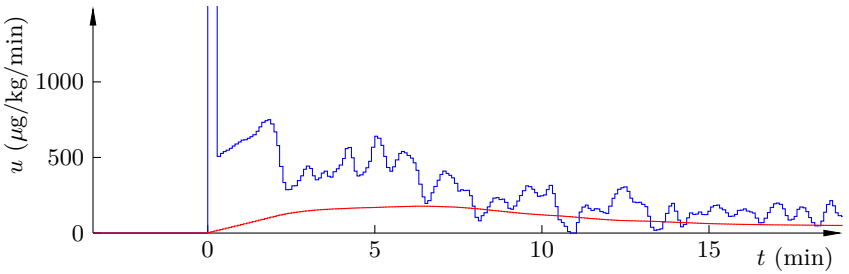

(b) Propofol infusion rate u (blue) and integral term of the control signal (red).

Figure 3.23 One case from the clinical study, showing how integrator build-up results in slow settling upon induction of anesthesia.

Standard integrator anti-windup strategies such as e.g. conditional integration mentioned in Appendix B.2, and dynamic tracking [Åström and Hägglund, 2006], are based on actuator saturation and hence do not prevent this behavior. A simple improvement to the system can be made by only activating integrator updates once a threshold clinical effect $y_{\min}$ has been reached for the first time. This is illustrated in Figure 3.24 through a a simulation example, based on a patient model identified from the data shown in Figure 3.23. The nominal measurement and control signals are shown in blue in Figure 3.24(a) and Figure 3.24(b), respectively. The corresponding outcome achieved by only activating the integrator once $y > y_{\min} = 0.21$ are shown in red. The integrator state is shown in green and black in Figure 3.24(b) for the nominal and proposed strategy, respectively.

For the strategy to be successful, it is essential that the clinical effect y indeed reaches the threshold value $y_{\min}$. In the example of Figure 3.24 this was ensured by dimensioning the initial bolus, described in Section 1.1, based on the 41 patient models identified from clinical data in Section 2.2. These models are normalized by patient body mass. Knowing the mass of the current patient, the bolus was designed to precisely bring the patient to 80 %

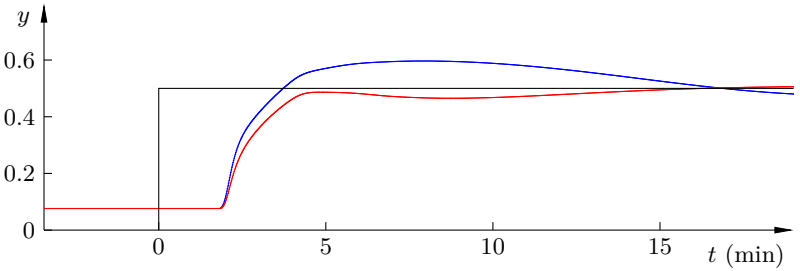

(a) DOH measurement y.

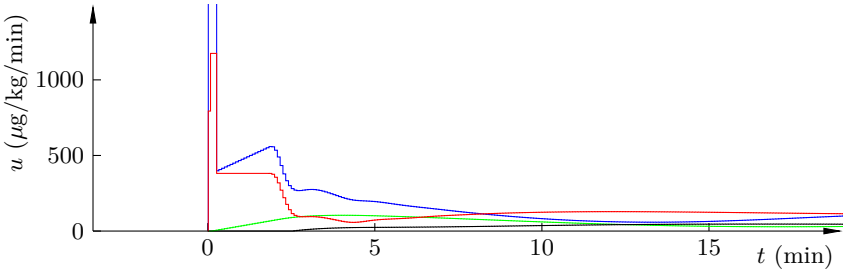

(b) Propofol infusion rate u and corresponding integral term.

Figure 3.24 A simulation showing the benefit of threshold-triggered integration. Measurement y and input u are shown in blue and red for the nominal and proposed strategies, respectively, with setpoint (black). The integrator state is correspondingly shown in green and black.

of the reference clinical effect assuming the most propofol sensitive model of the batch. I.e., for a reference of $r = 0.5$, the bolus was dimensioned to bring the most propofol sensitive model to $y = 0.4$. The threshold $y_{\min}$ was selected to be 80 % of the maximum clinical effect, which the bolus would result in assuming the least propofol sensitive patient model. The strategy will always be feasible assuming that the full propofol sensitivity variability is captured by the model population, with a margin of 20 %. In case this criterion is not met, the integrator is activated regardless of y, 3 min after the beginning of propofol infusion.

3.4 Control of Analgesia

Background

To this point, the focus of the thesis has been control of the DOH using propofol. It has been assumed that an adequate DOA can be achieved by

manual dosing of remifentanil, or another analgesic drug. There is a PD interaction between propofol and remifentanil, for which models were presented in Section 1.3 and further detailed in Section 2.3. No explicit attention was given to this interaction in the iControl study presented in Appendix B.2 and Section 3.2. Instead, the effect of remifentanil on the DOH was regarded as an output disturbance, similar to the ones caused by surgical stimulation. This was acceptable in the context of the study, as identical remifentanil dosing protocols were used during data collection for identification and the subsequent closed-loop controlled trials.

Directly controlling the DOA is problematic, as there exist no reliable monitors for it, which has already been mentioned in Section 1.1. However, it was outlined in Section 2.2 that changes in the surgical stimulation level, and hence the DOA, can be realistically modeled as additive output disturbances on the DOH. Such changes typically occur rapidly, while changes in the DOH caused by the infusion or metabolism of propofol occur at a much slower time scale determined by the propofol PK dynamics explained in Section 2.2. To illustrate this, the Bode magnitude curves for one representative propofol (blue) and remifentanil (red) PK model have been drawn side by side in Figure 3.25, together with their -3 dB bandwidths (dashed). The propofol PK is from a model identified using data from one of the iControl cases, published in [Soltész et al., 2012a]. The remifentanil PK was computed from biometric parameters of the same patient, using a formula for children with body mass as its only parameter and previous published in [Rigby-Jones et al., 2007]. For ease of comparison, both models have been scaled to unity static gain. The separation in time scale, apparent in Figure 3.25, makes it possible to detect changes in the DOA from the DOH signal y.

Due to the PD interaction, the DOH can be affected by altering the infusion rate of either drug. Remifentanil can be regarded as a fast actuator in this context, as it acts and is metabolized at a much faster time scale than propofol; seconds rather than minutes. While propofol has a large clinically feasible range in terms of v_p, the normalized effect site concentration v_r for remifentanil is confined to a narrower clinically feasible range. Consequently, when controlling the DOH, propofol can be viewed as a slow actuator with a wide range, and remifentanil as a fast actuator with narrow range. The fast actuator can be utilized to counteract disturbances in y, which are too rapid to be suppressed by the slow actuator. As mentioned above, such rapid changes in the DOH are most likely caused by underlying changes in the DOA. Correcting for them using the remifentanil infusion rate therefore makes sense; a rapid negative change in y indicates an inadequate level of analgesia and it is appropriate to counteract it with a momentary increase in remifentanil infusion rate and vice versa.

There have been previous attempts to simultaneously control the DOH and DOA using propofol and remifentanil, respectively. In [Liu et al., 2012]

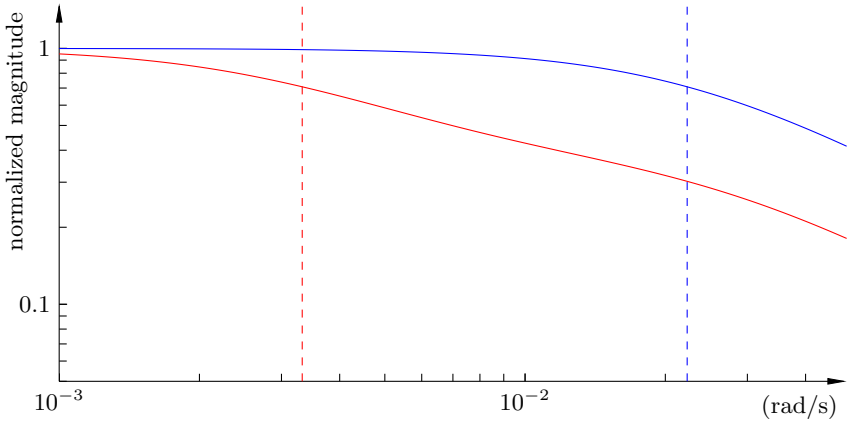

Figure 3.25 Bode magnitudes of one representative propofol PK model (blue) and one representative remifentanil PK model (red), both normalized to unity gain.

a rule-based approach, mimicking the behavior of an anesthesiologist is employed. A simulation study utilizing an MPC for the two drugs was presented in [Ionescu et al., 2011a]. Results from simulations using a fuzzy approach are presented in [Mahfouf et al., 2005].

The following section presents a control architecture for simultaneous control of the propofol and remifentanil infusion rates, based on a modified mid-ranging controller structure [Allison and Isaksson, 1998]. Advantages of the proposed architecture include modularity, in that the remifentanil loop is a pure addition to the existing propofol control system, and the possibility to gradually move from open- to closed-loop controlled remifentanil infusion, by increasing a single gain parameter.

Architecture and Tuning

With the availability of the measured DOH, propofol and remifentanil infusion rates and PK models as well as the PD interaction model, it is possible to construct a soft sensor for the DOA signal. Precise reconstruction is not feasible due to the sensitivity caused by the approximate nature of existing process models, as explained in Section 2.2. The approach taken in [Soltész et al., 2012a] and reviewed here, is rather to relate the high-frequency content in the DOH measurement y to changes in the DOA and consequently use it dose remifentanil. This single input, multiple output (SIMO) approach is justified by the previous discussion and its aim is to yield a mid-ranging control behavior, where propofol is the slow actuator with large range, while remifentanil is the fast actuator with narrow range. A block diagram illustrating how this can be achieved is shown in Figure 3.26. The signal y_f is a

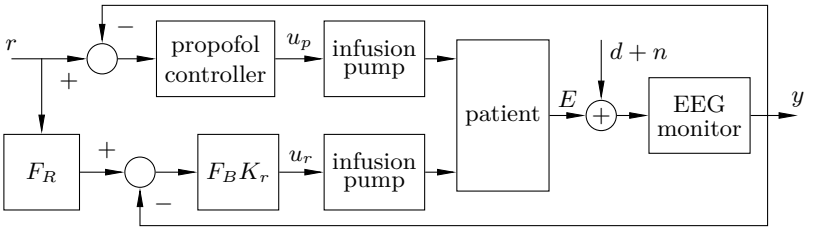

Figure 3.26 Block diagram showing the DOH control system structure used in iControl, augmented with the remifentanil controller proposed in the current section.

band-pass filtered version of the DOH measurement y. Its role is to reflect changes in the DOA and it can therefore be regarded as the output of a simple DOA soft sensor. Since the remifentanil controller only acts on transient changes in the DOA, the steady state behavior is not of particular interest. At the same time, there is no model which can be used to produce reliable DOA predictions. Consequently, a simple proportional controller is used.

The remifentanil controller is a pure augmentation to the existing DOH control system, which has not been modified in any way. The parameters introduced by the remifentanil controller are those of the band-pass filter F_B, the reference low pass filter F_R, the nominal remifentanil infusion rate u_r^o, the remifentanil infusion rate lower bound $u_r^{\min}$ and upper bound $u_r^{\max}$ and the controller gain K_r. The following values were assigned to the infusion rate parameters, based on advice from the clinical principal investigator of the iControl study: $(u_r^{\min}, u_r^o, u_r^{\max}) = (0.01, 0.03, 0.30)$ μg/kg/min. In fact $u_r^o = 0.03$ μg/kg/min was the infusion rate used during the study outlined in Appendix B.2.

In order to get an estimate, although somewhat optimistic, of what can be achieved with this structure, assume that remifentanil has an instantaneous PK model, i.e. a pure static gain. Looking at Figure 3.25, this is not an unrealistic approximation. The PD interaction is governed by the Hill function (1.17) applied to the virtual drug with normalized effect site concentration according to (1.22), where $\alpha = 5.1$ and $C_{e,50}^r = 12.5$ ng/ml in accordance with [Kern et al., 2004]. Based on this, Figure 3.27 shows the changes in DOH which can be achieved by changing the remifentanil infusion rate from u_r^o (blue) to $u_r^{\min}$ (red) and $u_r^{\max}$ (green). Note that the span (vertical distance between green and blue line) varies with the DOH, due to the nature of the PD interaction surface. The propofol related parameter values $\gamma = 1.5$ and $E_0 = 0.12$, being representative for models identified during the iControl study, were used.

A tuning strategy for the band-pass filter $F_B = F_H F_L$, where F_H is a high-pass filter and F_L is a low-pass filter, and the remifentanil controller

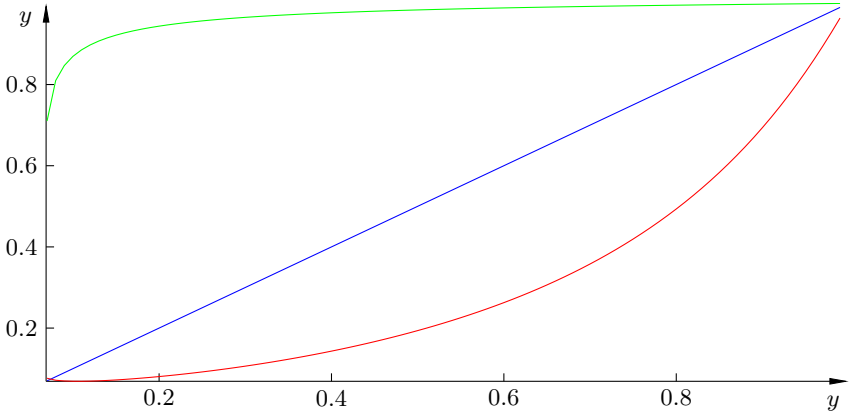

Figure 3.27 Upper bound on achievable DOH variation, which can be obtained by changing the remifentanil infusion rate from u_r^o to $u_r^{\min}$ (red) and $u_r^{\max}$ (green), respectively. The bound is plotted as a function of the nominal DOH (blue) corresponding to u_r^o.

gain K_r was proposed in [Soltész et al., 2012a]. The strategy is systematic, model based and is here illustrated on the set of 28 propofol patient response models identified from the initial cases of the iControl study. This model set consists of the 14 models identified from open-loop data ant the first 14 models identified from closed-loop data, as further described in Appendix B.

The Bode magnitude of the corresponding propofol loop sensitivity functions, linearized around $E_o = 0.5$ are shown in Figure 3.28. The vertical line at $\omega_{F_H} \approx 3.1 \cdot 10^{-3}$ rad/s marks the average -3 dB bandwidth among the models. Disturbance frequencies below ω_{F_H} are adequately attenuated by the propofol loop, motivating the use of the following high-pass filter:

$$F_H(s) = \frac{sT_{F_H}}{sT_{F_H} + 1}, \; T_{F_H} = \frac{1}{\omega_{F_H}} = 325 \text{ s}. \tag{3.16}$$

The filter in (3.16) sees to it that frequency content of the control error beyond what the propofol loop can handle is directed to the remifentanil controller.

With F_H determined and the low pass filter temporarily omitted, i.e. $F_B = F_H$, the gain K_r was chosen to yield a minimal gain margin of 2.0 among the models. This resulted in a corresponding phase margin of 56°.

Next, the low-pass filter F_L was designed to attenuate high-frequency components of y, which are most likely a result of measurement noise. The filter F_L is assumed to have the simple first-order structure

$$F_L(s) = \frac{1}{sT_{F_L} + 1}, \; T_{F_L} = \frac{1}{\omega_{F_L}}. \tag{3.17}$$

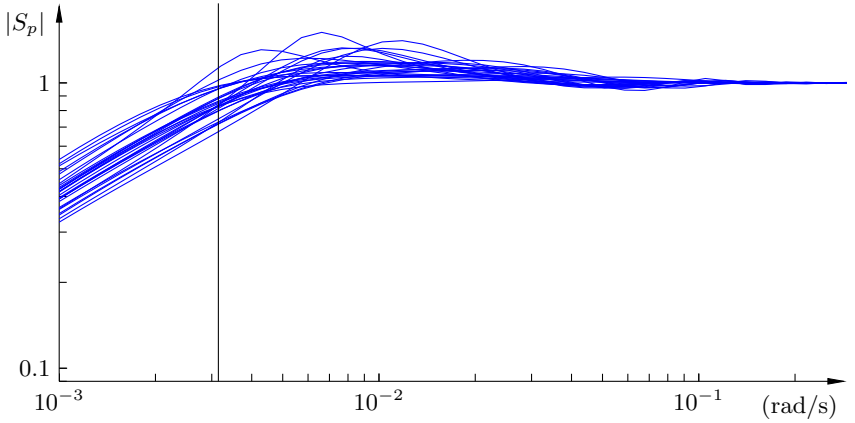

Figure 3.28 Sensitivity magnitudes and average −3 dB bandwidth of the 28 propofol control loops.

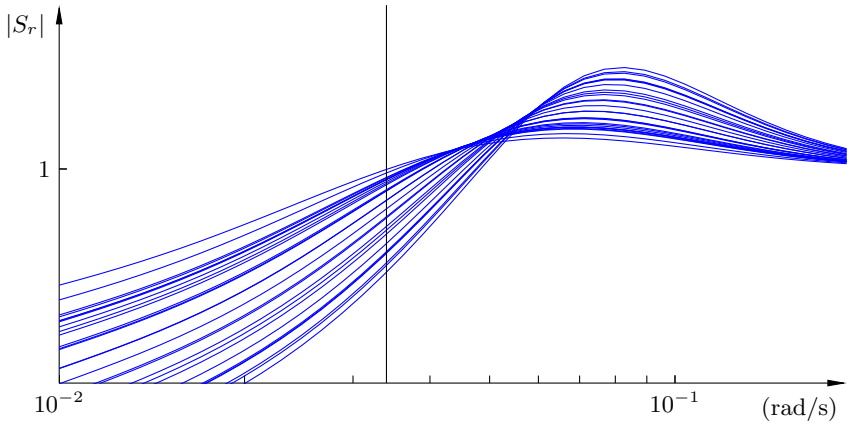

Figure 3.29 Sensitivity magnitudes and average −3 dB bandwidth of the 28 remifentanil control loops.

In a real implementation it would be wise to use a second-order filter, based on the findings reported in [Larsson and Hägglund, 2011]. However, in order to be consistent with [Soltész et al., 2012a], the structure of (3.17) will be used here. Figure 3.29 shows the Bode magnitudes of the 28 remifentanil loop sensitivity functions, with the average −3 dB magnitude marked. The corresponding angular frequency $\omega_{F_L} \approx 3.4 \cdot 10^{-2}$ rad/s was chosen as the corner frequency of (3.17).

Finally, the reference filter F_R of the remifentanil loop was designed. The high frequency content of a setpoint step could saturate the remifentanil

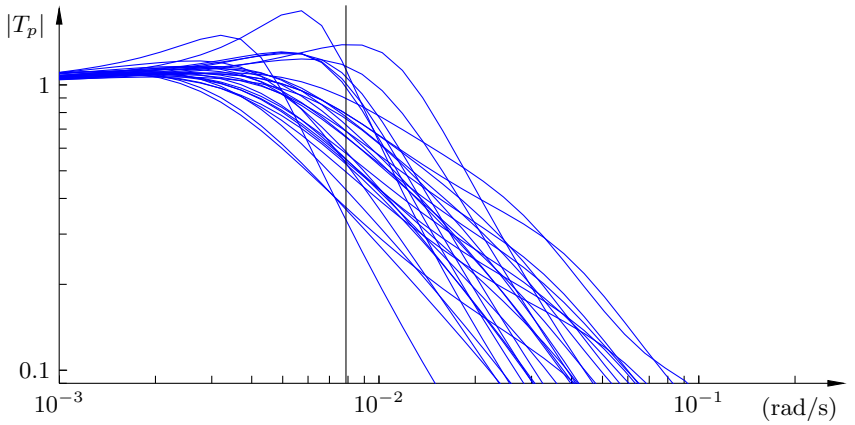

Figure 3.30 Complementary sensitivity magnitudes and average −3 dB bandwidth of the 28 propofol control loops.

control signal, momentarily reducing disturbance rejection ability. In order to avoid this, the reference is low-pass filtered by F_R before entering the remifentanil controller. Here F_R is chosen to have the same simple structure as F_L:

$$F_R(s) = \frac{1}{sT_{F_R} + 1}, \; T_{F_R} = \frac{1}{\omega_{F_R}}. \tag{3.18}$$

Figure 3.30 shows the complementary sensitivity Bode magnitudes corresponding to the sensitivity magnitudes in Figure 3.28 and their average −3 dB bandwidth. The average −3 dB bandwidth $\omega_{F_R} \approx 8.4 \cdot 10^{-3}$ rad/s was chosen as corner frequency of the reference low-pass filter (3.18), to block reference frequencies above what the propofol loop is expected to handle.

An alternative to the proposed strategy goes under the name habituating control and is thoroughly explained in [Henson et al., 1995]. It yields the same control structure topology, but the remifentanil and propofol control loops are simultaneously tuned in a model-matching fashion. The strategy is straight forward to apply and constitutes a good alternative if the constraint of keeping the propofol loop untouched is removed.

Simulation Example

The proposed controller structure and tuning were evaluated on simulated patients in [Soltész et al., 2012a]. Figure 3.31 shows a representative outcome of how the system handles output disturbances and measurement noise. The blue lines are from simulations with the controller used in the iControl study, while the red lines were obtained using the proposed SIMO controller. Figure 3.31(a) shows the reaction to the double step output disturbance profile

suggested in Section 2.2. The corresponding propofol and remifentanil infusion rates are shown in Figure 3.31(b) and Figure 3.31(c), respectively. Dark solid lines are from noise free simulations, while the lighter lines were obtained using the measurement noise model of Section 2.1. Note that the controller is more efficient in attenuating the initial positive output disturbance step than the subsequent negative one. This is because the nominal remifentanil infusion rate u_r^o lies closer to $u_r^{\min}$ than to $u_r^{\max}$.

Further details on the performance of the proposed controller, evaluated in simulation, are found in [Soltész et al., 2012a].

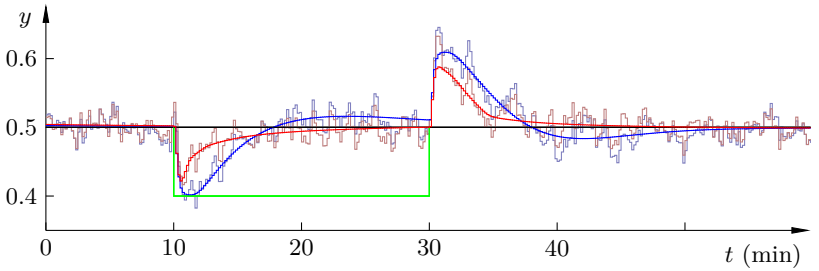

(a) DOH measurement y.

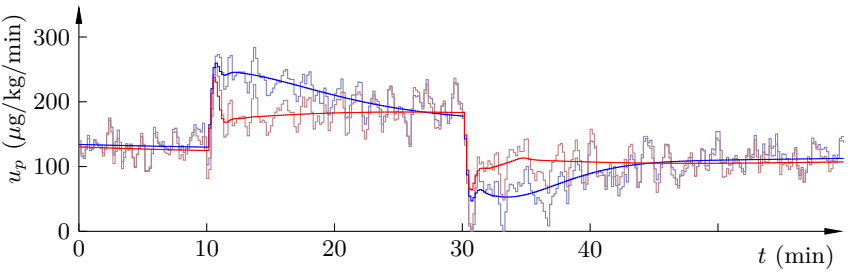

(b) Propofol infusion rate u_p.

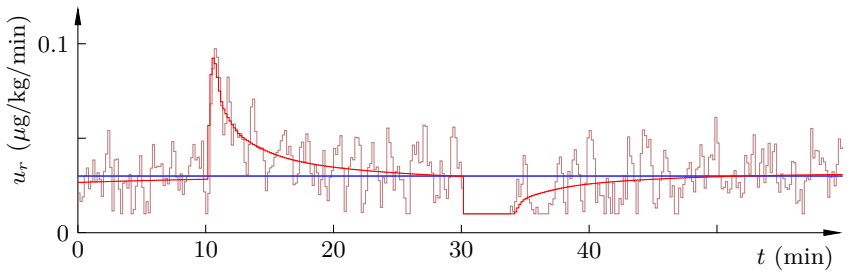

(c) Remifentanil infusion rate u_r.

Figure 3.31 Simulated response to output disturbance double step (green) using the iControl setup (blue) and proposed SIMO controller (red). The dashed green line marks the DOH reference r.

4

Discussion

4.1 Summary

The thesis has described the basic concepts and terminology of closed-loop controlled anesthesia in human patients. Models needed for the synthesis of safe controllers have been obtained from clinical data and a control system for the hypnotic depth component of anesthesia, guided by the NeuroSense EEG monitor and utilizing the intravenous drug propofol for actuation, has been described. This control system was clinically evaluated during the iControl study conducted at the University of British Columbia and the British Columbia Childrens Hospital, Vancouver, Canada.

One of the main benefits of closed-loop dosing of intravenous anesthetic drugs is that it lets the anesthesiologist focus on major events, rather than fine adjustments of the drug infusion rates. This has a potential of decreasing the use of drug as compared to current practice, resulting in faster recovery and a decrease in inter- and postoperative complications.

The evaluation of the closed-loop control system in the iControl study demonstrated that a PID controller is sufficient to provide adequate dosing of propol and its ease of operation was verified by the fact that several anesthesiologists found its use to be straight forward after only a brief introduction.

The control system used in the iControl study was deliberately designed to be simple and conservatively tuned. While providing adequate anesthesia, there is room for several improvements. A few such improvements have been demonstrated in simulation in the thesis and its underlying publications. The major one is a scheme for individualizing the controller tuning to the current patient upon induction of anesthesia. Minor improvements demonstrated in simulation include strategies for smooth switches between the manual, TCI and automatic operation modes of the system and a method to avoid integrator windup during induction of anesthesia.

It was shown that a representative closed-loop controlled induction of anesthesia does not provide sufficient excitation of the patient dynamics for

identification of a full model. The data typically allows for identification of a model of high precision (small output error) but low accuracy (poor predictive performance). As a response to this observation, an approach yielding deliberately conservative models was taken.

A strategy for additional closed-loop control of the analgesic component of anesthesia was suggested and demonstrated using realistic simulations. The strategy relies on a simple soft sensor approach and achieves a mid-ranging control behavior utilizing the analgesic drug remifentanil. Its advantages include increased disturbance rejection bandwidth of the hypnotic depth control loop and a decrease in the use of propofol.

A comprehensive reference to research groups which have been active on the EEG-guided closed-loop controlled total intravenous anesthesia scene is provided in one of the appendices. The other appendices hold technical detail related to conducted and ongoing clinical studies and identified patient model parameters.

It has been the intention of the author to make the thesis accessible to anyone with an undergraduate degree in control engineering or similar. Detail beyond what is presented in the thesis can be found in the underlying publications. These are listed in the Preface together with a description of which contributions were made by the author.

4.2 Future Work

There are several areas of future work with clinical potential, both technical and clinical. Some of these, which are anticipated to have the largest positive impact, are listed and described below.

It was shown that current clinical protocol does not provide adequate excitation for consistent model parameter identification, even when low-order models are used. Although it is not clinically feasible to excite the patient dynamics excessively by the introduction of e.g. random input signals, low amplitude signals can be superimposed on the nominal drug infusion rates. One way to achieve this is to use relay experiments, but there are also other possibilities.

The current work relies on that patient dynamics are similar during induction and maintenance of anesthesia. However, this has never been thoroughly investigated. Doing so is complicated by the lack of excitation combined with the presence of unmeasurable disturbances during the maintenance phase of anesthesia. However, a mechanism to detect disturbance-free episodes, combined with a superimposed exciting signal as proposed above, could help to provide a clearer picture.

Also related to increasing the excitation of the input is the clinical evaluation of controller individualization. The scheme for this proposed in the

thesis is based on re-tuning the controller upon induction of anesthesia. This concept of individualization has been demonstrated feasible in simulation and one direction of future work would be to bring it to clinical practice. With the addition of low-amplitude excitation during maintenance of anesthesia, it might be feasible to conduct more than one controller re-tuning during long surgeries, where patient dynamics may change due to e.g. loss of blood.

One possible strategy for controlling the depth of analgesia using the high frequency content of the hypnotic depth measurement was demonstrated in simulation. A clinical study utilizing a similar approach has been initiated at the University of British Columbia. However, it is still at an early stage and therefore not reported in the thesis, with the exception for a brief mention in Appendix B.3.

A future challenge not touched upon in the thesis is the utilization of the data rich environment of the operating room. For instance, the iControl system records and logs blood pressure, heart rate from the electrocardiogram, blood oxygen saturation, and electromyogram. During surgeries where the patient breathes spontaneously, the breathing pattern is available as an additional signal. These signals are currently not utilized by the control system, but could be potentially useful. In particular, changes in the electromyogram indicate possible artifacts in the hypnotic depth measurements while heart rate variability has previously been shown to correlate with changes in the level of nociception.

Furthermore, some minor clinical improvements could be anticipated by implementing the structures and strategies proposed in Section 3.3.

In a broader perspective, work needs to be done to promote the benefits of closed-loop controlled dosing of anesthetic drugs. Currently, the regimen has been successfully evaluated in several clinical studies, but there are no widespread units for it on the market. The foremost challenges here are regulation and clinical acceptance. Firstly, any unit to be used in everyday practice must pass the requirements dictated by the applicable regulatory agency. Secondly, the unit needs to gain clinical acceptance. Successful clinical studies are key in the certification process, while a close collaboration between clinicians and engineers is needed to assure that the systems are sound both clinically and engineering-wise.

References

Abdulla, S. and P. Wen (2012). "Depth of anaesthesia control investigation using robust deadbeat control technique". In: *2012 ICME International Conference on Complex Medical Engineering (CME)*. Kobe, Japan, pp. 107–111.

Absalom, A. and M. M. R. F. Struys (2007). *An overview of TCI & TIVA*. 2nd ed. Academia Press. ISBN: 978-90-382-1107-7.

Absalom, A., N. Sutcliffe, and G. Kenny (2002). "Closed-loop control of anesthesia using bispectral index". *Anesthesiology* **96**:1, pp. 67–73.

Absalom, A. R. and G. N. C. Kenny (2003). "Closed loop control of propofol anaesthesia using bispectral index: performance assessment in patients receiving computer-controlled propofol and manually controlled remifentanil infusions for minor surgery". *British Journal of Anaesthesia* **90**:6, pp. 737–741.

Absalom, A. R., R. de Keyser, and M. M. R. F. Struys (2011). "Closed loop anesthesia: are we getting close to finding the holy grail?" *Anesthesia & Analgesia* **112** (3), pp. 516–518.

Agrawal, G., S. Bibian, and T. Zikov (2010). "Recommended clinical range for WAV_{CNS} index during general anesthesia". In: *Annual Meeting of the American Society of Anesthesiologists*. Extended abstract. San Diego, USA.

Allison, B. J. and A. J. Isaksson (1998). "Design and performance of mid-ranging controllers". *Journal of Process Control* **8** (5–6), pp. 469–474.

Anderson, B. (2002). "Windsurfing approach to iterative control design". In: *Iterative Identification and Control*. Ed. by P. Albertos and A. Sala. Springer London, pp. 143–166. ISBN: 978-1-4471-1098-9.

Åström, K. J. and T. Hägglund (2006). *Advanced PID Control*. ISA. ISBN: 1-55617-942-1.

Åström, K. J. and B. Wittenmark (2008). *Adaptive Control*. Dover Publications, pp. 63, 64, 67, 285. ISBN: 0-201-55866-1.

Barash, P. G., B. F. Cullen, R. K. Stoelting, M. Cahalan, and M. C. Stock, eds. (2009). *Clinical Anesthesia*. 6th ed. ISBN: 978-0781787635.

Bhatt, T. V. (2009). "Fuzzy modeling and simulation for regulating the dose of anesthesia". In: *International conference on control, automation and energy conservation (INCACEC) 2009*. Tamilnadu, India, pp. 1–5.

Bibian, S. (2006). *Automation in Clinical Anesthesia*. PhD thesis. University of British Columbia, Vancouver, Canada.

Bibian, S., C. R. Ries, M. Huzmezan, and G. Dumont (2005). "Introduction to automated drug delivery in clinical anesthesia". *European Journal of Control* **11**:6, pp. 535–557.

Bibian, S., G. A. Dumont, M. Huzmezan, and C. R. Ries (2006). "Patient variability and uncertainty quantification in anaesthesia: part II – PKPD uncertainty". In: *Proc. 6th IFAC Symposium on Modeling and Control in Biomedical Systems*. Reims, France.

Bibian, S., G. A. Dumont, and T. Zikov (2010). "Dynamic behavior of BIS, M-entropy and NeuroSense brain function monitors". *Journal of Clinical Monitoring and Computing* **25**:1, pp. 81–87.

Borgeat, A., O. H. G. Wilder-Smith, M. Saiah, and K. Rifat (1992). "Subhypnotic doses of propofol possess direct antiemetic properties". *Anesthesia & Analgesia* **74**:4, pp. 539–541.

Bouillon, T., J. Bruhn, L. Radu-Radulescu, E. Bertaccini, S. Park, and S. Shafer (2002). "Non-steady state analysis of the pharmacokinetic interaction between propofol and remifentanil". *Anesthesiology* **97**:6, pp. 1350–62.

Breslin, D. S., R. K. Mirakhur, J. E. Reid, and A. Kyle (2004). "Manual versus target-controlled infusions of propofol". *Anaesthesia* **59**:11, pp. 1059–1063.

Brouse, C. J., W. Karlen, D. Myers, E. Cooke, J. Stinson, J. Lim, G. A. Dumont, and J. M. Ansermino (2011). "Wavelet transform cardiorespiratory coherence detects patient movement during general anesthesia". In: *Proc. International Conference of the IEEE EMBS*. Boston, USA.

Cameron, E., G. Johnston, S. Crofts, and N. S. Morton (1992). "The minimum effective dose of lignocaine to prevent injection pain due to propofol in children". *Anaesthesia* **47**:7, pp. 604–606.

Choo, E. K., W. Magruder, C. J. Montgomery, J. Lim, R. Brand, and J. M. Ansermino (2010). "Skin conductance fluctuations correlate poorly with postoperative self-report pain measures in school-aged children". *Anesthesiology* **113**:1, pp. 175–182.

Coppens, M. J., D. J. Eleveld, J. H. Proost, L. A. Marks, J. F. van Bocxlaer, H. Vereecke, A. R. Absalom, and M. M. R. F. Struys (2011). "An evaluation of using population pharmacokinetic models to estimate pharmacodynamic parameters for propofol and bispectral index in children". *Anesthesiology* **115**:1, pp. 83–93.

Cummings, G. C., J. Dixon, N. H. Kay, J. P. W. Windsor, E. Major, M. Morgan, J. W. Sear, A. A. Sepnce, and D. K. Stephenson (1984). "Dose requirement of ICI 35,868 (Propofol 'diprivan') in a new formulation for induction of anaesthesia". *Anaesthesia* **39**:12, pp. 1168–1171.

Derendorf, H. and B. Meibohm (1999). "Modeling of pharmacokinetic/pharmacodynamic (PK/PD) relationships: concepts and perspectives". *Pharmaceutical Research* **16** (2), pp. 176–185.

Diaz, J. C., A. Franco, D. R. Bacon, J. Rupreht, and J. Alvarez, eds. (2001). *The History of Anesthesia: Proceedings of the 5th International Symposium on the History of Anesthesia*. Santiago, Spain.

Dumont, G. A. (2012). "Closed-loop control of anesthesia – a review". In: *8th IFAC Symposium on Biological and Medical Systems*. Budapest, Hungary.

Dumont, G. A., A. Martínez, and J. M. Ansermino (2009). "Robust control of depth of anesthesia". *International Journal of Adaptive Control an Signal Processing* **23**:5, pp. 435–454.

Dzindolet, M. T., S. A. Peterson, R. A. Pomranky, L. G. Pierce, and H. P. Beck (2003). "The role of trust in automation reliance". *International Journal of Human-Computer Studies* **58** (6), pp. 697–718.

Egan, T. D., C. F. Minto, D. J. Hermann, J. Barr, K. T. Muir, and S. L. Shafer (1996). "Remifentanil versus alfentanil: comparative pharmacokinetics and pharmacodynamics in healthy adult male volunteers". *Anesthesiology* **84**:4, pp. 821–833.

Ejaz, K. and J.-S. Yang (2004). "Controlling depth of anesthesia using PID tuning: a comparative model-based study". In: *IEEE International Conference on Control Applications*. Taipei, Taiwan, pp. 580–585.

Fang, M., Y. Tao, and Y Wang (2013). "An enriched simulation environment for evaluation of closed-loop anesthesia". *Journal of Clinical Monitoring and Computing*. In press, pp. 1–14. DOI: 10.1007/s10877-013-9483-0.

Forssell, U. and L. Ljung (1998). *Closed-Loop Identification Revisited – Updated Version*. Tech. rep. LiTH-ISY-R-2021. Linköping University, Department of Electrical Engineering.

Gan, T. J., P. S. Glass, A. Windsor, F. Payne, C. Rosow, P. Sebel, and P. Manberg (1997). "Bispectral index monitoring allows faster emergence and improved recovery from propofol, alfentanil, and nitrous oxide anesthesia". *Anesthesiology* **87**:4, pp. 808–815.

Garpinger, O. and T. Hägglund (2008). "A software tool for robust PID design". In: *Proc. 17th IFAC World Congress, Seoul, Korea.*

Gentilini, A., M. Rossoni-Gerosa, C. W. Frei, R. Wymann, M. Morari, A. M. Zbinden, and T. W. Schnider (2001). "Modeling and closed-loop control of hypnosis by means of bispectral index (BIS) with isoflurane". *IEEE Transactions on Biomedical Engineering* **48**:8, pp. 874 –889.

Glen, J. B. (1998). "The development of 'Diprifusor': a TCI system for propofol". *Anesthesia* **53**:1, pp. 13 –21.

Haddad, W. M., K. Y. Volyanskyy, J. M. Bailey, and J. J. Im (2011). "Neuroadaptive output feedback control for automated anesthesia with noisy EEG measurements". *IEEE Transactions on Control System Technology* **19** (2), pp. 311–326.

Hägglund, T. and K. J. Åström (2002). "Revisiting the Ziegler-Nichols tuning rules for PI control". *Asian Journal of Control* **4**:4, pp. 364–380.

Hemmerling, T. M., S. Charabati, E. Salhab, D. Bracco, and P. A. Mathieu (2009). "The analgoscore: a novel score to monitor intraoperative nociception and its use for closed-loop application of remifentanil". *Journal of Computers* **4** (4), pp. 311–318.

Hemmerling, T. M., S. Charabati, C. Zaouter, C. Minardi, and P. A. Mathieu (2010). "A randomized controlled trial demonstrates that a novel closed-loop propofol system performs better hypnosis control than manual administration". *Canadian Journal of Anesthesia* **57** (8), pp. 725–735.

Henson, M. A., B. A. Ogunnaike, and J. S. Schwaber (1995). "Habituating control strategies for process control". *American Institute of Chemical Engineering Journal* **41** (3), pp. 604–618.

van Heusden, K., G. A. Dumont, K. Soltész, C. L. Petersen, A. Umedaly, N. West, and J. M. Ansermino (2013a). "Clinical evaluation of robust PID control of propofol anesthesia in children". *IEEE Transactions on Control System Technology.* In press.

van Heusden, K., J. M. Ansermino, K. Soltész, S. Khosravi, N. West, and G. A. Dumont (2013b). "Quantification of the variability in response to propofol administration in children". *IEEE Transactions on Biomedical Engineering.* In press.

Huang, J. W., Y.-Y. Lu, A. Nayak, and R. J. Roy (1999). "Depth of anesthesia estimation and control". *IEEE Transactions on Biomedical Engineering* **46** (1), pp. 71–81.

Huiku, M., K. Uutela, M. van Gils, I. Korhonen, M. Kymäläinen, P. Meriläinen, M. Paloheimo, M. Rantanen, P. Takala, H. Viertiö-Oja, and A. Yli-Hankala (2007). "Assessment of surgical stress during general anaesthesia". *British Journal of Anaesthesia* **98**:4, pp. 447–455.

Hume, R. (1966). "Prediction of lean body mass from height and weight". *Journal of Clinical Pathology* **19** (4), pp. 389–391.

Hunter, I. W. and M. J. Korenberg (1986). "The identification of nonlinear biological systems". *Biological Cybernetics* **55** (2–3), pp. 135–144.

Ionescu, C. M., R. D. Keyser, B. C. Torrico, T. D. Smet, M. M. R. F. Struys, and J. E. Normey-Rico (2008). "Robust predictive control strategy applied for propofol dosing using BIS as a controlled variable during anesthesia". *IEEE Transactions on Biomedical Engineering* **55**:9, pp. 2161 – 2170.

Ionescu, C. M., R. de Keyser, and M. M. R. F. Struys (2011a). "Evaluation of a propofol and remifentanil interaction model for predictive control of anesthesia induction". In: *Proc. IEEE Conference on Decision and Control and European Control Conference*. Orlando, USA.

Ionescu, C. M., R. Hodrea, and R. de Keyser (2011b). "Variable time-delay estimation for anesthesia control during intensive care". *IEEE Transactions on Biomedical Engineering* **58**:2, pp. 363–369.

Janda, M., O. Simanski, J. Bajorat, B. Pohl, G. F. E. Noeldge-Schomburg, and R. Hofmockel (2011). "Clinical evaluation of a simultaneous closed-loop anaesthesia control system for depth of anaesthesia and neuromuscular blockade". *Anaesthesia* **66** (12), pp. 1112–1120.

Jeanne, M., R. Loiger, J. de Jonckheere, and B. Tavernier (2009). "Heart rate variability during total intravenous anesthesia: effect of nociception and analgesia". *Autonomic Neuroscience: Basic and Clinical* **147**:1–2, pp. 91–96.

Jensen, E. W., H. Litvan, M. Reuelta, B. Rodriguez, E. Bernardo, P. Caminal, P. Martinez, H. Vereecke, and M. M. R. F. Struys (2006). "Cerebral state index during propofol anesthesia: a comparison with the bispectral index and the A-line ARX index". *Anesthesiology* **105**:1, pp. 28–36.

Johansen, J. W. and P. S. Sebel (2000). "Development and clinical application of electroencephalographic bispectrum monitoring". *Anesthesiology* **93**:5, pp. 1336 –1344.

Kelly, S. D. (2003). *Monitoring level of consciousness during anesthesia and sedation*. Aspect Medical Systems Inc. Newton, USA. ISBN: 0-9740696-0-4.

Kenny, G. N. and H. Mantzaridis (1999). "Closed-loop control of propofol anaesthesia". *British Journal of Anaesthesia* **83** (2), pp. 223–228.

Kern, S. E., G. Xie, J. L. White, and T. D. Egan (2004). "Opioid-hypnotic synergy: a response surface analysis of propofol-remifentanil pharmacodynamic interaction in volunteers". *Anesthesiology* **100**:6, pp. 1374 –1381.

Keys, T. E. (1978). *The History of Surgical Anesthesia*. 1st ed. R. E. Krieger. ISBN: 978-0882755700.

Kreuer, S., A. Biedler, R. Larsen, S. Schoth, S. Altmann, and W. Wilhelm (2001). "The Narcotrend – a new EEG monitor designed to measure the depth of anaesthesia. A comparison with bispectral index monitoring during propofol-remifentanil-anaesthesia". *Der Anaesthesist* **50**:12, pp. 921–925.

Larsson, P.-O. and T. Hägglund (2011). "Control signal constraints and filter order selection for PI and PID controllers". In: *Proc. American Control Conference*. San Francisco, USA.

Lecchini, A., A. Lanzon, and B. D. O. Anderson (2006). "A model reference approach to safe controller changes in iterative identification and control". *Automatica* **42** (2), pp. 193–203.

Liberman, M. Y., S. Ching, J. Chemali, and E. Brown (2013). "A closed-loop anesthetic delivery system for real-time control of burst suppression". *Journal of Neural Engineering* **10** (4). In press.

Liley, D. T. J., N. C. Sinclair, T. Lipping, B. Heyse, H. E. M. Vereecke, and M. M. R. F. Struys (2010). "Propofol and remifentanil differentially modulate frontal electroencephalographic activity". *Anesthesiology* **113**:2, pp. 292–304.

Lin, H.-H., C. L. Beck, and M. J. Bloom (2004). "On the use of multivariable piecewise-linear models for predicting human response to anesthesia". *IEEE transaction on biomedical engineering* **51**:11, pp. 1876–1887.

Litvan, H., E. W. Jensen, M. Revuelta, S. W. Henneberg, P. Paniagua, J. M. Campos, P. Martínez, P. Caminal, and J. M. Villar Landeira (2002). "Comparison of auditory evoked potentials and the A-line ARX index for monitoring the hypnotic level during sevofluane and propofol induction". *Acta Anaesthesiologica Scandinavica* **46**:3, pp. 245–251.

Liu, J., H. Singh, and P. F. White (1997). "Electroencephalographic bispectral index correlates with intraoperative recall and depth of propofol-induced sedation". *Anesthesia and Analgesia* **84**:1, pp. 185 –189.

Liu, N., T. Chazot, A. Genty, A. Landais, A. Restoux, K. McGee, P.-A. Laloe, B. Trillat, L. Barvais, and M. Fischler (2006). "Titration of propofol for anesthetic induction and maintenance guided by the bispectral index: closed-loop versus manual control: a prospective, randomized, multicenter study". *Anesthesiology* **104**:4, pp. 686–695.

Liu, N., T. Chazot, B. Tirillat, G. A. Dumont, and M. Fischler (2007). "Closed-loop titration of propofol guided by bispectral index". *Annales francaises d'anesthésie et de réanimation* **26**:10, pp. 850–854.

Liu, N., M. le Guen, F. Benabbes-Lambert, T. Chazot, B. Trillat, D. I. Sessler, and M. Fischler (2012). "Feasibility of closed-loop titration of propofol and remifentanil guided by the spectral M-entropy monitor". *Anesthesiology* **116**:2, pp. 286–295.

Liu, W. H. D., T. A. S. Thorp, S. G. Graham, and A. R. Aitkenhead (1991). "Incidence of awareness with recall during general anaesthesia". *Anaesthesia* **46**:6, pp. 435–437.

Luenberger, D. G. (1979). *Introduction to Dynamic Systems*. 1st ed. Wiley. ISBN: 0-471-02594-1.

Mackey, D. C. (2012). "Can we finally conquer the problem of medical quality?" *Anesthesiology* **117** (2), pp. 225–226.

Mahfouf, M., C. S. Nunes, D. A. Linkens, and J. E. Peacock (2005). "Modeling and multivariable control in anaesthesia using neural-fuzzy paradigms part II. closed-loop control of simultaneous administration of propofol and remifentanil". *Artificial Intelligence in Medicine* **35**:3, pp. 207 –213.

Manberg, P. J., C. M. Vozella, and S. D. Kelley (2008). "Regulatory challenges facing closed-loop anesthetic drug infusing devices". *Clinical Pharmacology & Therapeutics* **84** (1), pp. 166–169.

Mendonça, T., H. Magalhaes, P. Lago, and S. Esteves (2004). "Hippocrates: a robust system for the control of neuromuscular blockade". *Clinical Monitoring and Computing* **18** (4), pp. 265–273.

Miller, R. D. and M. Pardo (2011). *Basics of Anesthesia*. 6th ed. ISBN: 978-1437716146.

Minto, C. F., T. W. Schnider, T. D. Egan, E. Youngs, H. J. Lemmens, P. L. Gambus, V. Billard, J. F. Hoke, K. Moore, D. J. Hermann, K. T. Muir, J. W. Mandema, and S. L. Shafer (1997). "Influence of age and gender on the pharmacokinetics and pharmacodynamics of remifentanil: I. model development". *Anesthesiology* **86**:1, pp. 10–23.

Minto, C. F., T. W. Schnider, T. G. Short, K. M. Gregg, A. Gentilini, and S. L. Shafer (2000). "Response surface model for anesthetic drug interactions". *Anesthesiology* **92**:6, pp. 1603–1616.

Moerman, A. T., L. L. Herregods, M. M. de Vos, E. O. Mortier, and M. M. R. F. Struys (2009). "Manual versus target-controlled infusion remifentanil administration in spontaneously breathing patients". *Anesthesia & Analgesia* **108**:3, pp. 828–834.

Monk, T. G., V. Saini, B. C. Weldon, and J. C. Sigl (2005). "Anesthetic management and one-year mortality after noncardiac surgery". *Anesthesia & Analgesia* **100**:1, pp. 4–10.

Morley, A., J. Derrick, P. Mainland, B. B. Lee, and T. G. Short (2000). "Closed loop control of anaesthesia: an assessment of the bispectral index as the target of control". *Anaesthesia* **55** (10), pp. 953–959.

Oquendo, F. J. G., F. D. C. Arroyave, J. M. Fernández, and Á. G. Grisales (2013). "Total intravenous anesthesia in a closed loop system: report of the first case in Colombia". *Colombian Journal of Anesthesiology*. In press.

Phillips, R., J. Kondev, J. Theriot, and H. G. Garcia (2012). *Physical Biology of the Cell*. 2nd ed. Garland Science. ISBN: 978-0815344506.

Pouke, G. E. V., L. J. B. Bravo, and S. L. Shafer (2004). "Target controlled infusions: targeting the effect site while limiting peak plasma concentration". *IEEE Transactions on Biomedical Engineering* **51**:11, pp. 1869 – 1875.

Puri, G. D., B. Kumar, and J. Aveek (2007). "Closed-loop anaesthesia delivery system (CLADS) using bispectral index: a performance assessment study". *Anaesthesia and intensive care* **35** (3), pp. 357–362.

Ralph, M., C. L. Beck, and M. Bloom (2011). "L1-adaptive methods for control of patient response to anesthesia". In: *American Control Conference (ACC) 2011*. San Francisco, USA, pp. 1729–1735.

Revuelta, M., M. Paniagua, J. M. Campos, J. A. Fernández, A. Martínez, M. Jospin, and H. Litvan (2008). "Validation of the index of consciousness during sevoflurane and remifentanil anaesthesia: a comparison with the bispectral index and the cerebral state index". *British Journal of Anaesthesia* **101**:8, pp. 653–658.

Rigby-Jones, A. E., M. J. Priston, J. R. Sneyd, A. P. McCabe, G. I. Davis, M. A. Tooley, G. C. Thorne, and A. R. Wolf (2007). "Remifentanil – midazolam sedation for paediatric patients receiving mechanical ventilation after cardiac surgery". *British Journal of Anaesthesia* **99**:2, pp. 252–261.

Russell, D., M. P. Wilkes, S. C. Hunter, J. B. Glen, P. Hutton, and G. N. C. Kenny (1995). "Manual compared with target-controlled infusion of propofol". *British Journal of Anaesthesia* **75**:5, pp. 562–566.

Sawaguchi, Y., E. Furutani, G. Shirakami, M. Araki, and K. Fukuda (2008). "A model-predictive hypnosis control system under total intravenous anesthesia". *IEEE Transactions on Biomedical Engineering* **55**:3, 874 – 887.

Schnider, T. W., C. F. Minto, P. L. Gambus, C. Andresen, D. B. Goodale, S. L. Shafer, and E. J. Youngs (1998). "The influence of method of administration and covariates on the pharmacokinetics of propofol in adult volunteers". *Anesthesiology* **88**:5, pp. 1170 –1182.

Schüttler, J. and H. Ihmsen (2000). "Population pharmacokinetics of propofol: a multicenter study". *Anesthesiology* **92**:3, pp. 727–738.

Schwilden, H., H. Stoeckel, and J. Schüttler (1989). "Closed-loop feedback control of propofol anaesthesia by quantitative EEG analysis in humans". *British Journal of Anaesthesia* **62** (3), pp. 290–296.

Scott, R. P. F., D. A. Saunders, and J. Norman (1988). "Propofol: clinical strategies for preventing the pain of injection". *Anaesthesia* **43**:6, pp. 492–494.

Sebel, P. S. and J. D. Lowdon (1989). "Propofol: a new intravenous anesthetic". *Anesthesiology* **71**:2, pp. 260–277.

Servin, F. S. (1998). "TCI compared with manually controlled infusion of propofol: a multicenter study". *Anaesthesia* **53**:Supplement s1, pp. 82–86.

Shafer, S. L. and K. M. Gregg (1992). "Algorithms to rapidly achieve and maintain stable drug concentrations at the site of drug effect with a computer-controlled infusion pump". *Journal of Pharmacokinetics and Biopharmaceutics* **20** (2), pp. 147–169.

Sheiner, L. B. and S. L. Beal (1980). "Evaluation of methods for estimating population pharmacokinetic parameters". *Pharmacokinetics and Biopharmaceutics* **8** (6), pp. 553–571.

Sheiner, L. B., D. R. Stanski, S. Vozeh, R. D. Miller, and J. Ham (1979). "Simultaneous modeling of pharmacokinetics and pharmacodynamics: application to D-Tubocurarine". *Clinical Pharmacology and Therapeutics* **25**:3, pp. 358 –371.

da Silva, M. M., T. Mendonça, and T. Wigren (2010). "Online nonlinear identification of the effect of drugs in anaesthesia using a minimal parametrization and BIS measurements". In: *Proc. American Control Conference*. Baltimore, USA, pp. 4379–4384.

da Silva, M. M., T. Wigren, and T. Mendonça (2012). "Exactly linearizing adaptive control of propofol and remifentanil using a reduced Wiener model for the depth of anesthesia". In: *51st IEEE Conference on Decision and Control (CDC)*. Maui, Hawaii.

de Smet, T., M. M. R. F. Struys, M. M. Neckebroek, K. van den Hauwe, S. Bonte, and E. P. Mortier (2008). "The accuracy and clinical feasibility of a new Bayesian-based closed-loop control system for propofol administration using the bispectral index as a controlled variable". *Anesthesia and Analgesia* **107**:4, pp. 1200 –1210.

Smith, O. J. (1959). "A controller to overcome dead time". *ISA Journal* **6**:2, pp. 28–33.

Soltero, D. E., A. Faulconer, and R. G. Bickford (1951). "The clinical application of automatic anesthesia". *Anesthesiology* **12** (5), pp. 574–582.

Soltész, K., J.-O. Hahn, G. A. Dumont, and J. M. Ansermino (2011). "Individualized PID control of depth of anesthesia based on patient model identification during the induction phase of anesthesia". In: *Proc. IEEE Conference on Decision and Control and European Control Conference*. Orlando, USA.

Soltész, K., G. A. Dumont, K. van Heusden, and J. M. Ansermino (2012a). "Simulated mid-ranging control of propofol and remifentanil using EEG-measured hypnotic depth of anesthesia". In: *51st IEEE Conference on Decision and Control*. Maui, USA.

Soltész, K., G. A. Dumont, and J. M. Ansermino (2013a). "Assessing control performance in closed-loop anesthesia". In: *21st Mediterranean Conference on Control and Automation (MED13)*. Platanias-Chania, Greece, pp. 191–196.

Soltész, K., J.-O. Hahn, T. Hägglund, G. A. Dumont, and J. M. Ansermino (2013b). "Individualized closed-loop control of propofol anesthesia: a preliminary study". *Biomedical Signal Processing and Control* **8** (6), pp. 500–508.

Soltész, K., T. Hägglund, and K. J. Åström (2010). "Transfer function parameter identification by modified relay feedback". In: *Proc. American Control Conference, Baltimore, USA*.

Soltész, K., K. van Heusden, G. A. Dumont, T. Hägglund, C. L. Petersen, N. West, and J. M. Ansermino (2012b). "Closed-loop anesthesia in children using a PID controller: a pilot study". In: *Proc. IFAC Conference on Advances in PID Control*. Brescia, Italy.

Struys, M. M. R. F., T. de Smet, S. Greenwald, A. R. Absalom, S. Bingé, and E. P. Mortier (2004). "Performance evaluation of two published closed-loop control systems using bispectral index monitoring: a simulation study". *Anesthesiology* **100**:3, pp. 640–647.

Struys, M. M. R. F., T. de Smet, L. F. M. Versichelen, S. van de Velde, R. den Broecke, and E. P. Mortier (2001). "Comparison of closed-loop controlled administration of propofol using bispectral index as the controlled variable versus "standard practice" controlled administration". *Anesthesiology* **95**:1, pp. 6–17.

Tan, C. H. and M. K Onsiong (1998). "Pain on injection of propofol". *Anaesthesia* **53**:5, pp. 468–476.

Varvel, J. R., D. L. Donoho, and S. L. Shafer (1992). "Measuring the predictive performance of computer-controlled infusion pumps". *Journal of Pharmacokinetics and Biopharmaceutics* **20**:1, pp. 63–94.

Viertö-Oja, H., V. Maja, M. Särkelä, P. Talja, N. Tenkanen, H. Tolvanen-Laakso, M. Paloheimo, A. Vakkuri, A. Yli-Hankala, and P. Meriläinen (2004). "Description of the entropy algorithm as applied in the Datex-Ohmeda S/5 Entropy Module". *Acta Anaesthesiol Scandinavica* **48**:2, pp. 154 –161.

West, N., G. A. Dumont, K van Heusden, C. L. Petersen, S. Khosravi, K. Soltész, A. Umedaly, E. Reimer, and J. M. Ansermino (2013). "Robust closed-loop control of induction and maintenance of propofol anesthesia in children". *Pediatric Anesthesia* **23** (8), pp. 712–719.

Zikov, T., S. Bibian, G. Dumont, M. Huzmezan, and C. Ries (2006). "Quantifying cortical activity during general anesthesia using wavelet analysis". *IEEE Transactions on Biomedical Engineering* **53**:4, pp. 617 –632.

Nomenclature

Symbols

Symbol	Description	Unit or range
$C^r_{e,50}$	The $C_{e,50}$ for remifentanil towards DOH.	ng/ml
C_e	Effect site drug concentration.	[mass]/[volume]
C_m	Measured blood plasma drug concentration.	[mass]/[volume]
C_p	(Estimated) blood plasma drug concentration.	[mass]/[volume]
$C_{e,50}$	Effect site drug concentration corresponding to the effect half-way between E_0 and E_∞.	[mass]/[volume]
E^+	Percentage of time when maintenance phase $e > 0.1$.	%
E^-	Percentage of time when maintenance phase $e < -0.1$.	%
E_0	Patient specific clinical effect in absence of drug.	≈ 0
E_∞	Patient specific maximal clinical effect.	≈ 1
E_a	Analgesic effect.	(0,1)
E_h	Hypnotic effect.	(0,1)
E_o	Value of E at operating point.	≈ 0.5
E	Clinical effect.	(0,1)
F_B	DOA soft sensor band-pass filter.	
F_H	High-pass component of F.	

Symbol	Description	Unit or range
F_L	Low-pass component of F.	
F_R	Remifentanil controller reference filter.	
K'_o	Observer gain parameter.	
K_o	Observer gain.	
K_r	Remifentanil controller gain.	
K	Gain.	
L	Delay.	s
M_s	Maximum sensitivity.	
N	Generic dimension, e.g. vector length.	
R	Vector of samples of r.	(0,1)
S_p	Propofol loop sensitivity function.	
S_r	Remifentanil loop sensitivity function.	
T_F	Time constant of F.	s
T_p	Propofol loop complementary sensitivity function.	
T_r	Trending rate of the NeuroSense monitor.	s
T	Vector containing samples of t.	s
T	Time constant.	s
Y	Vector containing samples of y.	(0,1)
Δv	Deviation of v from operating point v_o: $\Delta v = v - v_o$.	
Δy	Difference in y caused by output disturbance.	
α	PD interaction model parameter.	>1
γ	Parameter (or degree) of Hill function.	≥ 1
$\hat{E}_0$	Estimate of v.	≈ 0
$\hat{K}$	Estimate of K.	
$\hat{L}$	Estimate of L.	s
$\hat{T}$	Estimate of T.	s

Symbol	Description	Unit or range
$\hat{\gamma}$	Estimate of γ.	>1
$\hat{v}'$	Model output $\hat{v}$ scaled by model gain.	
$\hat{v}$	Estimate of v.	
$\hat{y}_{\text{raw}}$	Model output corresponding to y_{raw}.	(0,1)
$\hat{y}$	Model output corresponding to y.	(0,1)
ω_F	Corner frequency of F.	rad/s
θ	Relative normalized remifentanil concentration: $\theta = v_r/(v_p + v_r)$.	
$\tilde{v}$	Estimation error for v: $\tilde{v} = v - \hat{v}$.	
c_i	Clearance of compartment i.	[volume]/[time]
d	Additive output disturbance.	
e	Control error: $e = r - y$.	
f	A function with biometric parameters as arguments and PK parameters as values.	
i, j, k	Generic vector or matrix indexing numbers.	
k_{e0}	PD parameter, corresponding to a pole at $-k_{e0}$.	1/[time]
k_{ij}	Equilibration rate constant relating compartment i to j.	1/[time]
m_i	Drug mass in compartment i.	[mass]
m	Vector of drug masses for compartmental model.	[mass]
n	Measurement noise.	
n	Generic dimension, e.g. number of states or vector length.	
p_i	System pole at $-p_i$.	1/[time]
r	Setpoint for y.	(0,1)
s	The Laplace variable.	
t_{ind}	Induction duration.	s
t	Time variable.	[time]

Symbol	Description	Unit or range
u_i	Drug infusion rate into compartment i.	[mass]/[time]
u_r^o	Nominal value of u_r.	[mass]/[time]
$u_r^{\max}$	Upper bound of u_r.	[mass]/[time]
$u_r^{\min}$	Lower bound of u_r.	[mass]/[time]
u_r	Remifentanil infusion rate.	[mass]/[time]
u	Drug infusion rate.	[mass]/[time]
v_i	Volume of compartment i.	[volume]
v_o	Value of v at operating point.	
v_p	Normalized propofol C_e.	
v_r	Normalized remifentanil C_e, with respect to DOH.	
v_{50}	$C_{e,50}$ of virtual drug modeled as $v_p + v_r$.	
v	Normalized effect site concentration: $v = C_e/C_{e,50}$.	
w_l	Weight used to blend y_l and y_r into y.	(0,1)
w_r	Weight used to blend y_l and y_r into y.	(0,1)
x_i	Drug concentration in compartment i.	[mass]/[volume]
x	Vector of drug concentrations for compartmental model.	[mass]/[volume]
y_f	DOA soft sensor output.	(0,1)
y_k	Sample number k in Y.	(0,1)
y_l	Left hemisphere y-value.	(0,1)
y_r	Right hemisphere y-value.	(0,1)
$y_{\min}$	Threshold at which the controller integrator is activated.	(0,1)
y_{raw}	Untrended measured effect y from the NeuroSense monitor.	(0,1)
y	Measured clinical effect E.	(0,1)
`SQI_alt`	Currently un-selected SQI signal.	
`SQI_curr`	Currently selected SQI signal.	

Symbol	Description	Unit or range
SQI	Signal quality index.	(0,1)
SQI_l	SQI of y_l.	(0,1)
SQI_r	SQI of y_r.	(0,1)
SR	Suppression ratio.	(0,1)
SR_l	SR of y_l.	(0,1)
SR_r	SR of y_r.	(0,1)

Acronyms

Acronym	Description
WAV_{CNS}	Wavelet-based anesthesia value for central nervous system.
AEP	Auditory evoked potential.
ASA	American Society of Anesthesiologists [physical status].
BIS	Bispectral index.
DOA	Depth of analgesia.
DOH	Depth of hypnosis.
EEG	Electroencephalogram.
EMG	Electromyogram or electromyograph.
ER	Emergence phase rise time.
FDA	The United States Food and Drug Administration.
FIR	Finite impulse response [filter].
FOTD	First-order time delay [system].
GS	Global score.
IAE	Integrated absolute error.
ID	Induction duration.
IE	Integrated error.
LTI	Linear time invariant [system].
MAP	Mean arterial pressure.
MDAPE	Median absolute performance error.
MDPE	Median performance error.
OS	Overshoot.
PD	Pharmacodynamic [model].
PE	Performance error.
PI	Proportional and integrating [controller].
PID	Proportional, integral and derivative [controller].

Acronym	Description
PK	Pharmacokinetic [model].
PKPD	Combined pharmacokinetic and pharmacodynamic [model].
SE	State entropy.
SIMO	Single input, multiple output [system].
SOTD	Second-order time delay [system].
SQI	Signal quality index.
SR	Supression ratio.
SSI	Surgical stress index.
TCI	Target controlled infusion [drug delivery system].
TIVA	Total intravenous anesthesia.
UPS	Uninterruptible power supply.
VI	Variability index.

A

Patient Parameters

Parameters of 41 identified models, relating the infusion rate of propofol u (μg/kg/min) to measured clinical effect $E \in (E_0, 1)$ in children, are enlisted in Table A.1. Note that no clinical monitor model is included. The models are characterized by delay L (s), lag T (s) and gain K ($1/(\mu\text{g/kg/min})$). The parameter of the output nonlinearity (1.17) has the value $\gamma = 1$ for all models, which is why it is not listed in the table. The identified parameters are the result of a fully automated schema proposed in Section 3.3. Although conceptually feasible, the results of the scheme will require further investigation before being incorporated in the tuning procedure of a closed-loop controlled system for clinical evaluation.

Table A.1 Identified patient model parameters for propofol: gain K ($1/(\mu g/kg/min)$), time constant T (s) and delay L (s).

$10^3 \cdot K$	T	L	$10^3 \cdot K$	T	L
0.3	11	51	1.4	96	93
0.5	11	84	1.4	148	90
0.8	121	41	1.4	91	56
0.9	178	45	1.4	139	55
0.9	142	58	1.5	160	37
1.0	82	41	1.5	165	71
1.0	174	49	1.5	241	132
1.0	158	69	1.6	128	57
1.0	86	61	1.6	15	147
1.0	184	116	1.6	129	72
1.1	125	42	1.6	112	107
1.1	178	121	1.7	185	82
1.1	229	89	1.7	143	91
1.1	181	149	1.8	124	124
1.2	171	42	1.9	79	224
1.2	138	40	1.9	176	165
1.2	152	81	2.0	160	138
1.2	164	73	2.0	126	101
1.3	18	9	2.3	169	145
1.3	131	79	2.5	94	161
1.4	140	53			

B

Clinical Studies

B.1 NeuroSense Data Ethics

The closed-loop controlled iControl study, presented in Appendix B.2 below, was preceded by the collection of open-loop data from 30 children undergoing elective surgery. The use of this data for modeling was granted by the University of British Columbia Children's and Women's Research Ethics Board (H11-02952, NeuroSense Data Ethics). Propofol and remifentanil was manually administered as initial boluses followed by continuous infusions. Dose adjustments were guided by the NeuroSense monitor. The initial propofol bolus and subsequent infusion rate were manually recorded and synchronized with the recorded log from the NeuroSense monitor. Out of the 30 collected data sets, 16 showed strong responses to stimulation, or other responses not explained by the intended model structure, early during the induction phase of anesthesia. Consequently, these data set were discarded and the remaining 14 data sets were kept for identification purposes, covering an age span of 6–16 years and a weight span of 22–71 kg.

B.2 iControl Testing

This section presents clinical and technical data related to the closed-loop study referred to as iControl. The study was approved by the University of British Columbia Children's and Women's Research Ethics Board (H10-01174, iControl Testing), which authorized a total of 125 cases.

Study Population

The study was conducted at the British Columbia Children's Hospital (BCCH), Vancouver, Canada. Out of 115 candidates, 108 subjects conformed with the inclusion criteria given below, and were hence enrolled for the study between 2011-08-02 and 2012-09-06. These subjects were children covering an

age span of 6–17 years and a weight span of 19–75 kg. Their American Society of Anesthesiologists (ASA) physical status was either I (a normal healthy patient) or II (a patient with mild systemic disease). All enrolled subjects were within the 5–95 percentile of weigh-for-age. Exclusion criteria included any contradiction to the administration of lidocaine, propofol or remifentanil and any chronic opioid analgesic or sedative drug therapy. Further exclusion criteria were suspected EEG abnormality, anticipated difficult airway, significant or uncontrolled reflux, delayed gastric emptying or requirements for endotracheal intubation.

Six of the 108 enrolled subjects were excluded from the study. Two of these were not subject to closed-loop controlled anesthesia due to insufficient measurement signal quality upon mounting of the NeuroSense electrodes. In one case it was not possible to gain intravenous access and a volatile anesthetic was consequently used for induction of anesthesia. One case was removed due to a practical issue with the infusion pump. In two cases signal quality from the monitor deteriorated and the system was switched to TCI mode by the anesthesiologist. Consequently, the study comprises 102 closed-loop controlled cases.

Clinical Protocol

Informed and written parental or guardian consent was obtained for all cases and patient assent for all subjects who were 7 years of age or older. Upon arrival in the operating room, biometric patient parameters (age, gender, body height, body mass) were entered into the iControl system by touch screen interface. The forehead of the patient was cleaned with an alcohol scrub upon which the NeuroSense sensor was applied. Signal quality was deemed adequate if the monitor displayed a sensor impedance of less than 10 kΩ. Apart from the NeuroSense, standard patient monitoring devices including electrocardiogram, non-invasive blood pressure measurement and pulse oximeter were applied and their output logged by the iControl system, explained below. An intravenous cannula was inserted, secured with tape and flushed with 0.5 mg/kg[1] lidocaine[2].

Remifentanil, with a concentration of 10 μg/ml (except one case where 5 μg/ml was used), was administered manually as an initial 0.5 μg/kg bolus at 200 ml/h, followed by a steady rate infusion at 0.03 μg/kg/min. A Graseby 3400 Anesthesia pump (Smiths Medical, Ashford, UK), not electronically connected to the iControl system, was used for remifentanil delivery.

Closed-loop administration of propofol using the iControl system was initiated, by press of a touch screen button. The upper and/or lower endoscopic

[1] In this context mg/kg refers to mg of drug per kg of patient.

[2] Lidocaine: a local anesthetic. Flushing the intravenous cannula with lidocaine helps in alleviating the pain associated with propofol infusion in aware patients.

investigation was initiated upon permission from the anesthesiologist.

The initial 25 cases were performed by anestesiologist Dr. J. M. Ansermino, who is one the principal investigators of the study and co-author of related publications [Soltész et al., 2012b], [van Heusden et al., 2013a], [West et al., 2013] and [van Heusden et al., 2013b]. Subsequent cases were performed by eleven different pediatric anesthesiologists. They received no formal training for the system, but most had experience of the interface from a previous usability study.

Throughout the cases, the anesthesiologist had the possibility to administer propofol boluses, change the setpoint or switch the system to either TCI or manual mode, by means of the touch screen interface. All such events were entered into the iContol log. The interface was additionally used to enter timed events into the log. Such events included loss of eyelash reflex, insertion of mouth gag and endoscope, patient movement and episodes of apnea. Technical complications resulting in the exclusion of cases as mentioned above, were also entered into the log by means of this mechanism.

Apart from the anesthesiologist, a research assistant was present during each case, ensuring that the protocol was followed and that all events mentioned above were adequately logged and documented.

The iControl System

The iControl system is a closed-loop controlled TIVA system. DOH is measured using the NeuroSense NS-701 Monitoring System (NeuroWave Systems Inc., Cleveland Heights, USA). Propofol is delivered using an Alaris TIVA pump (CareFusion, San Diego, USA). Apart from the clinical monitor and infusion pump, the system comprises a touch screen interface unit, a unit which runs the closed-loop controller software and an uninterruptible power supply (UPS)[3].

Apart from the PID controller and filter algorithms the system integrates safety features such as infusion rate bounds and automatic fall-back to TCI mode in case of inadequate signal quality. The anesthesiologist is notified by means of audible and visible alarms.

The touch screen display plots current and past measurements, infusion rates as well as estimated plasma (C_p) or effect site (C_e) drug concentrations. Case log and safety messages are displayed and buttons, enabling the user to perform the actions presented in the previous section, are part of the interface.

The system has undergone rigorous safety testing, risk analysis and a usability evaluation. It is authorized for investigational testing (class III) by Health Canada (application number: 168968).

[3] UPS: an uninterruptible power supply provides emergency power when the input power source, typically mains power, fails.

Controller Versions

A parallel form PID controller with $h = 5$ s sampling period was used throughout the study. All parameters in this section are given in continuous time. Zero-order hold sampling was used to obtain the values implemented in the actual controller, unless where otherwise stated.

The controller tuning used for the 23 first cases included in the study, based on the 14 available models mentioned in Appendix B.1, was $K = 5.4m$ h/ml, $T_i = 225$ s and $T_d = 33$ s. The input to the controller is the monitor output $y \in (E_0, E_\infty)$, explained in Section 1.3. The output of the controller is the infusion rate u in ml/h of a 10 ml/mg propofol solution. The gain of the controller is scaled by the patient mass m, measured in kg. The reference was filtered using a first-order low-pass filter with a time constant of 25 s. The measurement signal was filtered using a second-order filter with corresponding continuous time poles at $-1/T$, where $T = 15$ s. There was no path from the reference to the derivative term and integrator anti-windup was established by means of conditional integration, halting when the actuator was saturated. This controller tuning is referred to as *version 1*.

The derivative term was filtered using a backward difference[4] (with sampling period $h = 5$ s) discretization of the low-pass filter $1/(1+sT+(sT)^2/2)$, where $T = 15$ s, corresponding to a relative damping of $1/\sqrt{2}$. During included cases 1–10, an initial bolus was obtained by initializing the derivative term low-pass filter state to yield an initial output of $10.8m$ ml/h. This tuning is referred to as *version 1a*. For included cases 11–23, this was changed to correspond to an initial output of $16.2m$ ml/h, and the corresponding tuning is referred to as *version 1b*.

Out of the 23 initial cases, data sets from 14 were adequate for model identification. Based on these and the 14 models mentioned in Appendix B.1, i.e. a total of 28 models, the controller was re-tuned prior to case 24. The new controller parameters, referred to as *version 2*, were $K = 6.6m$ h/ml, $T_i = 180$ s and $T_d = 60$ s. The initialization of the derivative filter state to produce a bolus was replaced in favor of an initial 600 ml/h bolus with a duration of 15 s. The reference filter was changed to have a time constant of 180 s but with an initial state corresponding to an output of $9/20r$ at time 0^+, where r is the setpoint.

The *version 2* cases are further divided into *version 2a* and *version 2b*. *Version 2a* covers included cases 24–26 and was disclosed above. In *Version 2b*, the reference filter was removed altogether. For included cases 28 and onward, the body mass m for patients who had turned 16 was replaced by the lean body mass [Hume, 1966].

[4] The derivative filter is adopted from an implementation used in [Liu et al., 2007]. This explains why backward difference discretization is used here, whereas zero-order hold is used for all other discretizations within the controller.

In addition to the mentioned versions, minor adjustments were made during 8 cases as mentioned in [van Heusden et al., 2013a] and [West et al., 2013] in order to fine-tune the controller.

B.3 iControl-RP

The closed-loop control of DOA, see Chapter 3, is being evaluated in a clinical study, using the iControl-RP system, which is an extension of the iControl system of Appendix B.2 (”RP” is short for ”remifentanil – propofol”). The study has received Investigational Testing Authorization from Health Canada (Class IV, application number: 206188) and approval from the Fraser Health Research Ethics Board (Closed-Loop Control Of Anesthesia: Controlled Delivery Of Remifentanil And Propofol, FHREB File #: 2012-056). The approval is valid for 150 subjects, divided into two phases. Remifentanil is delivered by TCI during the initial 50 cases, upon which a closed-loop delivery scheme is to be evaluated. The first case was successfully conducted on February 22, 2013.

Results from the iControl-RP study are not presented in the thesis, as the study was not completed by the date of publication. However, the study is mentioned here for completeness and referred to in Chapter 3.

C

Prior Art

This appendix reviews prior art, divided by category into Table C.1 in Appendix C.1, listing reported clinical studies and Table C.2 in Appendix C.2, listing simulation work. Inclusion criteria, motivated by the context of the thesis, are the use of propofol as the main hypnotic drug if DOH was closed-loop controlled, the use of remifentanil as the main analgesic drug if DOA was closed-loop controlled and the use of an EEG monitor as the main source of measurement signal for the closed-loop controller. An attempt has been made to cover all research groups[1] which have reported work matching these criteria. In the interest of space, the survey has been limited to one publication per research group in each category.

Note that only groups considering EEG-guided closed-loop control using propofol or remifentanil are listed. Additionally, there exist several groups, including those of Morari (Switzerland) [Gentilini et al., 2001], Ejaz (USA) [Ejaz and Yang, 2004], Bhatt (India) [Bhatt, 2009] and Beck (USA) [Ralph et al., 2011], who have researched closed-loop controlled anesthesia using volatile drugs.

C.1 Clinical Studies

A survey of closed-loop controlled anesthesia studies (including one on animals), as outlined above, is provided in Table C.1. The table contains one horizontal section per publication. A reference to the publication is listed together with geographical location of the research group and the name of the group leader in the first column. The second column indicates which hypnotic or analgesic drugs were closed-loop controlled in the study and which EEG monitor or monitoring technique was used. The type of controller (and tuning, when reported) are given in column three. It is also indicated in the third

[1] As research group constellations vary over time, Table C.1 in Appendix C.1 and Table C.2 in Appendix C.2 might not accurately represent the research scene at all past times.

column whether induction was performed manually[2], by TCI or in closed-loop and whether the controller was cascaded around an inner TCI loop or controlling drug infusion directly. The method by which control performance was evaluated is displayed in column four. The Varvel method refers to a set of measures introduced in [Varvel et al., 1992] and further discussed in Section 3.1. Patient demography, the number of patients receiving closed-loop controlled anesthesia, their ASA[3] status, types of surgery are reported in column five. This last column also lists, when available, whether patients were breathing spontaneously or mechanically ventilated and, if not closed-loop controlled, how analgesia was provided.

Groups are listed in chronological order of their cited work. This work is not necessarily the most representative of each research group, but serves the purpose of providing one reference from which it is possible to trace other contributions.

[2] Fixed, computer controlled induction profiles which are not based on PK models are referred to as manual in this context.

[3] ASA is the American Society of Anesthesiology. They provide a patient physical classification by systemic disease from I (normal, healthy) to VI (brain-dead).

Table C.1 Examples of clinical studies in which propofol or remifentanil infusion was closed-loop controlled, guided by EEG measurements.

Group, Nationality, Publication	Closed-loop drugs, Monitor	Controller (Tuning), Induction, TCI	Evaluation	Comments
Schüttler, Schwilden Germany, [Schwilden et al., 1989]	Propofol, Median EEG frequency	Model-based (Adaptive), Manual induction, No TCI cascade	Custom	Adults (11), ASA I-II. No surgery (volunteer study).
Roy, United States, [Huang et al., 1999]	Propofol AEP	Fuzzy (Neural), Manual induction, TCI cascade	Custom	*Mongrel dogs* (2). No surgery. Mechanical ventilation. Nitrous oxide was co-administered.
Kenny, United Kingdom, [Kenny and Mantzaridis, 1999]	Propofol, AEP	PI (Tuning not disclosed), Closed-loop induction, TCI cascade	Mean and std errors, Questionnaire	Adults (100), ASA I-II. Body surface surgery. Spontaneous breathing. Nitrous oxide was co-administered.
Short, Hong Kong, [Morley et al., 2000]	Propofol, BIS	PID (Ziegler-Nichols), Manual induction, No TCI cascade	Custom	Adults (30), ASA I-II. Mostly gynecological surgery. Mechanical ventilation.

Continued on next page

Table C.1 Continued.

Group, Nationality, Publication	Closed-loop drugs Monitor	Controller (Tuning), Induction, TCI	Evaluation	Comments
Absalom, United Kingdom, [Absalom et al., 2002]	Propofol, BIS	PID (Tuning not disclosed), TCI induction, TCI cascade	Varvel	Adults (10), ASA I-II. Hip or knee surgery. Spontaneous breathing.
Puri, India, [Puri et al., 2007]	Propofol, BIS	Rule-based (Adaptive), Closed-loop induction, No TCI cascade	Varvel, Patient interview	Adults (20), ASA I-III. Gallbladder, upper and lower gastrointestinal and hernia[4] surgery. Mechanical ventilation.
Fukuda, Japan, [Sawaguchi et al., 2008]	Propofol, BIS	MPC (Adaptation during induction), Manual induction, No TCI cascade	Varvel, Custom	Adults (160), ASA I-II. Various surgery. Mechanical ventilation. Analgesia by manual fentanyl infusion.
Struys, Benelux, [de Smet et al., 2008]	Propofol, BIS	Nonlinear (Model-based), Closed-loop induction, TCI cascade	Varvel, Emergence time	Adult women (20), ASA I-II. Ovum[5] removal. Spontaneous breathing.

Continued on next page

[4] Hernia: a bulge or protrusion of an organ through the structure or muscle that usually contains it.
[5] Ovum: The female reproductive cell.

Table C.1 Continued.

Group, Nationality, Publication	Closed-loop drugs Monitor	Controller (Tuning), Induction, TCI	Evaluation	Comments
Hemmerling, Canada, [Hemmerling et al., 2010]	Propofol, BIS	PID-like (Tuning not disclosed), Manual induction, No TCI cascade	Varvel, Custom	Adults (20), ASA I-III. Various surgery. Mechanical ventilation.
Haddad, United States, [Haddad et al., 2011]	Propofol, BIS	Neuroadaptive (Online training), Closed-loop induction, No TCI cascade	Varvel, Custom	Adults (15), ASA status not disclosed. Type of surgery not disclosed. Spontaneous breathing or mechanical ventilation not disclosed
Janda, Germany, [Janda et al., 2011]	Propofol, BIS	Fuzzy PID (Heuristic tuning), Manual induction, No TCI cascade	Varvel, Manual assessment	Adults (22), ASA I-III. Intra-abdominal or orthopedic surgery. Mechanical ventilation.
Liu, France, [Liu et al., 2012]	Propofol and remifentanil, M-entropy	PID (Tuning not disclosed), Closed-loop propofol and TCI remifentanil induction, TCI cascade	Varvel	Adults (30), ASA I-IV. Various surgery. Mechanical ventilation.

Continued on next page

Table C.1 Continued.

Group, Nationality, Publication	Closed-loop drugs Monitor	Controller (Tuning), Induction, TCI	Evaluation	Comments
Dumont, Canada, [West et al., 2013]	Propofol, NeuroSense	PID (Robust), Closed-loop induction, No TCI cascade	Varvel, Custom	Children (102), ASA I-II. Gastroscopy. Spontaneous breathing.
Grisales, Colombia, [Oquendo et al., 2013]	Propofol, BIS	PID-like (Tuning not disclosed), TCI induction, No TCI cascade	None	Woman (1) ASA I. prosthetic mammary implantation. Mechanical ventilation.

C.2 Simulation Studies

A survey of simulated closed-loop controlled anesthesia studies is provided in Table C.2. The concept and format are identical to those of Table C.1 in Appendix C.1. However, the last column, *Comments*, of Table C.1 is omitted from Table C.2, as its content was specific to clinical evaluations.

Table C.2 Examples of simulation studies in which propofol or remifentanil infusion was closed-loop controlled, guided by EEG measurements.

Group, Nationality, Publication	Closed-loop drugs, Monitor	Controller (Tuning), Induction, TCI	Evaluation
Linkens, Nunes, United Kingdom, [Mahfouf et al., 2005]	Propofol and remifentanil, AEP	PI and fuzzy (Custom), Manual induction, No TCI cascade	Custom
Ionescu, de Keyser, Belgium, [Ionescu et al., 2008]	Propofol, BIS	MPC (Custom), Closed-loop induction, No TCI cascade	Varvel, Custom
Wen, Australia, [Abdulla and Wen, 2012]	Propofol, No monitor model	Dead beat, Closed-loop induction, No TCI cascade	Custom
Mendonça, da Silva Portugal and Sweden, [da Silva et al., 2012]	Propofol and remifentanil, BIS	LQG, Closed-loop induction, No TCI cascade	Varvel, Custom
Brown USA, [Liberman et al., 2013]	Propofol, Custom	PI (IMC), Closed-loop induction, No TCI cascade	Custom
Wang China, [Fang et al., 2013]	Propofol and remifentanil, BIS	PID and MPC (IMC, not disclosed), Closed-loop induction, No TCI cascade	None